Assessing the Impact of Different Pollution Sources on the Type of Microplastics, Associated Microbial Communities, Antimicrobial Resistance and Transport of Microplastics in Selected Urban Rivers in South Africa

Final Report

to the

WATER RESEARCH COMMISSION

Report by:

Malla MA, Malambule N, Moodley T, Amoah ID, Kumar A, Nnadozie C, Indhur R, Bux F, Kumari S

Institute for Water and Wastewater Technology, Durban University of Technology

Institute for Water Research, Rhodes University

WRC report no. 3230/1/25

ISBN 978-0-6392-0737-7

WATER RESEARCH COMMISSION

October 2025

Obtainable from

Water Research Commission

Private Bag X03

GEZINA, 0031

This is the final report of WRC project no. C2022/2023-00886.

DISCLAIMER

This report has been reviewed by the Water Research Commission (WRC) and approved fo publication. Approval does not signify that the contents necessarily reflect the views and policies of the WRC, nor does mention of trade names or commercial products constitute endorsement or recommendation for use.

EXECUTIVE SUMMARY

Background

Plastic polymers, while revolutionising modern industries with their affordability, durability, and versatility, have created a global environmental crisis: the accumulation of non-biodegradable microplastics (MPs). These MPs contaminate aquatic ecosystems, including rivers, lakes, and oceans, posing significant ecological and health risks. Sources of this pollution are diverse, encompassing improper waste disposal, wastewater discharge, and agricultural runoff. Notably, MPs can act as substrates for microbial biofilm formation, fostering diverse microbial communities with potential ecological implications. This study aimed to evaluate the impact of various pollution sources on the type, associated microbial communities, and transport of MPs in selected urban rivers in South Africa.

Methodology

This study investigated microplastic (MP) pollution in two South African rivers: the Msunduzi River (KwaZulu-Natal Province) and the Swartkops River (Eastern Cape Province). To assess the impact of various pollution sources, samples were collected from urban areas (UA), agricultural areas (AA), industrial areas (IA), and wastewater treatment plants (WWTPs) along both rivers. Surface water and sediment samples were obtained using grab sampling techniques. MPs were isolated through filtration and size-fractionated (0.5 mm to 0.025 mm) using mesh sieves. Isolated MPs were then microscopically identified and classified by shape. Polymer identification was performed using Fourier Transform Infrared (ATR-FTIR) and Pyrolysis-Gas Chromatography-Mass Spectrometry (Py-GCMS). Additionally, shotgun metagenomics was employed to explore the relationship between MP pollution sources and the structure, composition, and assembly of microbial ecosystems. The resulting metagenomic sequencing data were analysed using SqueezeMeta and R (R Core Team 2016).

Results

Microplastics (MPs) were detected in both surface water and sediment samples across the studied rivers. The identified MPs included polypropylene (PP), polystyrene (PS), polyethylene terephthalate (PET), polyethylene (PE), polycarbonate (PC), and polyamides (Nylon), with concentrations and types varying significantly across sampling sites.

Metagenomic analysis revealed a diverse range of bacterial phyla and species associated with MPs, showing significant differences in microbial diversity, structure, and functional abundance between surface water and plastisphere habitats ($p < 0.05$). On average, surface water exhibited approximately 7% higher bacterial taxa richness than plastisphere. Mantel analysis indicated that dissolved oxygen (DO) and temperature significantly influenced the surface water microbiome ($r = -0.62$, $p = 0.003$; $r = 0.50$, $p = 0.003$, respectively), while DO and salinity were key environmental drivers for the plastisphere microbiome ($r = 0.33$, $p = 0.003$; $r = 0.47$, $p = 0.003$, respectively). Additionally, significant variations in pathogenic bacterial diversity, structure, and composition were observed between surface water and plastisphere samples across different sampling locations, further demonstrating that pollution sources and environmental factors play a crucial role in shaping both the microbiome and antibiotic resistome profiles within these distinct aquatic compartments. Notably, the plastisphere exhibited an enrichment of mobile genetic elements (MGEs), increased antibiotic resistance genes (ARGs), and a higher abundance of potentially pathogenic bacteria, suggesting it acts as a hotspot for the acquisition and dissemination of pathogens and antibiotic resistance.

The transport model yielded satisfactory simulations of observed MP concentrations in both water and sediment samples, validating its effectiveness in representing real-world conditions. The model also highlighted significant variations in MP transport dynamics, influenced by reach-specific hydrodynamic conditions. Notably, biofilm formation on MPs affected their buoyancy and degradation rates, further complicating their transport mechanisms. Overall, these findings underscore the complex interactions between MPs, hydrodynamic conditions, and biological factors within these river systems.

Conclusions

The comprehensive investigation into MP contamination in the understudy river systems has yielded significant insights into the intricate relationship between different pollution sources and microplastic types, associated microbial communities, and transport models. All selected pollution sources had a significant impact on the type and abundance of MPs in the riverine environment, with PE and PS being the most dominant plastics identified. The identification of various plastic polymer types and their abundance highlights the pressing need to address the growing issue of MP pollution in aquatic environments from various sources. Furthermore, these pollution sources are also shown to drive the microbial community type attachment to the plastic surface. The presence of distinct microbial communities in MPs distinguishes the plastisphere from surrounding habitats by selectively recruiting microbial communities, thus

underscoring the complex ecological dynamics at play. The functional implications of such a unique habitat (the -plastisphere) assemblage are also reflected in its distinct metabolic potential for different biogeochemical cycling and other organic compounds and potential pathogens.

Additionally, modelling the MP transport mechanisms in riverine environments offers a valuable tool for predicting MP behaviour and guiding mitigation efforts. This, in turn, provides a comprehensive framework for assessing MP pollution in freshwater systems and highlights the need for targeted interventions to reduce MP inputs from various sources. Our results can provide a basis for quantifying the effects of plastisphere on various planetary issues, such as ecosystem monitoring, sustainable development, greenhouse gas emission, climate change, pathogenicity and One-Health. Overall, this study contributes valuable knowledge to the ongoing efforts to promote a sustainable coexistence of humanity and the environment, safeguarding our planet for current and future generations.

ACKNOWLEDGEMENTS

The authors extend their gratitude to all collaborators for their unwavering support throughout the study period and to the reference group of the WRC project for their assistance and constructive discussions. Special thanks are due to the WRC for funding the research and to DUT for providing administrative support and research facilities.

REFERENCE GROUP MEMBERS

Name	Organisation
Dr E Ubomba-Jaswa	Research manager, Water Research Commission (Chairperson)
Ms Penny Jaca	Research coordinator, Water Research Commission
Mr Mncedisi Malungana	
Ms Megan Schalkwyk	Umgeni Water
Mr Nico van Blerk	Ekurhuleni Water Care
Mr Sydney Masha	eThekwini Water and Sanitation Department (ERWAT)
Dr Swastika Surujlal-Naicker	Scientific services, City of Cape Town
Mr Hennie Kotze	Scientific services: City of Cape Town
Mr Mcebo Mkhize	Research and Development Unit: Umgeni
Prof Henk Bouwman	North West University
Dr Deidre Van Wyk	Senior Lecturer: North West University, Mafikeng
Prof Memory Tekere	University of South Africa
Prof Beatrice Opeolu	Cape Peninsula University of Technology
Dr Rembu Magoba	Water Centre Manager, CSIR

RESEARCH OUTPUTS:

Journal articles:

1. Comprehensive profiling and risk assessment of antibiotic resistomes in surface water and plastisphere by integrated shotgun metagenomics, MA Malla, NL Malambule, J Featherston, A Kumar, ID Amoah, A Ismail, *Journal of Hazardous Materials*, 137180
2. The plastisphere ecology: Assessing the impact of different pollution sources on microbial community composition, function and assembly in aquatic ecosystems, MA Malla, NL Malambule, ID Amoah, J Featherston, A Ismail, F Bux, *Environmental Chemistry and Ecotoxicology* 7, 75-83
3. Applications of mathematical modelling for assessing microplastic transport and fate in water environments: a comparative review, T Moodley, T Abunama, S Kumari, D Amoah, M Seyam, *Environmental Monitoring and Assessment* 196 (7), 667
4. Muneer Ahmad Malla, Riona Indhur, Nomalihle Malambule, Kelebogile Mosagale, Tyrone Moodley, Faizal Bux, Sheena Kumari, Microplastic in Ecosystems: Abundance, Transportation, and Biodegradation (In: Bioremediation: Removing Microplastics from Soil), Chapter 1pp 1-18

Additional outputs related to the study area:

1. A Kumar, R Indhur, F Bux, S Kumari. 2024. Recent advances in mechanistic insights into microplastics mitigation strategies via emerging advanced oxidation processes: Legislation, challenges, and future direction, *Science of the Total Environment* 957, 177150
2. R Indhur, I Amoah, F Bux, S Kumari 2024 Nanomaterials for microplastic removal from wastewater: current state of the art nanomaterials and future prospects, *ACS ES&T Water* 3 (12), 3741-3754

Conference presentations:

1. Malla MA, Malambule NL, Magray O, Bux F, Kumari S. 2024. Impact of different pollution sources on the plastisphere microbiome in aquatic ecosystems. IWA World Water Congress & Exhibition. 11-15 August 2024, Toronto, Canada.
2. Malambule, N,. Malla, MA., Amoah, ID., Nnadozie, C., Kumari, S. 2024. Impact of different pollution sources on microplastics in the Msunduzi river. WISA 2024 Biennial Conference & Exhibition, 12 - 14 June 2024, Durban ICC.
3. Malla, MA., Malambule, N., Bux, F., Kumari, S. 2024 Pollution sources impact on plastisphere microbiome in aquatic ecosystems. WISA 2024 Biennial Conference & Exhibition, 12 - 14 June 2024, Durban ICC.

CAPACITY BUILDING

POST GRADUATE STUDENTS		
Ms Nomalihle Malambule	Master's (Applied Science)	Durban University of Technology (DUT)
Mr Tyrone Moodley	PhD (Civil Engineering)	DUT
Ms Riona Indhur	PhD (Biotechnology) DUT	DUT
Mr Siyabonga Muna Ms Havilah	Master's (Water Resource Science	Rhodes University
Onyinyechi Nnadozie Mazibuko	Master's (Water Resource Science	Rhodes University
Ms Kelebogile Mosagale	Honours (Biotechnology),	DUT
Ms Anele Khumalo	Honours (Biotechnology),	DUT
EMERGING RESEARCHERS		
Dr Muneer Malla	Post Doctoral Fellow	DUT
Dr Arvind Kumar	Post Doctoral Fellow	DUT

LIST OF TABLES

LIST OF FIGURES

ACRONYMS & ABBREVIATIONS

AA	Agricultural area
AOPs	Advanced Oxidation Processes
ATR-FTIR	Attenuated Total Reflectance Fourier Transform Infrared
BOD	Biological Oxygen Demand
COD	Chemical Oxygen Demand
COG	Clusters of Orthologous Groups
DEM	Digital Elevation Model
DNA	Deoxyribonucleic acid
DO	Dissolved oxygen
EC	Electrical Conductivity
EPS	Extra polymeric substances
FAPROTAX	Functional Annotation of Prokaryotic Taxa
Fc	Cohesion
Fd	Hydrodynamic drag
Ff	Friction
Fl	Hydrodynamic Lift
Fn	Bed Support Force
FTIR	Fourier Transform Infrared Spectroscopy
GES DISC	Goddard Earth Science Data and Information Services Centre
GIS	Geographic Information System
HDPE	High density polyethylene
HGT	Horizontal gene transfer
IA	Industrial Area
INCA-MP	Integrated Catchment Model of MPs Transport
ISA	Impervious Surface Area
IUCN	International Union for Conservation of Nature
KEGG	Kyoto Encyclopaedia of Genes and Genomes
KZN	KwaZulu-Natal
LDA	Linear Discriminant Analysis

LEfSe	Linear Discriminant Analysis Effect Size
MC	Monte Carlo
MERRA	Modern-Era Retrospective Analysis for Research and Applications
MODIS	Moderate Resolution Imaging Spectroradiometer
MP	Microplastics
Mt	Metric Ton
NASA	National Aeronautics and Space Administration
NEWS	Nutrient Export from WaterSheds
NP	Nanoplastics
NSE	Nash-Sutcliffe Model Efficiency Coefficient
NTU	Nephelometric Turbidity Units
ODE	Ordinary Differential Equations
ORFs	Open Reading Frames
PBS	Phosphate Buffer Saline
PCoA	Principal Coordinated Analysis
PE	Polyethylene
PERMANOVA	Permutational multivariate analysis of variance
PERSiST	Precipitation, Evapotranspiration and Runoff Simulator for Solute Transport
PET	Polyethylene Terephthalate
PP	Polypropylene
PS	Polystyrene
PTFE	Polytetrafluoroethylene
PVC	Polyvinylchloride
Pyro-GCMS	Pyrolysis-Gas Chromatography Mass Spectrometry
RPKM	Reads Per Kilobase Million
SRTM	Shuttle Radar Topography Mission
TDS	Total Dissolved Solids
TMPA	TRMM-Multi-Satellite Precipitation Analysis
TRMM	Tropical Rainfall Measurement Mission
TUFLOW FV	Two-dimensional Unstructured Flow Finite Volume Model
UA	Urban Area

USGS	United States Geological Survey
WAQ	Water Quality Model
W	Submerged weight
Wb	Bottom weight
WGS	World Geodetic System
WR	Water Resources
Wt	Top width
WWTP	Wastewater treatment plants

TABLE OF CONTENTS

CHAPTER 1: INTRODUCTION

1.1 Background

Plastic polymers have become an integral part of modern society, finding utility across various domains of daily life due to their cost-effectiveness, durability, lightweight nature, and flexibility. Plastic accretion in the environment is becoming a significant problem owing to its exponentially expanding manufacturing rate (Eriksen *et al.* 2014; Boyle and Örmeci 2020). The inflow of mismanaged plastics into the environment has grown from 4.8 to 12.7 million tonnes (Uzun, Farazande and Guven 2022).The gradual fragmentation of larger plastic materials, coupled with the inability of MPs to undergo complete degradation, has led to their widespread presence across aquatic environments, including rivers, lakes, and oceans (Karbalaei et al., 2018). Their accumulation in water, soil and sediments has raised substantial concerns globally (Ratre et al., 2024; Thakur et al., 2023a). The global plastic production has risen significantly and has reached ~ 10 billion metric tons (Mt), with an annual production of 400 million metric tons (Brown et al., 2023; Omura et al., 2024). Out of the total waste generated, 9% is recycled and about 80% ends up in landfill sites and other natural environments (Li et al., 2021). It has been reported that every year, about 8 million tons of MP waste end up in aquatic ecosystems (Meijer et al., 2021). The sources, fate and transport of these MPs are diverse, presenting a significant threat to both terrestrial and aquatic ecosystems, with adverse effects on their flora and fauna (Malla et al., 2023; Ratre et al., 2024; Rüthi et al., 2023). Once released the MP debris is transported across ecosystem boundaries and remains in the environment for longer periods, representing an emerging perturbation with unknown biogeochemical and long-term ecological consequences (Omura et al., 2024; Turner et al., 2020). The aquatic ecosystems are of particular concern owing to high MP inputs and hence higher contamination. The proliferation of MPs in aquatic ecosystems stems from a multitude of sources, contributing to the complex contamination of these fragile habitats. Improper waste management, inadequate disposal practices, and the persistence of plastic materials in the environment all contribute to the escalation of MPs. Furthermore, effluents released from wastewater treatment plants, often containing MP fragments from personal care products and synthetic fibres, also contribute to this predicament. Agricultural runoff, laden with plastic fragments and residues from farming practices, further amplifies the issue, particularly in regions with intensive agricultural activity (He et al., 2020).

Recently, the microplastic-microbe interplay has moved into focus (Bhagwat et al., 2021; Yang et al., 2020), as these MPs provide a new niche for microbes in the environment (Yang et al., 2020;

Zhu et al., 2022). Understanding the mechanisms driving the microbial community composition and function in aquatic ecosystems and plastisphere is essential. Significantly, recent research has unveiled that the presence of MPs extends beyond surface water samples, permeating even sediment samples. This emphasizes the pervasive nature of MPs within aquatic ecosystems, indicating the potential for these particles to infiltrate various levels of the aquatic environment and interact with diverse ecological components (Gola et al., 2021). Model estimates indicate that more than 5 trillion plastic particles float on the ocean surface, and approximately 348 million tonnes of plastic were produced worldwide in 2017 compared to 1.5 million tonnes in 1950 (Boyle and Örmeci 2020). It is estimated that 75% of the oceans' waste is plastic, with the majority being classed as MPs (Uzun, Farazande and Guven 2022). MPs, distinguished by being smaller than 5 mm in length, are present in all aquatic environments, including lakes, rivers, oceans, and aquifers. These MPs are typically composed of fibres and films and are either PE, PP, polychloride, PS or PET (Zhang *et al.* 2020). The ocean is considered the largest sink of MPs, of which 98% originate from land-based sources, with riverine runoff being the primary method of transport (Yang *et al.* 2021). It is estimated that 1.15-2.41 million tonnes of plastic are deposited into the ocean via rivers annually (Pereao, Opeolu and Fatoki 2020). MPs enter the aquatic system in two types: primary and secondary MPs. Primary MPs are manufactured products and secondary MPs are the subsequent breakdown of large plastics (macroplastics) existing in the environment (Boyle and Örmeci 2020).

MPs defined size range are typically subcategorized as plastic fragments ranging from 0.1 to 1000 μm (small MPs), whilst MPs in the range of 1-5 mm are regarded as large MPs (Dos Santos et al., 2023). Plastic particles classified as nano-plastics (NPs) measure ≤ 0.1 μm, and are widely recognised as a global pollutant. The threat posed by MPs to human health varies depending on their size. For example, MPs smaller than 110 μm can travel through the portal vein, which carries blood from the intestines, pancreas, and spleen to the liver (Gao et al., 2023). Moreover, MPs smaller than 20 μm may infiltrate organs such as the liver and kidneys, while those larger than 150 μm are not absorbed by the human body (Uheida et al., 2021). Furthermore, MPs can disrupt habitats by altering the physical and chemical properties of sediments, impacting the health and biodiversity of aquatic ecosystems (Ahmed et al., 2022; Lu et al., 2023). Chronic exposure to the human, MPs potentially creates serious health issues, including immune dysfunction, reproductive abnormalities, and neurological disorders (Gao et al., 2023). Additionally, once in aquatic systems, MPs are ingested by various marine species, including fish, plankton, and shellfish, causing physical damage, impaired feeding, and decreased growth and reproductive success (Yang et al.,

2023). Ingestion of MPs can also transfer toxic chemicals, which adhere to the plastic surfaces, up the food chain, potentially reaching humans. The MPs' inhalation and ingestion routes accumulated by the human body, and their toxic effects on human organisms are shown in Fig. 2b. The pervasive nature of MPs, coupled with their persistence and ability to accumulate, presents a formidable challenge to maintaining the health and sustainability of aquatic environments globally (Jaiswal et al., 2022). The major sources of MPs to the environment are hospital, industrial, and domestic waste, as shown in Fig. 2a. Furthermore, Fig. 2c depicts bioaccumulation processes of MPs/nanoplastics, and their detrimental impacts on human health, whereas Fig. 2b illustrates environmental transportation pathways of MPs. These MPs result from the breakdown of larger plastics at a wastewater treatment plant (Sharma et al., 2021). Municipal wastewater treatment plants (WWTPs) have recently garnered heightened scrutiny as possible contributors to plastic pollution in surface water (Okoffo et al., 2023). These MPs, however, can have multiple entry points to the environment, such as sewage sludge used as agricultural fertilizer and direct urban discharges (Sharma et al., 2021). The milestone timeline of research related to MP detection and treatments has been shown in Fig. 1a. European WWTPs report MP levels ranging from 0.25 to 15 MPs per litre across all treatment stages, with effluent levels around 1-3 MPs per litre (Dos Santos et al., 2023). Plastic production has experienced a significant escalation, reaching 288 million tons annually, and is projected to reach 33 billion tons by the year 2050 (Domínguez-Jaimes et al., 2021) as shown the trend in Fig. 1a. The current cumulative plastic production has surpassed 8 billion MT worldwide and is anticipated to continue escalating in the forthcoming decades (Ricardo et al., 2021). In the recent study reported by Leslie et al., MPs particles, including polyethylene (PE), Polypropylene (PP), and Polyethylene terephthalate (PET) were detected in human blood at a concentration of 1.6 μg/mL. Even in freshwater, MPs, particularly PE, PET, PP and PS have been commonly identified, constituting 70% of the total MP count (Hossain et al., 2024; Nabi et al., 2020). Given the exponential increase in publications over the past 10 years, there is an urgent need to develop advanced techniques for the removal of MPs, as highlighted by the aforementioned issue. This trend is depicted in Fig. 1a. However, the strategies for eliminating MP pollution from the environment are still in their early stages. Considering the complexity and severity of the MP problem, it is crucial to develop rapid and sustainable techniques for MP treatment. MPs degradation techniques should aim to break down the polymer chains and simultaneously generate highly valuable intermediate products, posing a significant challenge on a global scale. Recently, MP have emerged as a hazardous environmental pollutant due to their impact on biota and human health (Sharma and Chatterjee 2017). It has been calculated that there are 630 000 metric tonnes of mismanaged plastic waste in the coastal areas of South Africa, placing

it eleventh worldwide in contributing to marine plastic debris (Verster, Minnaar and Bouwman 2017). In South Africa, MP studies are currently being conducted; however, most of the studies are limited to marine MPs (Verster, Minnaar and Bouwman 2017). Due to MPs having many forms, additivities, sources, pathways and sinks, their quantification and evaluation in river environments is extremely difficult, which limits the ability to mitigate their impacts and has caused it to become one of the most prevalent and damaging environmental contaminants (Boyle and Örmeci 2020).

Urban rivers are increasingly impacted by a complex interplay of environmental factors, including seasonality, sedimentation, and varying water quality, all of which can significantly influence their microbial ecosystems. This study investigates the microplastics abundance and microbiome of surface water and plastisphere (the microbial community inhabiting plastic debris) within the Msunduzi and Swartkops river systems in KwaZulu-Natal and the Eastern Cape provinces, respectively. Specifically, the study aims to elucidate how different pollution sources, alongside these environmental factors, shape the composition and function of microbial communities associated with microplastics, including functional microbes and pathogens. Furthermore, leveraging remote sensing, Geographic Information System (GIS), and modelling software, this study assesses the microplastic fluxes within these river systems, providing a comprehensive understanding of their transport and distribution. Ultimately, this study aims to shed light on the ecological mechanisms governing microbial community assembly in these environments and to contribute to a deeper understanding of the broader implications of microplastic pollution on aquatic ecosystem health.

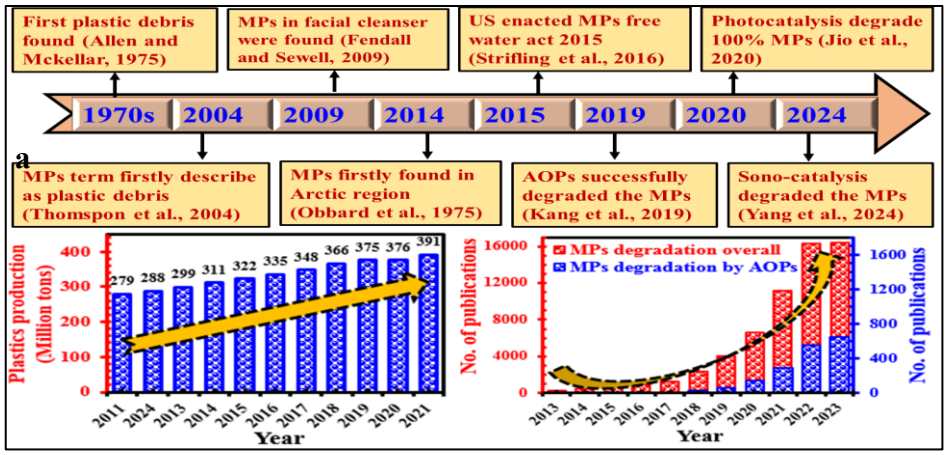

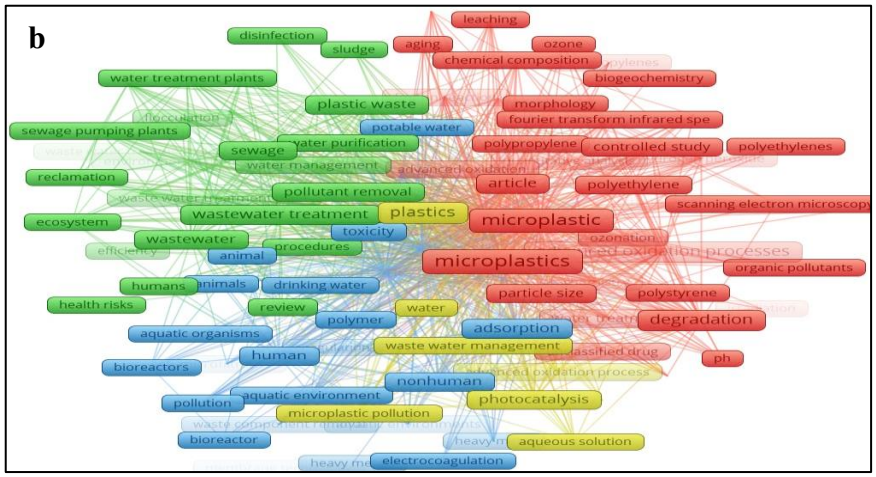

Fig. 1 (a): Milestone timeline of research related to MP, global plastic production, last 10-year publications on MP degradation by AOPs (Google Scholar, MP degradation as keyword search made in August 2024), **(b)** Existing literature based on Scopus database searched by keyword "MP removal" and "MP degradation".

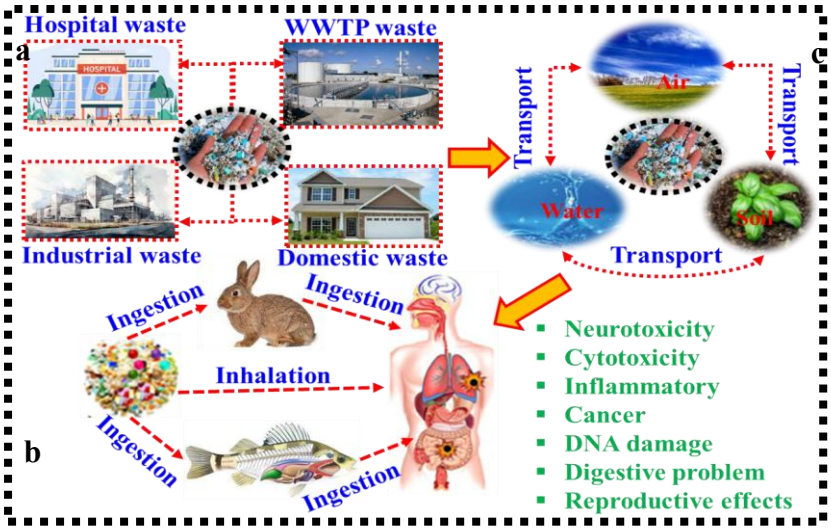

Figure 2: Potential primary sources, environmental transportation pathways of MPs, bioaccumulation processes of MPs/NPs, and their detrimental impacts on human health.

The specific aims of the projects are as follows:

1. To detect, quantify, and characterise microplastics from different pollution points in the Msunduzi and Swartkops rivers in KwaZulu-Natal and Eastern Cape provinces.
2. To apply shotgun sequencing and bioinformatics to determine attached microbial communities on MP surfaces, with special emphasis on pathogens, antibiotic-resistant genes, mobile genetic elements and other functional microbes.

3. To identify the leading sources of microplastics, link the types to identified sources to the biofilm/microbial diversity, and hence provide an indication of local ‘hot spots’ of occurrence.

4. To investigate the influence of seasonal variation, sedimentation and water quality on biofilm formation and its diversity on MP surfaces.

5. To model the transport and fate of microplastics in the selected rivers, accounting for the impact of microbial association with the microplastics.

CHAPTER 2

LITERATURE ON MICROPLASTICS OCCURRENCE IN SURFACE WATER

2.1 Main sources of MP in the river

MP are characterised as being less than 5 mm in diameter and are grouped between macro- and nano-plastics (Yang *et al.* 2021). In recent literature the upper limit of MP diameter is restricted to 1 mm as microbeads, which are manufactured MP, fall in the size range of 5μm to 1mm (Hernandez, Yousefi and Tufenkji 2017; Bouwman *et al.* 2018). However, the characterisation can be further classified according to source; location; use; release patterns; shape and polymer composition, which, in MP research are crucial parameters especially in transport and distribution modelling (Bouwman *et al.* 2018; Wagner and Lambert 2018). MP are grouped based on origin and shape as primary particles, fragments and fibres. Primary MP particles are plastics that are manufactured as plastic pellets and cosmetic plastic particles, and secondary MPs are macro-plastics that are fragmented by biological and mechanical action and sunlight (Van Cauwenberghe et al. 2015). Fibres are MPs that originate from the washing of clothes (Bouwman et al. 2018).

Several studies have recently revealed a broad presence of MP in riverine ecosystems, as well as their origins, transit, and negative impacts on freshwater biota. Only a small amount of study has shown evidence of MP origins in riverine ecosystems so far. Anthropogenic sources of MP in riverine ecosystems, such as industrial effluents, household activities, WWTP reclamation operations, surface discharge, and so on, are described in this section. According to the International Union for Conservation of Nature (IUCN), machine-washed synthetic fabrics were the single greatest source of MPs in the water, accounting for 35 percent of the total (Kumar et al., 2021). As the intake of MPs grows, the concentration of MPs often exceeds the ambient threshold. MP entry channels, sinks, and accumulation zones in terrestrial, aquatic, and atmospheric environments were studied by (Lechthaler et al., 2020). MP contamination has been discovered in riverine ecosystems all around the world, in both sediments and water (Alam et al., 2019; Fan et al., 2019; Zhang et al., 2020). The riverine ecosystem has been contaminated by plastics from agricultural activities (Guerranti et al., 2017; Kumar et al., 2021), WWTP (de Villiers, 2019; McCormick et al., 2014; Schmidt et al., 2020), fishing nets and cages (Kasamesiri and Thaimuangphol, 2020), municipal wastewater (Zheng et al., 2019).

MPs have long been recognised as a hazardous contaminant impacting land and marine environments due to their abundance and persistence, making it one of the most urgent global

problems in recent years (Berezina *et al.* 2021; Whitehead *et al.* 2021). However, little is known about MP transport and distribution, especially in riverine environments, which is evident in lack of published studies compared to oceanic modelling (Whitehead *et al.* 2021; Uzun, Farazande and Guven 2022; Moodley *et al.* 2024). Rivers are one of the most dominant pathways of MPs into the ocean, with pollution from surface runoff, land disposal, air deposition, wastewater treatment effluent and sewage sludge used in agriculture (Allen *et al.* 2019). The transport of MPs in rivers is subject to various processes depending on the environmental conditions and particle characteristics viz. MP fragmentation, chemical degradation, colonisation by biofilm and its physical properties (shape, size and density) (Domercq, Praetorius and MacLeod 2022). The combined complexity of the various processes governing MP distribution and transport restrains current literature on these mechanisms, limiting our ability to accurately forecast concentration for different plastic types at various locations and to assess potential risk (Domercq, Praetorius and MacLeod 2022).

Mathematical modelling has the potential to understand MP transport, fate and distribution in riverine environments, which is demonstrated in various recently developed modelling approaches (Whitehead *et al.* 2021; Nizzetto *et al.* 2022; Norling *et al.* 2024). Recent research by Uzun, Farazande and Guven (2022) and Moodley et al. (2024) consolidated, characterised and critically analysed modelling frameworks used in MP transport research globally, and highlighted that all modelling frameworks resulted in relatively reliable findings, with each having its strengths and weaknesses in simulating MP transport and fate. It was also highlighted that the bulk of research generally concentrates on MP modelling in the oceans rather than in rivers, which is a significant contributor of MP into the ocean. Landscape-scale riverine modelling of MP transport and fate is needed to fill the gap in monitoring data, quantify fluxes to the marine environment and identify environmental distribution processes, however, only a few such models exist which limits the capacity to assess MP transport and fate and prioritise MP reduction interventions (Norling et al. 2024). This is evident in the study by Moodley et al. (2024), the authors screened 631 articles to identify water environment-specific MP modelling studies and resulted in 61 articles, of which 16 focused on riverine-based MP modelling. The study also highlighted various factors that are often omitted from modelling studies and reduce model reliability, which are included in this study, such as the use of sampled MP data from the river column and river bed; sedimentological information viz. MP size, type, density, depositional environment and water depth; MP-shaped fibres rather than near-spherical shapes; the inclusion of vertical mixing in the water column and the inclusion of modelling the potential sources.

Twelve relevant MP modelling studies, including this one are presented in Table 1. The table highlights each study's location, aim, applied model, model inputs, and findings. The comparison illustrates the current state of MP riverine modelling, revealing that only two studies have modelled the entire river catchment. Both Whitehead *et al.* (2021); Nizzetto *et al.* (2022) used INCA models, but compared to this study, they unutilized minimal input data did not model different pollution sources. Notably, none of the analyzed studies were conducted in Africa, limiting the environmental conditions to the European, American, Australian and Asian climates, characterized by moderate and evenly distributed rainfall.

Table 1: Comparison of articles employing models to describe the transport of MP in riverine environments

Author	Location	Aim/Objectiv	Applied mod	Model inpu data	Main findings
(Atwood *et al.* 2019)	Po River, Northern Italy	The study aims to model the coastal build-up of MP particles generated by th Po River.	Ichthyop lagrangian particle trackin model and a remote sensing model.	Images of the Landsat 8, and the European Space Agency Sentinel-2 we used for the remote sensin model, and river discharg and wind spee were used in the hydrodynamic model.	The results indicate that the released particle quantity is semi-coupled to beaching rates, which are mouth dependent. Remote sensing better captured river mouth relative strength, and accumulatio patterns were consistent with t hydrodynamic model.
(Bondelind *et al.* 2020)	Göta River, Sweden	The study aims to analyse the influence of siz and density of tyre wear particles in roac run-off.	MIKE 3 FM software	MP quantity, particle sizes, density and settling velocities.	Large quantities MPs were observed on the south side of the river owing to higher annual average daily traffic loads. The mixing processes in the river and t MP concentratio were influenced by the vertical

					water density gradient.
(Nizzetto *et a* 2016)	Thames River - UK	The study aims to model MP transport across the pedosphere and hydrospher	INCA-Contaminant fa model.	Data on the river geometry sub-catchmen boundaries, slopes, land use, and soil properties.	MPs of 0.2 mm are not retained, whereas larger MPs with densities higher than water are retained in the sediment. However, high flow periods can cause resuspension.
(He *et al.* 202	Brisbane River, Australia	The study aims to model the transport processes of sedimental MPs	TUFLOW FV Particle Trackii Module	Flow velocity water levels, water temperature, salinity, wave and tidal data and sinking velocity data.	The study outcomes confir that sedimental MPs with low density have high mobility and hig flow velocity in the bottom water layer of the wate column enabling sedimental MP transport.
(Whitehead *et al.* 2021)	River Thames-UK	The study aims to model the impacts of MPs on river water quality and quantify the amount moving along the river.	Integrated catchments (INCA) MPs model	MP data from effluent discharges and sewage sludge disposal.	The results show that there is a significant amou of MPs moving down the river with increasing deposition on the riverbed.
(Babajamaaty, Mohammadian and Pilechi 2022)	Fraser Rive Georgia	The study aims to model the transport of MP in a highly urbanised and industrialised area.	Telemac modelling system and BlueKenue.	Bathymetry data, water level, flow velocity, salinity	The results indicated that the hydrodynamic mesh solution in both horizontal and vertical directions, the discharge rate upstream, time step size, boundary treatment metho and quality of th bathymetry data

					were the main factors which influenced the behaviour of the particles.
(Sani-Kast *et a* 2015)	Rhone Rive France	The study aims to investigate th influence of various parameters on t fate of engineered nanoplastics.	A modified version of the river multimedi box model	Water composition data, river morphology and flow velocity.	The results indicate that the fate of nanoparticles car be described by relatively small concentrations ar is significantly dependent on conditions near their seeding source.
(Besseling *et a* 2017)	Dommel River, Netherlands	The study aims to analyse the fate and retentic of plastic in the river.	NanoDUFLOW model and R Studio software v0.98.976	Experimental attachment efficiency, sedimentation aggregation, degradation, resuspension, and burial dat	The data shows that particle size significantly influences the simulated retention and accumulation ho spots in the sediment, with retention being lowest for intermediate-size particles (5 μm).
(Siegfried *et a* 2017)	European Rivers	This study aims to estimate MP fluxes from lan to sea.	Global NEWS (Nutrient Expo from WaterSheds) model.	MP estimates, land use, agricultural ar socio-econom parameters.	The study did no provide a validated model. However, the results indicate that synthetic polymers from tyres and road wear comprise th largest source of MP pollution.
(Mai *et al.* 2019)	Pearl River Delta, Chin	The study aims to conduct sampling to provide field-measured data for validating modelling results.	Mass-balance model	MP field data	The annual riverine input of MPs was estimated at 240 3800 tons of plastic debris. These values we substantially below the

					mismanaged plastic waste-based model estimates (91,00(170,000 tons). Tl large difference between measure and modelled results may have derived from the large uncertainty in the mismanag plastic waste values assigned t the world's countries/regions
(Unice *et al.* 2019)	Seine River France	The study aims to develop a ma balance model t assess the fate c tyre and road wear particles.	Delft-3D WAQ	Tyre wear and generation rat particle densit particle diameter, biofilm thickness and density,	The modelled pseudo steady state sediment concentrations were consistent with measurements from the Seine watershed supporting the plausibility of th predicted trappin efficiency of approximately 90%.
(Lee *et al.* 2022)	Langat Rive Malaysia	The study aims using machine learning techniques to automatically segment and count MPs in a given image.	U-Net convolutional neural network	Images of MP sieved throug a 53 μm mesh	The results indicate that U-Net can achieve human-level performance in counting MPs in cluttered images.

MPs can be found in everyday products such as cosmetics, shampoo, and toothpaste. The release of microfibers occurs as a result of normal fabric washing and laundering (Jiang, 2018). In fact, when cleaning synthetic clothing in a wash machine, approximately 2000 microfibers can be released (Browne et al., 2011; Carney Almroth et al., 2018) . A large body of research has been conducted on MP pollution in rivers based on numerous factors, including the watershed area,

population density, wastewater treatment level, and effluent discharge volumes (Blair et al., 2019; Eriksen et al., 2013).

In addition to industrial pollution (Mani et al., 2015; Scherer et al., 2020), natural sediment erosion, surface runoff, and urbanization has been highlighted as a major source of MP pollution (Horton et al., 2017; Mani et al., 2015). In India, Singh et al. (Singh et al., 2022) discovered MP in the sediments of the Ganga River in Patna, with concentrations of 144 to 250 particles per 25 mg of soil sediments (equivalent to 576,000 to 1,000,000 particles per kg). A significant concentration of MPs has been found downstream of Patna, indicating that urbanization and human activities are major contributors to river pollution.

The contamination of freshwater habitats with MPs has been driven by human sources such as sewers and wastewater treatment facilities. Sewers and treatment facilities accept sewage waste and effluents generated by homes, businesses, and storm drains that are discharged directly into rivers (Schmidt et al., 2020). Effluents collected in rivers are classified into two basic sources: point and non-point (diffuse) sources. Both of which contribute to MP contamination. WWTPs are considered a source of MP contamination in waterways. The role of WWTPs in identifying, monitoring, and removing MPs cannot be overstated.

MPs are mainly present in WWTPs as a result of the sewage system and various wastewater sources, such as residential, commercial, and industrial. MP concentrations in the combined sewer system have been observed as a result of surface runoff (Mason et al., 2016; Sun et al., 2019). In addition to industrial and commercial wastes, WWTPs contain a significant amount of MPs and microbeads from personal care products (Atugoda et al., 2021; Golwala et al., 2021; Mason et al., 2016; Sun et al., 2019). The microfibers found in South African WWTPs are a result of household activities (de Villiers, 2019).

In a WWTP, MPs can be removed with a 95% efficiency at various stages of the treatment process, including screening, sedimentation, biological treatment, secondary and tertiary treatment (Blair et al., 2019; Mason et al., 2016; Shen et al., 2019; Sun et al., 2019; Ziajahromi et al., 2016). Even though wastewater treatment plants have a high removal efficiency, the increased rate of effluent discharge per day results in an increased amount of MPs accumulating in rivers (Dris et al., 2018; Murphy et al., 2016). In the United States, WWTPs have been observed to generate high MP concentrations downstream of the Chicago River (McCormick et al., 2014). In addition to wastewater treatment plants, landfills release MPs into the environment, which leads to MPs leaching (Hou et al., 2021), which then enters surface runoff and enters the environment.

2.2 Distribution of MPs in river ecosystem

MP studies in river ecosystems are difficult and sensitive because hydrological parameters, morphology, and physicochemical features of rivers are the main variables that influence distribution and abundance (Campanale et al., 2020; Horton et al., 2017). Several studies have shown that MPs are accumulating in river sediments all around the world (de Villiers, 2019; Guerranti et al., 2017; Wang et al., 2017). MP forms have been found in river water and sediment samples on a regular basis (He et al., 2020; Scherer et al., 2020; Van Emmerik et al., 2018; Xu et al., 2020)(. MP pollution has been reported in rivers around the world, including the Danube River in Europe (Lechthaler et al., 2020), the San Gabriel River in the United States (Moore et al., 2011), the Hudson River in the United States (Miller et al., 2017), the Snake River in the United States (Kapp and Yeatman, 2018), the Pearl River in China (Fan et al., 2019), the Orange-Vaal River in South Africa (Weideman et al., 2019).

Asia adds a huge amount of plastic to the aquatic environment's water and sediments on a worldwide scale (Lebreton et al., 2017)(Adam et al., 2019)(Singh et al., 2022). As previously noted, China has the highest concentration of MPs in surface water and sediments in Asia, followed by India, Taiwan, South Korea, and Indonesia. A high concentration of MPs has been documented from a number of different nations, including the United Kingdom, Canada, Germany, the United States, South Africa, and France. MPs concentrations in sediments were determined to be 18–629 items kg^{-1} in the Antua River in Portugal (Rodrigues et al., 2018). In comparison, large levels of MPs have been found in Chinese river sediments (Peng et al., 2018)(Ding et al., 2019). MP contamination occurs for a variety of reasons, including a large population, established businesses with high plastic output, and inefficient and inadequate waste management. Urbanization, on the other hand, is reported to be the leading cause of MP pollution in the Rhine-Main River in Germany (Klein et al., 2015; Mani et al., 2015), the St. Lawrence River in Canada(Castañeda et al., 2014), and the River Ganga in India (Singh et al., 2022).

Similarly, high concentrations of MPs due to urbanization in river sediments were investigated in other locations, including the Beijing River, China (Wang et al., 2017), the Ombrone River, Italy (Guerranti et al., 2017) the Roter River, Germany (Frei et al., 2019) and the Solimoes, Negro, and Amazon Rivers in Brazil (Gerolin et al., 2020). This indicates high concentration of MPs in sediments compared to water samples. For instance, (Scherer et al., 2020) found a significant concentration of MPs in the Elbe River silt in the Czech Republic, with an average concentration of 3,350,000 particles m^3 compared to 5.57 particles m^3 in water samples.

MPs of all forms have been studied in rivers all over the world, with fibres, pieces, films, foams, pellets, and micro-beads being the most common (Alam et al., 2019; Klein et al., 2015). Following that, several polymeric kinds such as PE, PS, PP, PVC and others were studied in river sediments and surface water samples (Kapp and Yeatman, 2018) (Van Emmerik et al., 2018)).

In South Africa, MP pollution of rivers has received less attention than pollution of marine environments. In the peer-reviewed literature, (Weideman et al., 2019) reported an average concentration of microfibres and MPs of 1.7 ± 5.1 L^{-1} of water from the Orange-Vaal River system. Dams from the same river system had a much lower concentration (0.23 ± 0.27 items$\cdot L^{-1}$)(Weideman et al., 2019). However, in Braamfontein Spruit, a higher concentration of 2080 particles per cubic meter was reported by (Dahms et al., 2020). These data illustrate differences in the concentration of MPs in different areas of the country. River sediment contamination with MPs has also been reported in South Africa. For instance, Nel et al., (Nel et al., 2018)**,** reported MP concentrations up to 160.1 ± 139.5 particles kg^{-1} of sediments from the Bloukrans River in the Eastern Cape Province. The study by Dahms et al., (Dahms et al., 2020) on the Braamfontein Spruit also reported similar concentration (166.8 particles kg^{-1} dw) in river sediments. These studies highlight the high concentration of MPs in river ecosystems within South Africa. This calls for further studies to understand the source of these MPs, their transport processes and fate.

2.2.1 Seasonality and distribution of MPs

Environmental conditions are key determinants of microbial plastic colonization (De Tender et al., 2015; Oberbeckmann et al., 2014). Abiotic factors, such as temperature, warmer waters and salinity, are known to influence diversity and biofilm growth on plastics (Xianchuan Chen et al., 2019; Li et al., 2021; Philippe et al., 2023). Additionally, seasonality is known to influence the microbial community structure and composition in surface water and plastisphere (Marsay et al., 2023; Pinnell and Turner, 2020; Zhang et al., 2022). Van et al., (Van Emmerik et al., 2018) identified seasonal variation in plastic movement in the riverine environment, which might contribute to monitoring and mitigation of plastic pollution. China's freshwater sediments contain more MPs during the dry season than during the wet season due to low fluidity. According to Zhu et al. (Zhu et al., 2018), average MPs were determined to be 4360 items kg^{1} during the dry season and 3160 items kg^{1} during the wet season. A comparable abundance was also discovered in China's Ganjiang River, with a considerable change in MP concentration during the wet (103 3247 items kg^{1}) and dry (193 688 items kg^{1}) seasons (Lu et al., 2019). In contrast, increased MP content has

been observed in several rivers during rainfall, for example, 5 items m^3 in the dry season to 153 items m^3 in the rainy season in Los Angeles River, USA (Moore et al., 2011).

CHAPTER 3: METHODOLOGY

3.1 Sampling site selection

Two main sites were chosen for this study, these are the Msunduzi river in KwaZulu Natal province and Swartkops River in the Eastern Cape Province. These two rivers pass through highly industrialized areas, receives runoff from agricultural sector, effluent from wastewater treatment plant, runoff from rural and urban communities which provides an understanding of the different pollution sources of MPs in the river. Four sampling sites in the Msunduzi River in KwaZulu-Natal and six sites on the Swartkops River in the Eastern Cape province were selected to purposely represent different pollution sources (Figure 3). Table 2 presents detailed description of these sampling sites. A map of sampling sites in the Msunduzi and Swartkops rivers is shown in Figure 4 and 5 respectively.

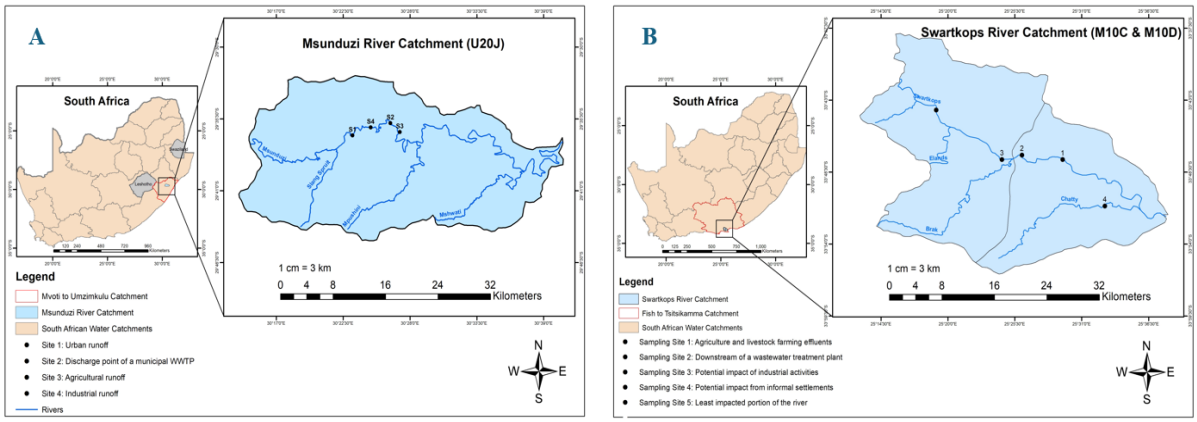

Figure 3 A: Study area: Msunduzi river; B: SwartsKop river

Table 2: Characteristics of sampling sites on the two rivers

SITE	GPS Coordinates	Potential activities impacting the river
	Msunduzi river	
#1	29°35'49.3"S 30°26'21.3"E	Downstream of a wastewater treatment plant
#2	29º36’29.3” 30º27’09.0”E	Potential runoff from agricultural sector and rural communities
#3	29°36'43.2"S 30°23'13.8"E	Runoff from Urban communities
#4	29°36'07.9"S 30°24'48.5"E	Potential impact of industrial waste
	Swartkops river	
#1	33º47’31.93” 25º29’26.99 E	Potential impact from agriculture and livestock farming effluents

#2	33°47’11.11” 25°26’48” E	Downstream of a wastewater treatment plant
#3	33°47’34.2” 25°24’27.0” E	Potential impact of industrial activities
#4	33°47’31.50” 25°24’27.25” E	Potential impact of industrial activities
#5	33°51’04.88” 25°32’54.98” E	Potential impact from informal settlements
#6	33°44’12.33” 25°19’08.91” E	Least impacted portion of the river

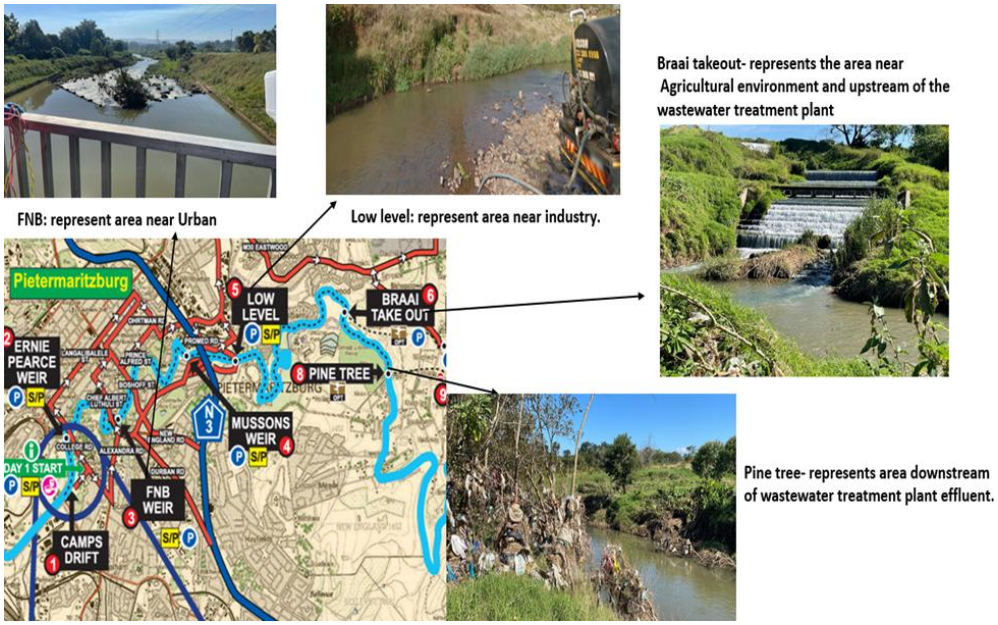

Figure 4: Map with an indication of Msunduzi River in KwaZulu-Natal and Four sampling locations (FNB (3), Low level (5), Braai takeout (6), and Pine tree (8).

Figure 5: Images from the sampling sites on the Swartkops River.

3.2 Sampling approach

Four sampling sites were selected according to the degree of anthropogenic impact, as shown in Figure 3. Site 1 was located in an area affected by runoff from urban communities, Site 2 was located downstream of the Municipal Darvill Wastewater Treatment Plant, Site 3 was in an area influenced by agriculture and anthropogenic discharges from rural communities and Site 4 was in an industrial area. The sampling took place during three sampling dates covering the summer and winter months from 2022 – 2023. A composite sampling methodology was employed to collect both water and sediment samples. Initially, 10 litres of surface water underwent filtration on-site through a 0.18 mm steel mesh sieve. The residues retained on the sieves, along with 200 ml of surface water, were transported to the laboratory for subsequent processing. The samples then underwent successive filtration through steel mesh sieves with pore sizes of 0.5mm, 0.18mm, 0.1mm, and 0.025mm to segregate MPs by size. Density separation was then conducted using sodium chloride, facilitating the flotation of lightweight particles, which were subsequently filtered through a 20µm mesh sieve and a glass fibre filter paper with a pore size of 1.22µm. At each site surface water and the sediment samples were collected in two sites. Physicochemical parameters (pH, electrical conductivity (EC), temperature, Dissolved oxygen (DO) were measured in situ. .

3.3 Isolation of MPs

Surface water and sediment samples were filtered using 0.5, 0.18, 0.1-, and 0.025-mm mesh size sieves (Hidalgo-Ruz et al., 2012). The filtered residues on the sieves were washed off into the

beaker with 50 mL distilled water (dH_2O) and allowed to dry in the oven at 90 ºC overnight. The step for removal of natural organic and inorganic components was done by adding 30% hydrogen peroxide (H_2O_2) to the dried samples (Huang et al., 2023; Nuelle et al., 2014). Furthermore, the mixture was heated and stirred at 75 ºC until dry. The lightweight particles were allowed to float by performing the density separation method using sodium chloride (NaCl) solution with a density of 1.2 g cm^{-3} (Hidalgo-Ruz et al., 2012). The residues were transferred into conical flasks and were left to settle overnight. Materials with a density above 1.2 g cm^{-3} settled to the bottom and the floating materials were carefully transferred into fresh conical flasks. All the light materials were filtered over a 20 µm mesh size sieve and rinsed with 50 mL dH_2O and then washed off into the clean beaker with 50 mL dH_2O. The materials were once more filtered utilizing a 1.22 µm pore size glass fiber filter paper using a vacuum system. Subsequently, the filter was placed in a clean petri dish and allowed to dry in the oven at 60ºC.

3.4 Characterization of MPs

3.4.1 Visual characterization

A light microscope with a magnification of 4x (Nikon, Y-TV55 microscope) equipped with a MoticamBTW camera was used for visual identification the MP particles on the filter paper. The images were taken with MoticamBTW connected to the microscope. The observed MPs were classified as four types (Figure 6) based on their shape: fiber, pellet, fragment, and film (Huang et al., 2023). Fiber is a long and thin line with a slender shape, and they come in different colors (transparent, red, blue, black etc.). The fragment was characterized as a piece of debris. The film appears in the shape of broken pieces or slices. The pellet was considered to be a dimensional sphere (Hidalgo-Ruz et al., 2012; Huang et al., 2023).

3.4.2 Polymer characterization

The chemical composition of each piece of plastic debris on the filter paper collected was identified using ATR-FTIR spectroscopy using Perkin Elmer, Spectrum two with ATR. Wavelength spectra were recorded in the mid-infrared range (4000-400 cm^{-1}) and at resolution 4 cm^{-1}. The plastic characterization was performed by looking at the absorption bands (AB) of samples with those in the published literature (Coates, 2000, Khan *et al.*, 2018, Nandiyanto *et al*., 2019) based on the infrared spectrum. The polymer characterization was done using the Pyro-GC/MS. Prior to Pyro-GC/MS, samples were viewed under the Stereo Olympus with Euromex fiber optic light source EK-1 light microscopy to identify the MPs. The samples were then pyrolyzed in a multi-shot pyrolyzer, EGA/PY-3030 D, (Frontier Lab, Japan) attached to an ultra-alloy capillary column (30

m x 0.25 mm, 0.25 μm). Approximately 100 to 150 μg of the sample were pyrolyzed at 550°C for 20 seconds and the interface temperature to the analytical column was set at 350°C. The chromatographic separation of the pyrolysis products was performed using an ultra-alloy capillary column (Frontier Lab, Japan) (30 m × 0.25 mm, 0.25 μm). The injection temperature was set to 280°C and the column flow rate was set to 1.0 mL/min with helium used as a carrier gas. The GC temperature program used was: (i) held at 50°C for 2 min; (ii) ramped from 50°C to 200°C at a rate of 3°C/min; (iii) then hold for a further 4 min. The ion source and interface temperatures in the mass spectrometer were set to 200°C and 300°C, respectively. The scan range used for the mass selective detector was from m/z 40-650. The pyrolysis products were identified by comparing their mass spectra with the mass spectra in a library database (NIST14 and WILEY10).

Table 3: Range in wavenumber (cm^{-1}) with the regions

Range of wavenumber (cm^{-1})	**Regions**
2500-4000 cm^{-1}	Single bond region (e.g., O-H, N-H, and C-H)
2000-2500 cm^{-1}	Triple bong region (e.g., C≡C, and C≡N)
1500-2000 cm^{-1}	Double bond region (e.g., C=C, and C=O)
600-1500 cm^{-1}	The fingerprint region.
	The region from 1000 to 1500 cm-1 some classify it for C- and C-C and other bending vibrations. While region 400-7(cm-1 classify it as fingerprint region.

3.5. Microbial community structure and function in surface water and plastisphere

3.5.1. Sample collection and processing

A composite sampling method was used for sample collection. 10 L of surface water was filtered through a 0.18 mm mesh sieve size on-site, the residues on the sieves were transport along with 200 ml of surface water to the laboratory for further processing.

3.5.2 MPs isolation and DNA extraction

The filtered residues from the mesh sieves were washed off with phosphate buffer saline (PBS) solution (pH 7.4) into a glass beaker. The PBS with residues was filtered through 1.2 μm pore-size glass fiber-filtered papers using a vacuum system. Each filter paper was divided into four quadrates, to easily count the number of MPs on filter paper under the light microscope with a magnification of 4x (Nikon, Y-TV55 microscope). The filter papers were cut into smaller pieces

to transfer into beat beads from the Power Soil DNA extraction kit. The beat beads were placed on rotor bead for 10 min at medium speed to rupture all the cells attached to MP surfaces. Thereafter, DNA was extracted from MP surfaces following the manufacturer's manual. Quantification and purity testing of DNA was done using the Nano spectrophotometer (Implen, USA). DNA samples with ratio of absorbance of 1.8 -2.0 at 260 and 280 nm were accepted as pure and stored, to be used for sequencing.

3.5.3 Metagenomic sequencing and analysis

DNA fragmentation of the extracted DNA was performed by Covaris M220 and the obtained fragments (400bp) size were used to construct a paired-end library using NEXTFLEX Rapid DNA-Seq as per manufacturer's guidelines. An Illumina NovaSeq 6000 (Illumina Inc., San Diego, CA, USA), was selected to sequence the paired-end library *via* with NovaSeq Reagent Kits. For the obtained raw metagenomic data, we used Trim Galore (Xiaoli Chen et al., 2019) to trim the adapter sequences ($l < 50$ bp and N bases) and to remove low quality ($q < 20$) reads. SqueezeMeta was used to perform the taxonomic analysis, functional identification and quantification (Tamames and Puente-Sánchez, 2019). We then used MEGAHIT (Li et al., 2015), to assemble the sequences and selected the contigs ($l \geq 300$ bp) for further taxonomic, functional annotation and gene prediction. MetaGene (Noguchi et al., 2006), was employed to perform ORFs (Open reading frames) prediction of the assembled contigs and genes with length ($l \geq 100$bp) were retrieved and translate into amino acid sequences. We used CD-HIT (Fu et al., 2012) and SOAP aligner (Li et al., 2008) to construct a non-redundant gene catalogues and to calculate gene abundance based on 90 % and 95% similarity threshold, respectively, and the gene abundance was indicated using Reads Per Kilobase Million (RPKM). Finally, the taxonomic and functional gene annotations were obtained by aligning the representative sequences to NCBI, NR and KEGG databases (e-value: $1e^{-5}$), using diamond (Buchfink et al., 2015).

3.6 The modelling approach

The modelling approach was set up for the Msunduzi River quaternary catchment (678 km^2) in Pietermaritzburg, South Africa. The catchment starts at the Henley Dam, passes through Pietermaritzburg Town where it is joined by small tributaries, picks up treated effluent from one of the municipal wastewater treatment works, Darvill, situated along the sites and ends at the confluence of the Msunduzi and Umgeni Rivers. The catchment is divided by the significant variations in settlement types, with the upper and lower catchment being rural, and the middle being urban. The rural areas are dominated by subsistence farming and rural developments and the

urban area, Pietermaritzburg, is a mix of urban, industrial and informal settlements (Ngubane *et al.* 2022). The topology of the catchment is mountainous having various hills, valleys, wetlands, marshes and flat areas (Shozi 2015). The area has an average precipitation of 832 mm and a subtropical climate, with hot and wet summers and warm and dry winters. Figure 1 presents the study area.

3.6.1 Secondary data collection and processing

This subsection describes the data sources, formats and processing techniques used for the setup and calibration of the transport model simulation. The data sources used were the National Aeronautics and Space Administration (NASA) Giovanni database, Water Resources of South Africa, 2012 Study (WR2012), Department of Water and Sanitation and uMngeni-uThukela Water. The collected, generated, and digitized data on the Msunduzi Catchment (U20J) were stored and analysed on ArcGIS 10.8.2 using the World Geodetic System (WGS) 1984 Universal Transverse Mercator Zone 36 coordinate system. Remote sensing images together with existing catchment data, sourced WR2012, were used to spatially delineate the catchment and produce input data for the MP transport model.

Table 4: Summary of secondary data

Data type	Figure	Source	Description	Importance	Resolution	Catchment data ranges/classes
Slope Data	Figure 2 (a), (b), and (c) illustrates the contour, hillshade, and slope map	USGS/NASA Shut Radar Topograph Mission (SRTM)	Digital elevation model (DEM) used to generate layers depictir contours, slope, and hillshade.	Slope data influences runoff characteristics, with steeper slopes accelerating surface runoff and soil erosion, whil gentler slopes enhance infiltration rates.	90 meters	Slope: 0 – 92.8 degree Contours: 300 - 1400 mm amsl
Rainfall		Tropical Rainfalll Measurement Mission (TRMM) / NASA Giovanni	TMPA rainfall estimate produ combining satellite rainfall estimates with gauge data int gridded estimates on a calend month temporal resolution.	Rainfall data is crucial for understanding the water in into the catchment, which affects river flow, runoff, a the transport of MPs.	0.25 by 0.2 spatial resolution	0.168 – 0.478 mm/hr
Landcover	Figure 2 (d).	USGS Earth Explorer / NASA MODIS MCD12Q1 V6 product	Global land cover data at 500m spatial resolution annually, usir supervised classifications of MODIS Terra and Aqua reflectance data.	Land cover data helps in understanding the distributio of different land types, whicl affects runoff, infiltration, ar MP transport.	500 meters	• Evergreen needleleaf forest • Deciduous needleleaf forest • Deciduous broadleaf forest • Mixed forest • Open shrublands • Woody savannas

	Figure 2 (e)					• Savannas • Grasslands • Croplands • Urban and built-up land • Natural vegetation • Coastal tropical fores types • False grassveld types • Karoo and karroid types • Temperate and transitional forest and scrub types
Vegetation Data		WR2012 database	GIS shapefiles containing information on vegetation cove type.	Vegetation data provides insights into the types of vegetation present, which influences soil stability, infiltration, and the ecologic aspects of the catchment.	Various (GI shapefiles)	
	Figure 2(f)					• Msunduzi River • Slang Spruit River • Mpushini River • Mshwati River
Stream Data		Extracted from DEM using ArcGIS	Visual representation of the catchment streams as polylines located in low-lying areas whe water accumulates.	Stream data is essential for mapping the flow paths of water within the catchment, aiding in understanding how water and MPs are transported.	Derived fro DEM	

River Flow	Department of Water and Sanitation / uMngeni-uThukela Water	River flow data from four flow stations, including daily averag data spanning a decade (2012-2024).	River flow data is critical for modelling water movement, determining flow rates, and understanding the transport and distribution of MPs.	Daily averag data spannir a decade	• Henely dam flow station • Masons Mill flow station • Hamstead Park flow station • Inanda Loc flow station
Canopy Cov	NASA Giovanni	Data from the GLDAS Catchment Land Surface Mode L4, with a spatial resolution of 0.25 x 0.25 degrees.	Canopy cover data helps in understanding the extent of vegetation cover, which affects evapotranspiration rates, shading, and the microclimate within the catchment.	0.25 x 0.25 degrees	0.023 – 0.233 $Kg/m^2/day$
Evapotransp ation	NASA Giovanni	Dataset from the GLDAS Noal Land Surface Model L4 month 0.25 x 0.25-degree V2.1.	Evapotranspiration data is important for understanding water loss from the catchmei due to evaporation and plant transpiration, influencing water availability and MP transport.	0.25 x 0.25 degrees	1.559e-05 – 3.747ek05 $kg/m^2/s$
Soil Infiltration	NASA Giovanni	Dataset from the MERRA-2 tavgM_2d_lnd_Nx: 2d, Monthl mean, Time-Averaged, Single-Level, Assimilation, Land Surface Diagnostics V5.12.4.	Soil infiltration data helps in understanding the rate at which water enters the soil, affecting runoff, groundwate recharge, and the potential transport of MPs.	Monthly mean data	1.363e-05 – 4.526e-05 mm/
Soil Moistur	NASA Giovanni	Dataset from the GLDAS_CLSM025_DA1_D.	Soil moisture data is crucial for understanding the water	Various	4.31 – 8.35 mm/d

			content in the soil, which influences plant growth, infiltration rates, and the movement of water and MPs through the soil.		
Surface Runoff	NASA Giovanni	Dataset from the GLDAS_NOAH025_M.	Surface runoff data is important for modelling the flow of water over the land surface, which affects erosio nutrient transport, and the distribution and movement o MPs in the catchment.	Various	4.173e-07 – 8.475e-06 mm/
Surface Temp **Sk**	NASA Giovanni	Dataset from the M2TMNXLND.	Surface skin temperature dat helps in understanding the thermal properties of the lan surface, which influences evaporation rates, plant growth, and the microclimat within the catchment.	Various	15.85 – 22.85 º

3.6.2 Slope Data

The topographical slope of an area plays a crucial role in determining runoff characteristics. Steeper slopes accelerate surface runoff and soil erosion rates, impeding the process of infiltration. Conversely, gentler slopes extend the residence time of runoff, thereby enhancing infiltration rates (Moodley 2022).

Digital elevation models (DEMs) play a crucial role in hydrology and engineering by enabling the calculation of various parameters such as slope steepness, hill shade, contours, and catchment drainage (Moodley 2022). In this study, the DEM utilized originates from the United States Geological Survey (USGS)/NASA Shuttle Radar Topography Mission (SRTM), having a resolution of 90 meters. The DEM served as the foundation for generating layers depicting contours, slope, and hill shade. The hill shade layer presents a grayscale 3-dimensional depiction of the surface, considering the relative position of the sun for shading. Slope steepness at each cell was determined using the planar method, measuring the maximum rate of change in value from a cell to its immediate neighbor. Additionally, the contour layer was integrated to provide precise height values during map analysis. Figure 6 illustrates the contour, hill shade, and slope maps for the Msunduzi River Catchment.

3.6.3 Stream data

Stream data was extracted from the DEM using ArcGIS. Firstly, the DEM was clipped for the Msunduzi Catchment, and then the Hydrology tools in the ArcGIS Toolbox were used to calculate flow direction, flow accumulation, stream order and stream to feature. These tools visually represent the catchment streams as polylines located in low-lying areas where water accumulates. Figure 6 illustrates the streams within the Msunduzi River Catchment.

3.6.3 Rainfall

Rainfall data used in the study was obtained from the Tropical Rainfall Measurement Mission (TRMM) observatory and its partner satellites. This mission is a joint effort between NASA and the Japanese Aerospace Exploration Agency. The TRMM Multi-Satellite Precipitation Analysis (TMPA) rainfall estimate product, 3B43 version 7 used in the study combines satellite rainfall estimates with gauge data into gridded estimates on a calendar month temporal resolution and a 0.25 by 0.25 spatial resolution from 50◦ S to 50◦N latitude.

The Dataset was sourced from the NASA Giovanni, which is a web-based data centre developed by NASA Goddard Earth Science (GES) Data and Information Services Centre (DISC).

3.6.4 Land cover

Remote Sensing land cover data was freely downloaded from the USGS Earth Explorer website. The downloaded data was from the NASA MODIS MCD12Q1 V6 product, which is the Terra and Aqua combined Moderate Resolution Imaging Spectroradiometer (MODIS) Land Cover Type (MCD12Q1) Version 6 data product. The product provides data sets that map global land cover at 500m spatial resolution annually. The data is derived using supervised classifications of MODIS Terra and Aqua reflectance data and then undergoes additional processing that incorporates prior knowledge and ancillary information to refine specific classes. Each year five land cover classification schemes are developed by different research organizations. The five research organizations developed their land cover classification schemes using one year of Terra and Aqua MODIS data. The International Geosphere-Biosphere Programme type 1 land cover scheme was used to classify land use/land cover data for the Msunduzi Catchment and is shown in Table 5.

Table 5: Landcover categories (Adapted from Friedl et al. 2010)

Class	IGBP (Type 1)	UMD (Type 2)	LAI/fPAR (Type 3)
1	Evergreen needle leaf forest	Evergreen needle leaf forest	Evergreen needle leaf forest
2	Deciduous needle leaf forest	Deciduous needle leaf forest	Deciduous needle leaf forest
3	Evergreen broadleaf forest	Evergreen broadleaf fores	Evergreen broadleaf fores
4	Deciduous broadleaf forest	Deciduous broadleaf fore	Deciduous broadleaf fore
5	Mixed forest	Mixed forest	
6	Closed shrublands	Closed shrublands	Shrublands
7	Open shrublands	Open shrublands	Shrublands
8	Woody savannas	Woody savannas	Savannas
9	Savannas	Savannas	Savannas
10	Grasslands	Grasslands	Grass/cereal crops
11	Permanent wetlands		-
12	Croplands	Croplands	Broadleaf crops
13	Urban and built-up	Urban and built-up	Urban
14	Cropland/natural vegetation mosaic	-	-
15	Snow and ice	-	-
16	Barren or sparsely vegetated	Barren or sparsely vegetated	Unvegetated
17	Water	Water	Water

The data set were imported into ArcGIS using the type 1 classification. Data for the Msunduzi River Catchment was extracted and converted to a feature class polygon. The data were then

classified using the grid codes, representing the land cover classification codes shown in Table 1. The land cover of the Msunduzi River Catchment by the type 1 grid code classification scheme is represented in Figure 6e**.**

Vegetation data were used in conjunction with the land cover data for an in-depth analysis. Vegetation data were taken from the WR2012 database in the form of GIS shapefiles which contain information on vegetation cover type as shown in Figure 6d**.** The WR2012 is a study that began in 2012, intending to build on the previous WR2005 study, which is consolidated on a web-based platform. The website defines the water resources of South Africa, Lesotho and Swaziland, and consolidates results from several water resource studies that have been conducted over the past four decades.

3.6.5 River flow

Msunduzi River flow data from four flow stations, the Hamstead, Henely, Inanda and Masons Mill were sourced from the South African Department of Water and Sanitation website. The site provides flow station monthly and daily volume data. Daily average data spanning a decade (2012-2024) was used in the study as model inputs. The Darvill Wastewater Treatment Plant outflow data, sourced from uMngeni-uThukela Water, was also used as model input flow data.

3.6.6 Canopy cover

Canopy cover data was obtained from the NASA Giovanni database. This dataset originates from the GLDAS Catchment Land Surface Model L4, with a spatial resolution of 0.25 x 0.25 degrees, known as GRACE-DA1 V2.2 (GLDAS_CLSM025_DA1_D). GLDAS-2.2 is a recent addition to the GES DISC archive, featuring the primary product from CLSM-F2.5 with Data Assimilation for the Gravity Recovery and Climate Experiment (GRACE-DA) spanning from February 2003 to the present.

3.6.7 Evapotranspiration

Evapotranspiration data was sourced from the NASA Giovani database and is a dataset of the GLDAS Noah Land Surface Model L4 monthly 0.25 x 0.25-degree V2.1 (GLDAS_NOAH025_M). The GLDAS-2.1 is forced with a combination of model and observation data from 2000 to the present.

3.6.8 Soil infiltration

Soil water infiltration rate data was sourced from the NASA Giovani database and is a dataset of the MERRA-2 tavgM_2d_lnd_Nx: 2d, Monthly mean, Time-Averaged, Single-Level,

Assimilation, Land Surface Diagnostics V5.12.4 (M2TMNXLND). M2TMNXLND is a time-averaged 2-dimensional monthly mean data collection in Modern-Era Retrospective analysis for Research and Applications version 2 (MERRA-2).

3.6.9 Soil moisture

Soil moisture data was sourced from the NASA Giovani database and is a dataset of the GLDAS_CLSM025_DA1_D.

3.6. 10 Surface runoff

Surface runoff data was sourced from the NASA Giovani database and is a dataset of the GLDAS_NOAH025_M.

3.6.11 Surface skin temperature

Surface skin temperature data was sourced from the NASA Giovani database and is a dataset of the M2TMNXLND.

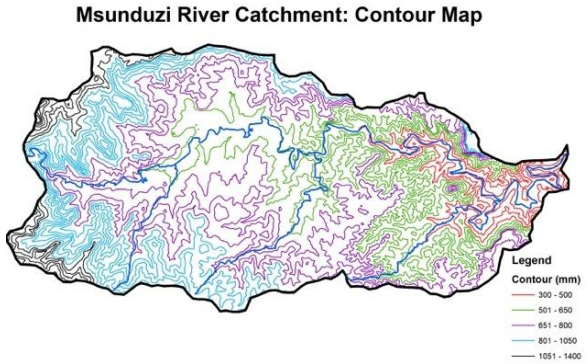

(a)

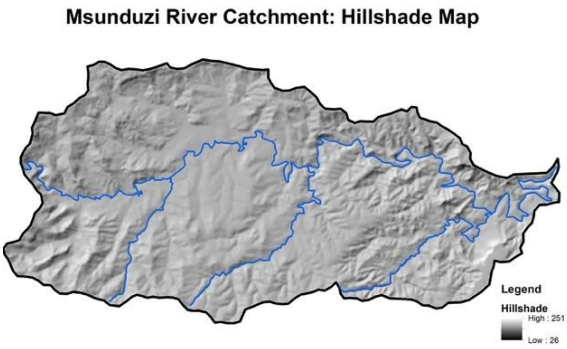

(b)

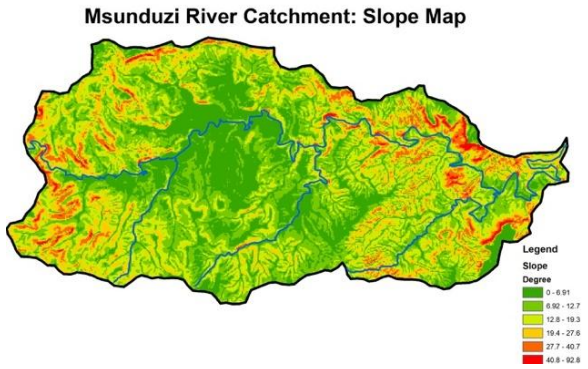

(c)

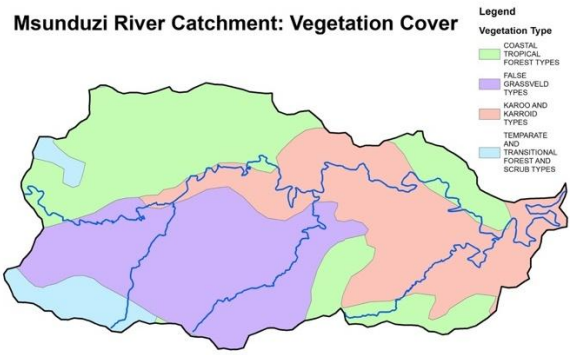

(d)

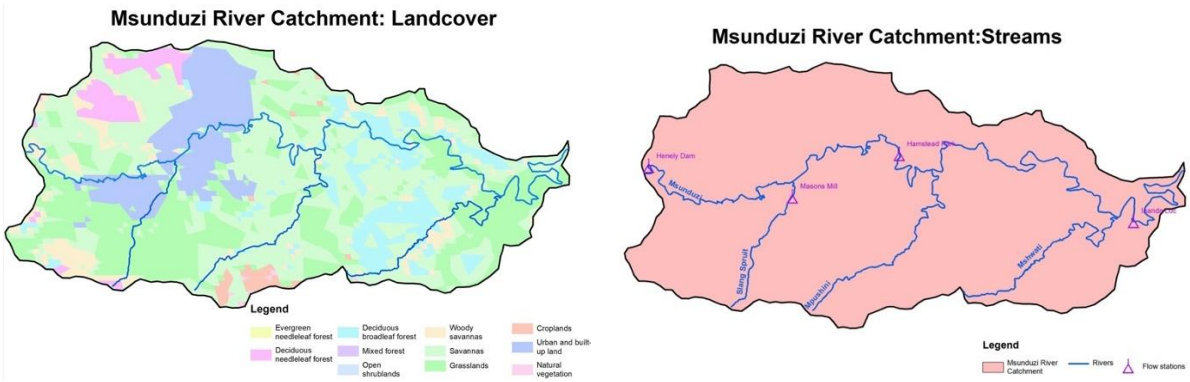

(e) (f)

Figure 6: Msunduzi River Catchment contours (a), hillshade (b), slope (c), vegetation cover (d), landcover (e) and stream maps (f)

3.7 Model description and development

Integrated Catchment model of MPs transport (INCA-MP) is a semi-distributed daily-timestep model which forms part of the INCA family of models (Nizzetto et al. 2022). The model consists of the hydrological module, PERSiST (Precipitation, Evapotranspiration and Runoff Simulator for Solute Transport), and a MPs module which together simulate the on-land and in-stream mobilization and transport of MPs. PERSiST is a semi-distributed bucket hydrology model which allows for a user-specific runoff generation process (Futter *et al.* 2014). The in-stream model uses the Rosenbrock4 solver from boost: odeint to solve its ordinary differential equations (ODE) and the other ODEs are solved with the Runge-Kutta 4 DASCRU solver (Nizzetto et al. 2022). The MPs module uses direct runoff fluxes and predicted streamflow regimes to simulate the deposition and entrainments of MPs within a catchment. Additionally, arbitrary inputs can be included at multiple locations within a catchment. The model is built in the Mobius modelling framework and the simulation is done on the graphical user interface, MobiView. The modelling framework was developed and coded by Magnus Norling and is available at https://github.com/NIVANorge/Mobius/blob/master/Modules/INCA/INCA-Microplastics.h.

The model has two main parts, the land-phase delivery model which simulates MPs generation and transport processes on land; and the in-stream component which simulates the transport processes and storage within the river. The model assimilates the catchment area, river network structure, elevation, and land use together with weather data to define a semi-distributed MP transport model. The conceptual model that governs the INCA MP transport model, which is based on the INCA-Sed model described by Lazar et al. (2010), as presented in Figure 7.

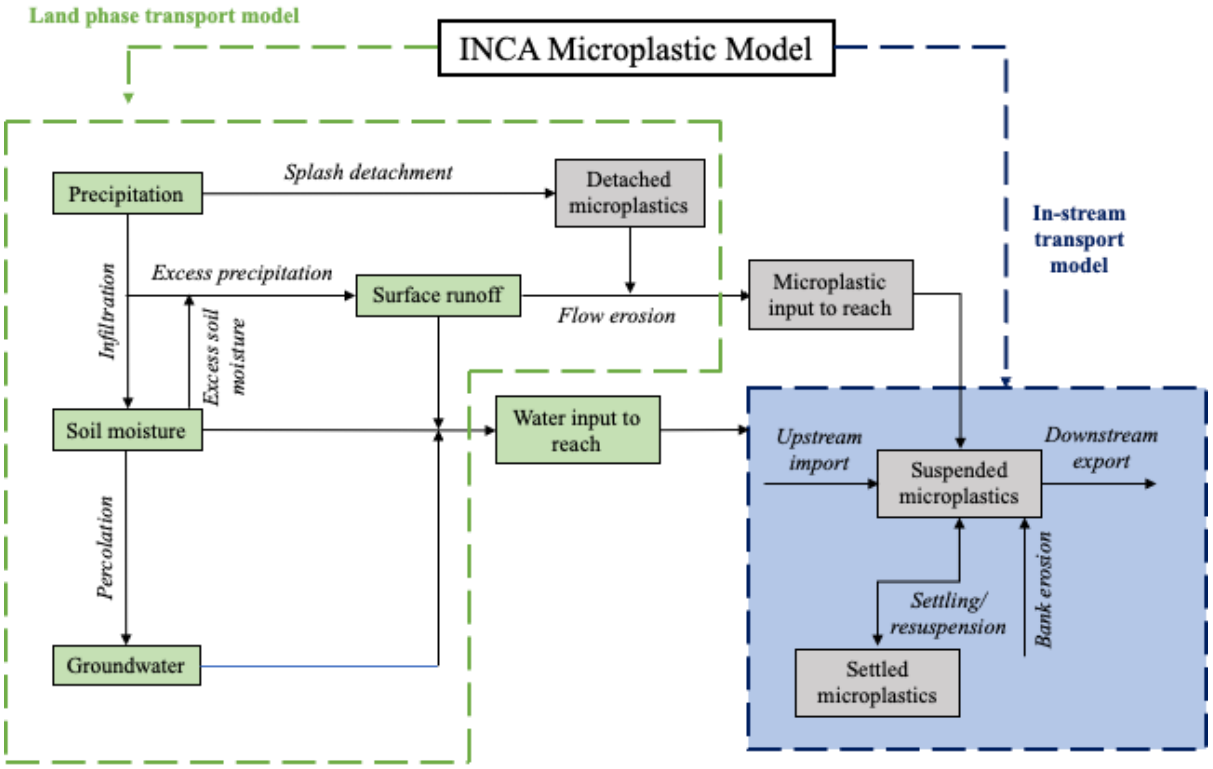

Figure 7: INCA MP conceptual model (Lazar *et al.* 2010)

3.8 Model setup and calibration

The modelling simulation followed a pragmatic approach using a quantitative method of data collection, analysis, and simulation. Geographic Information Systems (GIS) and remote sensing techniques were used with the INCA-Microplastics modelling framework to examine inputs, loads and concentrations, highlighting the dominant transport processes and the pathways of MPs in the Msunduzi River Catchment. The general methodology for MP transport modelling, as depicted in Figure 8, begins with the collection of model input data from two sources (secondary): remote sensing data and conventional data. Once collected, the input data undergoes several processing and integration steps. Initially, data processing is performed to clean, format, and prepare the raw data for analysis. Following this, model scenario configuration is conducted to establish different simulation scenarios. Subsequently, hydrology calibration is carried out to ensure the model accurately represents the hydrological processes within the catchment area, involving the adjustment of model parameters to match observed data. The next phase involves configuring on-land transport, modeling the movement of MPs across the land surface, and in-stream dynamics, simulating MP transport within the stream network. The simulation phase is then conducted, where the configured model is executed to generate MP transport time-series data. The model results is

then validated using the Nash-Sutcliffe model efficiency coefficient (NSE) and the coefficient of determination (R2) by measuring the goodness of fit when compared with the observed data. The NSE values range from negative infinity to 1 and R2 is a number between 0 and 1.

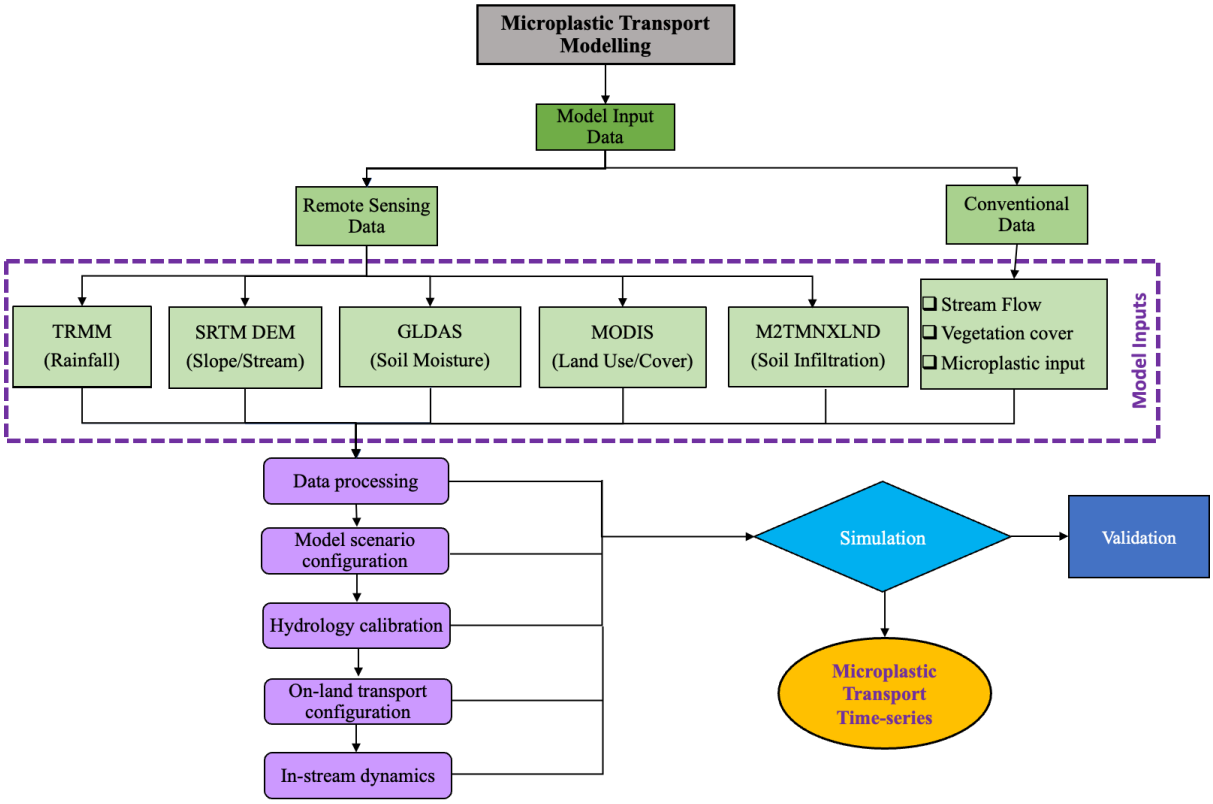

Figure 8: Flow chart of the methodology used for the MP transport modelling

3.9 Model boundary

The catchment is divided into subcatchments, with each subcatchment being divided into landscape units, soils and MP class, which are defined by the percentage of surface area coverage, soil characteristics, climate parameters and MP inputs. The landscape units were categorised, based on figure 6e, being natural, agricultural and built-up per sub catchment as indicated in Table 6. Fluxes from land to the river are computed once per landscape unit and aggregated over each sub-catchment. In-stream processes are computed per river section within a sub-catchment. Figure 9 illustrates the three Msunduzi River subcatchment boundaries, within which the simulations were conducted, and presents the subcatchment characteristics. The sub catchments were created based on the landcover types, MP sampling locations and catchment drainage patterns.

Table 6: Sub catchment characteristics

Subcatchment no.	Subcatchment area (km^2)	Sampling point	Characteristic	Coordinates	River flow station	River name	Landscape units
Msunduzi Subcatchment 1	201.66	Site 1	Runoff from Urban communities	30.387861, -29.612466	Henely Dai	Msunduzi, Slang Sprui	Natural:86% Agricultural: 0% Built-up: 14%
Msunduzi Subcatchment 2	93.33	Site 4	Industrial waste	30.413472, -29.602194	Masons Mi	Msunduzi	Natural:88% Agricultural: 6% Built-up: 6%
Msunduzi Subcatchment 3	377.90	Site 2	Downstream of the wastewater treatment plant	30.439972, -29.596762	Hamstead Park	Msunduzi	Natural:89% Agricultural: 10% Built-up: 1%
Msunduzi Subcatchment 3	377.90	Site 3	Runoff of agricultural secto & rural communities	30.452500, -29.608139	Inanda Loc	Msunduzi, Mpushini, Mshwati	

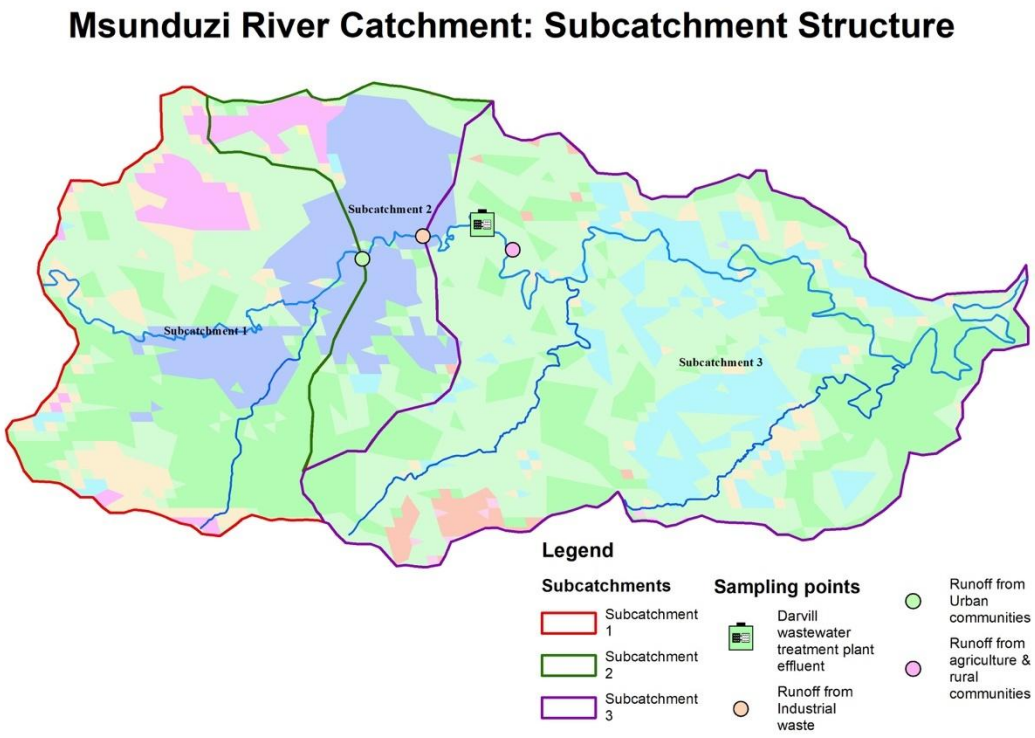

Figure 9: Msunduzi River sub-catchment boundaries

3.10 Model scenario

The model was run using various time series data, such as rainfall, hydrological effective rainfall, soil moisture deficit and air temperature. Due to the lack of an MP emission and concentration

database for the catchment, the model scenario in terms of MP input was defined by generic sources encompassing atmospheric and anthropogenic deposition and fragmentation of macro-plastics from rural, urban and industrial areas, wastewater effluent and sludge application to agricultural land. MPs from direct source points per sub-catchment were continuously emitted using an arbitrary steady flow of 300 tonnes per year of each selected size class, which is estimated based on the amount of sampled MPs found at the four sampling location, and estimates reported by (Bratovcic, Nithin and Sundaramanickam 2022; Kataoka *et al.* 2023; Saad *et al.* 2024; Samuels, Awe and Sparks 2024). MP input from the application of sewage sludge from the Municipal Darvill Wastewater Treatment Works to agricultural soils was set as 3000 kg/km^2 during 2 days per year of simulation for a total application of 6 000 kg/km^2 per year, based on estimates from (Weber, Santowski and Chifflard 2022; Radford *et al.* 2023) and using scientific judgement and estimation considering agricultural activities in the area focusing on timber, beef, dairy, sugarcane, citrus, exotic fruits and cut flowers. MP input of 1000 tonnes per year of MPs emitted continuously from a source point in catchment 3, representing emissions from the Municipal Darvill Wastewater Treatment Works. Given the absence of current measurements of MPs in the treatment plant effluent, the model's estimates are based on the study by Enespa and Chandra (2024), which indicated that effluent from tertiary treatment plants can contain between 0 and 51 particles per litre. Considering that Darvill Wastewater Treatment Works is a tertiary treatment plant with an average effluent discharge of 72 million litres per day, the upper end of the MP particle range (0 and 51 particles per litre) was used for the model.

The model was simulated for the period 1 January 2013 to 1 January 2024, which incorporated a burn-in period allowing the model to reach a state of equilibrium, reducing the influence of initial conditions of the simulation results, and to cater for the lack of/poor data for certain years. A spatial average of precipitation and temperature was computed over the catchment for the setup of the model input file. Hydrologically effective rainfall and soil moisture deficit were computed using PERSiST. No continuous monitoring of MP emissions takes place at the Msunduzi River Catchment, and therefore no direct calibration of the MP transport module could be performed.

3.11 Model limitations and assumptions

The model limitations and assumptions associated with the model scenario are as follows:

I. The model scenario details the input of MPs in the catchment as a generic source, due to a lack of an MP database within the catchment, representing the contribution of atmospheric

deposition, fragmentation of litter, application of sewage sludge for agricultural purposes, wastewater treatment effluent and any other sources of fragments and fibres. Due to there being no direct observations of atmospheric deposition in the catchment and the limited global representation of atmospheric MPs due to the limited studies and lack of comparability (Allen *et al.* 2022), a homogenous distribution was assumed as a broad range of 0-1000 particle/m^2/day (Wright *et al.* 2020; Hee *et al.* 2023).

II. The model scenario does not consider tyre wear particles and is therefore excluded from the calibration and validation. Given that the study did not address the mass budget of all MPs within the catchment, the omission of tyre wear sources did not invalidate the results and conclusion of the study.

III. The simulation was conducted to predict masses of MPs of three classes, being fibres, fragments and pellets, as per the sampled datasets used for calibration. Fragments were categorised by not having the elongated shape of fibres, and pellets were round, manufactured particles. All particles were separated further into size and density. Fragmentation processes, aggregation and particle ageing affecting particle density and size were not considered in the simulation, given the lack of knowledge on the rate of these processes.

IV. In the first approximation simulation, parameters relating to on-land sources, mobilisation and transport were constant across all landscape units due to the lack of information on the spatial distribution of source intensity.

V. An initial burn-in period was taken as the first 6 years of modelled data.

VI. The observed flow for reach 2, sourced from the flow station, was missing a portion of data, and therefore the flow calibration was done for 3 years compared to 5 years.

VII. Given the lack of empirical data on MP concentration in soils within the catchment, it was assumed an initial pool of 100 t of MPs (fragments, fibres and pellets) in the topsoil layer at the beginning of the simulation , which is based on estimates reported by Islam, Islam and Islam (2024) and using scientific judgement, considering the landcover attributes of the Msunduzi catchment.

VIII. The densities of MPs were assumed to be 1000, 1050, 1150 and 1250 kg/$m^{3,}$ respectively. The densities were chosen based on the density range of the most common MPs, being polyethylene, polypropylene, polystyrene, polyamide, polyester and acrylic (Bråte *et al.* 2014; Li *et al.* 2018)

3.12 Parameter calibration and model assessment

In-stream hydrology

The first step in calibrating the model for MP transport prediction was to set up the catchment hydrology as described by (Norling *et al.* 2024). The reach profiles, velocity, flow, and shear stress of the reaches were calculated using the formulas and input values, governing the in-stream hydrology, described below.

The reach profiles were considered trapezoidal configurations having a bottom width (Wb) and a bank slop (Sb). The top width (Wt), cross-sectional area (A) and depth of the river were calculated using:

$$w_t = w_b + 2\frac{d}{s_b}$$

$$\frac{V}{L} = A = \frac{d}{2}(w_t + w_b)$$

$$d = \frac{1}{2}(\sqrt{(w_b s_b)^2 + 4As_b} - w_b s_b)$$

The velocity of the reaches was computed using the wetted perimeter (p), hydraulic radius (R), Manning's roughness coefficient and the slope of the reach (Sr).

$$v = \frac{1}{n}R^{\frac{2}{3}}s_r$$

$$\text{Where: } wt = w_b + 2d\sqrt{1 + \frac{1}{{s_b}^2}}$$

$$R = \frac{A}{p}$$

Flow (Q) was calculated using:

$$Q = Av = Vv/L$$

The shear stress of the reach acting on the sediment bottom was calculated using:

$$\tau = a_{shear} s_r R \rho_f g$$

Where the density of water is 1000 kg/m^3, the Earth's gravitational acceleration is 9.81m/s^2 and the a_{shear} was a default value of 1 representing the turbulence or uneven geometry.

Table 7 presents the model input values that govern the in-stream hydrology.

Table 7: Model values associated with the in-stream hydrology

Symbol	Unit	Name
$\boldsymbol{L}$	m	Reach length
$\boldsymbol{A_c}$	km^2	Terrestrial catchment area
$\boldsymbol{w_b}$	m	Reach bottom width
$\boldsymbol{s_b}$	$-$	Reach bank slope
$\boldsymbol{s_r}$	$-$	Reach slope
$\boldsymbol{n}$	$s/m^{1/3}$	Manning's roughness coefficient
$-$	$-$	Reach rain multiplier
$\boldsymbol{Q_e}$	m^3/s	Effluent flow
$\boldsymbol{Q_a}$	m^3/s	Abstraction flow
$\boldsymbol{Q}$	m^3/s	Initial stream flow
$\boldsymbol{a_{shear}}$	1	Shear stress coefficient
$\boldsymbol{A}$	m^2	Reach cross-section area
$\boldsymbol{d}$	m	Reach depth
$\boldsymbol{w_t}$	m	Reach top width
$\boldsymbol{p}$	m	Reach wetted perimeter
$\boldsymbol{R}$	m	Reach hydraulic radius
$\boldsymbol{v}$	m/s	Reach velocity
$\boldsymbol{\tau}$	N/m^2	Reach shear stress
$\boldsymbol{Q}$	m^3/s	Reach flow
$\boldsymbol{Q_{us}}$	m^3/s	Reach flow from upstream
$\boldsymbol{Q_l}$	m^3/s	Total diffuse flow input from lan
$-$	mm/C°day	Degree day evapotranspiration
$-$	C°	Growing degree threshold
$-$	mm/day	Canopy interception
$-$	mm/C°day	Degree day melt factor
$\boldsymbol{V}$	m^3	Reach volume
$-$	mm	Initial water depth
$-$	$-$	Relative area index
$-$	mm/day	Infiltration
$-$	mm/day	Retained water depth
$-$	$-$	Drought runoff fraction
$-$	days	Time constant
$-$	$-$	Evapotranspiration
$-$	$-$	Relative evapotranspiration inde
$-$	mm	Maximum capacity (in bucket)

For the application of the hydrological PERSiST model, three hydrological response units, where water is routed into the stream as described in Figure 3, were used to represent natural and agricultural vegetation and urban land use. Areas of different hydrologic response types were derived from the catchment landcover data with natural vegetation representing the forest types,

savannas, grasslands and shrublands; agricultural being croplands; and urban representing urban and built-up land.

The model was driven by temperature and precipitation time series and each hydrological response unit was modelled as three vertically stacked buckets representing surface runoff, soil moisture and groundwater. The model was calibrated assuming all precipitation entering the surface runoff bucket percolates into the soil moisture bucket. Water can leave the soil moisture bucket via surface runoff, percolation to the groundwater bucket or directly into the reaches due to the soil reaching moisture capacity. It was assumed that all water entering the groundwater bucket flowed into the stream.

The model was calibrated against stream flow data from three flow stations within the catchment, presented in Table 7. The model was first manually calibrated by adjusting the rain multiplier to improve the correlation between the simulated and observed stream flows. The model performance was assessed using untransformed and log-transformed data for each flow station resulting in six goodness-of-fit statistical tests which was used to evaluate the parameter set. The manual calibration was attempted to obtain the best fit for reach 1 (subcatchment 1) first and then subsequent reaches by maximizing the sum of the NSE and logNS statistics. The calibration was then used as a starting point for a simple Monte Carlo (MC) analysis in which 21 parameters were allowed to vary, shown in Table 8. At each run the MC algorithm used a set of parameters randomly sampled from a-priori distribution resulting in a posterior distribution encompassing an estimation of the most likely parameters. Five parameters being the growing degree threshold, evapotranspiration adjustment and time constant for direct runoff, soil water and groundwater, were allowed to vary for each hydrologic response type. The reach rain multiplier and initial stream flow were allowed to vary for each of the three subcatchments. The MC tool was run 100 times, with each chain consisting of 4000 runs to generate an ensemble of parameter sets.

Table 8: Parameter ranges used in the MCMC

Location	Parameter	Min	Max	n	Units
Hydrologic response typ	Growing degree threshold	-4	4	3	˚C
Hydrologic response typ	Evapotranspiration adjustmen	0	10	3	Days
Hydrologic response typ	Time constant: Direct runoff	1	30	3	Days
Hydrologic response typ	Time constant: Soil water	1	10	3	Days
Hydrologic response typ	Time constant: Groundwater	1	500	3	Days
Subcatchment	Reach rain multiplier	0.5	2	3	

Reach	Stream flow	0.0001	10	3	m^3/s

3.13 On-land transport of MPs

The MP particle classes used in the study were categorised into four size class ranges, being 0.025, 0.18, 0.5 and 1 mm; and having a density of 1000, 1050, 1150 and 1250 kg/m^3 respectively. The transport of on-land MPs is computed per sub-catchment by aggregating the values per land-use class and reach. For each particle class the on-land store of MPs is divided into an immobile ($m_{immob,i}$) and a surface ($m_{surf,i}$) store. Due to the lack of a MP river database, the influx on new MPs to the surface store was assumed as 100 t across all landscape unis and MP shapes and the immobile store increases due to the infiltration ($a_{inf,i}$) from the surface store. Particles can also be transferred from the immobile store to the surface store via splash detachment ($f_{splash,i}$) as described below.

$$m'_{surf,i} = m^{t-1}_{surf,i}(1 - a_{inf,i}) + f_{add,i}$$

$$m'_{immob,i} = m^{t-1}_{immob,i} + m^{t-1}_{surf,i} a_{inf,i}$$

$$f_{splash,i} = \min(m'_{immob,i},\ 10^{-3} a_{splash,i} RE_{splash}^{\frac{10}{10-I_{veg}}})$$

For splash detachment, $a_{splash,i}$ is the scaling parameter per class, R is the rainfall, E_{splash} is a specific soil erosion potential parameter and I_{veg} is a vegetation cover index.

The transport capacity (S_{TC}) of MPs from the surface store to the river was computed per landscape type and reach.

$$S_{TC} = a_{TC,1}\left(10^3 \frac{A_c}{L} \max(0, Q_{dr} - a_{TC,2})\right)^{a_{TC,3}}$$

A_c is the subcatchment area, L the reach length, Q_{dr} is the direct runoff flow and $a_{TC,1}$, $a_{TC,2}$ and $a_{TC,3}$ are sub-catchment-specific calibration parameters. If the transport capacity exceeds particles in the surface store after splash detachment, then all the detached particles are transported to the reach ($f_{land,i}$). If the capacity is smaller than the surface store, then the mass of particles of a class *j* transported to the river is given by:

$$S_{TC}\frac{m''_{surf,i}}{\sum_j m''_{surf,j}}$$

$m''_{surf,i}$ is the surface store after splash detachment. If the transport capacity is not exceeded, the remaining capacity can be used for flow erosion from the immobile store to the reach using a flow erosion flux $f_{flow,i}$, which gets added to $f_{land,i}$. The potential flow erosion from each class is:

$$f_{flow,i} = \min\left(m''_{immob,i},\ a_{flow,1}E_{flow,i}\left(10^3\frac{A_c}{L}\max(0, Q_{dr} - a_{flow,2})\right)^{a_{flow,3}}\right)$$

$E_{flow,i}$ is a per-particle-class flow erosion potential, $a_{flow,1}$, $a_{flow,2}$ and $a_{flow,3}$ are subcatchment-specific calibration parameters, and $m''_{immob,i}$ is the immobile store after splash detachment.

There are also matrices $M_{land} = (M_{land,i,j})$ and $M_{reach} = (M_{reach,i,j})$ describing transfer of particles between classes on land and in the reach. This can represent processes like the fragmentation of particles, degradation and aggregation of particles. M_{land} is used to transform the on-land stores, and M_{reach} for the suspended and sediment bed particles: At the end of each timestep, for a given store and a given particle class j, it is computed:

$$m'_j = m_j + \sum_i M_{i,j}m_i - m_j\sum_i M_{j,i}$$

where m_j is the mass of class j in the store before the transfer, and m'_j is the new mass after the transfer and $M_{i,j}$ is the proportion of the mass that is transferred from class i to class j each time step.

Table 9 presents the model input values that govern the on-land mobilization of MPs.

Table 9: Model values associated with on-land mobilization of MPs (Norling *et al.* 2024).

Symbol	Unit	Name
$\boldsymbol{a_{inf}}$	$1/day$	Grain infiltration rate
$\boldsymbol{f_{add}}$	kg/day	Grain input to land
$\boldsymbol{a_{splash}}$	kg/m	Splash detachment scaling factor
$\boldsymbol{E_{splash}}$	1	Splash detachment soil erodibility
$\boldsymbol{I_{veg}}$	1	Vegetation index
$\boldsymbol{a_{TC,1}}$	$kg/(m^2km^2)$	Transport capacity scaling factor
$\boldsymbol{a_{TC,2}}$	mm/day	Transport capacity direct runoff threshol
$\boldsymbol{a_{TC,3}}$	1	Transport capacity nonlinear coefficient
$\boldsymbol{a_{flow,1}}$	1	Flow erosion scaling factor
$\boldsymbol{a_{flow,2}}$	mm/day	Flow erosion direct runoff threshold
$\boldsymbol{a_{flow,3}}$	1	Flow erosion nonlinear coefficient

$\boldsymbol{E_{flow}}$	1	Flow erosion potential
$\boldsymbol{M_{land}}$	$1/day$	Mass transfer matrix (land)
$\boldsymbol{M_{reach}}$	$1/day$	Mass transfer matrix (reach)
$\boldsymbol{R}$	mm/day	Precipitation
$\boldsymbol{Q_{dr}}$	mm/day	Direct runoff flow
$\boldsymbol{f_{splash}}$	$kg/(km^2day$	Splash detachment
$\boldsymbol{S_{TC}}$	$kg/(km^2day$	Surface transport capacity
$\boldsymbol{f_{flow}}$	$kg/(km^2day$	Flow erosion
$\boldsymbol{m_{surf}}$	kg/km^2	Surface grain store
$\boldsymbol{m_{immob}}$	kg/km^2	Immobile grain store

3.14 In-stream dynamics of MPs

The transport dynamics of MP class in the river is determined using the following parameters: i) the minimum and maximum size of the major (longest) axis of MPs in the class ($D_{min,i}$) and $D_{max,i}$); ii) the ratio of the major axis to the minor axis (r_i); and iii) the density of MPs ($\rho_{p,i}$) and is computed using the equations below.

The in-stream MP transportation is described per class i of particles. The masses of suspended particles ($m_{sus,i}$) and bed sediment particles per unit area ($m_{bed,i}$) are governed by the equations:

$$\frac{dm_{sus,i}}{dt} = f_{us,i} + f_{land,i} + f_{d,i} + Lw_b\left(f_{ent,i} - f_{dep,i}\right) - Q\frac{m_{sus,i}}{V}$$

$$\frac{dm_{bed,i}}{dt} = f_{dep,i} - f_{ent,i}$$

$f_{us,i}$ is flux from upstream and $f_{land,i}$ is input from land. $f_{dep,i}$ is the settling of suspended MPs to the riverbed, and $f_{ent,i}$ is the remobilization of settled MPs to the water column. Suspended MPs are assumed to be in free fall, so that:

$$f_{dep,i} = \frac{m_{sus,i}}{V}\omega_i$$

where ω_i is the terminal settling velocity per particle class i. The terminal settling velocity is computed whereby the equivalent diameter is:

$$d_{equi,i} = \begin{cases} c_i, \\ \sqrt[3]{a_i b_i c_i}, \end{cases}$$

The Corey shape factor is defined below with a_ib_i represented the particle projected area and c_i being the thickness:

$$CSF_i = \frac{c_i}{\sqrt{a_i b_i}}$$

The reach kinematic viscosity is given as:

$$\nu = 0.00285e^{-0.27(T_w+273.15)}$$

T_w is the water temperature which is approximated from air temperature using a time lag model. The Reynold's number, drag coefficient and terminal settling velocity are circular referenced and are solved starting with an initial guess using the Stokes equation ($\omega_{i,0}$) until ω_i has converged within an absolute error of 10^{-6}:

$$\omega_{i,0} = \frac{(\rho_{p,i} - \rho_f) g d_{equi,i}}{18\nu}$$

$$Re_i = \frac{\omega_i d_{equi,i}}{\nu}$$

$$C_{D,i} = \begin{cases} \frac{4.7}{\sqrt{Re_i}} + \sqrt{CSF_i}, \\ \frac{3}{CSF_i \sqrt[3]{Re_i}}, \end{cases}$$

$$\omega_i = \sqrt{\frac{4}{3} \frac{d_{equi,i}}{C_{D,i}} \frac{\rho_{p,i} - \rho_f}{\rho_f} g}$$

To compute the remobilization, we first compute the critical shear stress. The non-dimensional Shields parameter of a given particle class is:

$$\theta_i = 0.5588\theta^* \left(\frac{d_{equi,min,i}}{d}\right)^{-0.503}$$

Where θ^* is the critical Shields parameter of the sediment bed and d is the median bed grain diameter. $d_{equi,min,i}$ was used to compute the critical shear stress for mobilizing the smallest particles in the class. The critical shear stress is:

$$\tau_{c,i} = \theta_i (\rho_{p,i} - \rho_f) g d_{equi,min,i}$$

To compute the largest equivalent diameter a particle can have for it to be mobilized ($d_{equi,c}$), we solved the previous equation for d_{equi} with the actual shear stress τ standing in for the critical shear stress, which is:

$$d_{equi,c} = \left(\frac{\tau}{0.5588\theta^{*} d_{50}^{0.503} (\rho_{p,i} - \rho_f) g} \right)^{\frac{1}{1-0.503}}$$

The proportion of a given class that can be entrained is estimated as:

$$p_{ent,i} = \begin{cases} 1, & \text{if } d_{equi,c} < d_{equi,min,i} \\ 0, & \text{if } d_{equi,c} > d_{equi,max,i} \\ \dfrac{d_{equi,c} - d_{equi,min,i}}{d_{equi,min,i} - d_{equi,max,i}}, & \text{othewise} \end{cases}$$

Table 10 presents the model input values that govern the in-stream dynamics of MPs.

Table10: Model values associated to the in-stream dynamics of MPs (Norling *et al.* 2024).

Symbol	Unit	Name
$\boldsymbol{D_{min}}$	m	Major axis of smallest particle in class
$\boldsymbol{D_{max}}$	m	Major axis of largest particle in class
$\boldsymbol{r}$	m	Ratio of major to minor particle axis
$\boldsymbol{\rho_p}$	kg/m^3	Particle density
$\boldsymbol{d_{50}}$	m	Median diameter of bed sediment
$\boldsymbol{a_{ent}}$	$day \cdot m^2/$	Entrainment coefficient
$\boldsymbol{c_e}$	kg/m^3	Concentration of particles in effluent inputs
$\boldsymbol{f_d}$	kg/day	Direct deposition of particles to reach
$\boldsymbol{a}$	m	Particle major axis (representative)
$\boldsymbol{b}$	m	Particle second longest axis (repr.)
$\boldsymbol{c}$	m	Particle minor axis (repr.)
$\boldsymbol{d_{equi}}$	m	Particle equivalent diameter (repr.)
$\boldsymbol{d_{equi,min}}$	m	Equivalent diameter of smallest in class
$\boldsymbol{d_{equi,max}}$	m	Equivalent diameter of largest in class
$\boldsymbol{CSF}$	1	Corey shape factor
$\boldsymbol{T_w}$	℃	Water temperature
$\boldsymbol{\nu}$	m^2/s	Reach kinematic viscosity
$\boldsymbol{Re}$	1	Particle Reynold's number
$\boldsymbol{C_D}$	1	Particle drag coefficient
$\boldsymbol{\omega}$	m/s	Particle terminal settling velocity

$\boldsymbol{\theta}$	1	Particle non-dimensional Shields par.
$\boldsymbol{\theta^*}$	1	Sediment bed critical Shields parameter
$\boldsymbol{\tau_c}$	N/m^2	Critical shear stress for entrainment
$\boldsymbol{d_{equi,c}}$	m	Smallest equiv. diam. that can be entrained
$\boldsymbol{p_{ent}}$	1	Proportion of particles in class entrainable
$\boldsymbol{f_{ent}}$	kg/day	Entrainment flux
$\boldsymbol{f_{dep}}$	kg/day	Settling flux
$\boldsymbol{f_{us}}$	kg/day	Particle flux from upstream
$\boldsymbol{f_{land}}$	kg/day	Total particle flux from land
$\boldsymbol{f_a}$	kg/day	Particles removed by abstraction
$\boldsymbol{f_e}$	kg/day	Particles entering stream from effluents
$\boldsymbol{m_{sus}}$	kg	Mass of suspended particles in reach
$\boldsymbol{m_{bed}}$	kg	Mass of particles in sediment bed

3.15 Statistical analysis

All the statistical analysis of the obtained data was done using different packages in R v4.2.3 (R Core Team 2016). We compared the microbial community assemblage both across the sampling locations and habitats (surface water and plastisphere). Observed, Simpson, Shannon and Chao1 indices were used to estimate species abundance and richness and alpha diversity. Wilcoxon and Kruskal-Wallis rank sum tests were used to test the significance of differences of community composition between the sampling sites and habitat. Bray-Curtis distance based unconstrained principal coordinate analysis (PCoA) was used to observe the differences in community composition and function between different sampling sites and habitats (surface water vs plastisphere) using *vegan* package (Oksanen, 2010). To evaluate microbial compositions both across the sites and habitat, we conducted PERMANOVA with 999 permutations using Adonis function from the *vegan* package (Anderson, 2001). In case where the homogeneity of variances was not fulfilled between the groups, ANOSIM was performed using Anosim function in *vegan* package (Oksanen et al., 2007). Mantel and redundancy analysis (RDA) were performed to evaluate the effects of different environmental variables on microbial communities both across the sites and habitat. Spearman's correlation was used to estimate the relationship between the microbial diversity and the physiochemical properties *corrplot* function in R v 4.2.3. We then

applied machine learning based random-forest model (Liaw and Wiener, 2002) to obtain important biomarkers both across the sampling sites and between plastisphere and surface water. We also calculated the environmental difference and the corresponding community similarities between sites and surface water and plastisphere and used linear regression model analysis to test the relationship between environmental differences and bacterial similarity. Information on the ecologically functional signatures of the microbes was obtained by using the FAPROTAX database. Network analysis was performed to discern the patterns of microbial interaction and to estimate species co-existence across the sampling regions and habitats using Gephi v.0.10.1. In order to reduce the taxa, we removed the taxa whose relative abundance was less then < 0.01%. Using Spearman's rank correlation with coefficients greater than 0.6 ($\rho > 0.6$) and p-value < 0.05 used to construct the networks. The niche breadth values of species across the habitats and sampling locations were calculated *via spaa* package (Zhang and Ma, 2014). Sloan's Neutral based model was applied to investigate the community assemblage of surface water and plastisphere. Finally, we applied null model to measure the significance of deterministic and stochastic processes in community assemblage using *NST* package.

CHAPTER 4

RESULTS AND DISCUSSION

4.1 Physicochemical characteristics of the river water

Temperature and pH in the Msunduzi River showed no significant variation across sampling sites and periods (Table 11). However, dissolved oxygen (DO) levels fluctuated, although all measurements remained within the acceptable range of 4.15-6.66 mg/L (45-70.4%) (Horton et al., 2017). Based on DO levels, Sites 2 and 3 are potentially polluted. Site 2, affected by agricultural runoff (a known source of river pollution that lowers DO), and Site 3, impacted by urban runoff, support this conclusion. While other physicochemical parameters exhibited some variation, these differences were not statistically significant. Therefore, the data in Table 11 suggests that agricultural and urban runoff are likely the primary sources of pollution in the Msunduzi River.

Physicochemical water quality in the Swartkops River varied significantly across sampling sites. Notably, electrical conductivity and turbidity differed significantly between the five sampling sites and the control site. For example, Site 5 exhibited the highest conductivity (32.1 µS/cm²) but the lowest turbidity (3.42 NTU). As site 5 is reportedly influenced by urban settlements, the variation in land use along the river's catchment likely explains these differences. This conclusion is supported by the control site's significantly different conductivity and turbidity values, given its lack of land use impact (Table 12)

Table 11: Physicochemical quality of water samples from Msunduzi River

Site	Physicochemical Parameters						
	Temp (ºC	pH	DO mg/l	Salinity (g/L)	TDS	Spec. conductivity (µS/cm)	DO%
#1	17	7.05	5.4	0.15	0.204	314	56
#2	18.37	7.12	4.15	0.13	0.178	224	48.2
#3	17.08	7.21	4.32	0.14	0.185	283	45
#4	17.66	7.22	6.66	0.08	0.115	176	70.4

Table 12: Physicochemical quality of water samples from Swartkops River

Site	Temp (ºC)	pH	Conductivity(µS/cm^2)	Turbidity (NTU)
#1	20.53	7.40	2667	16.44
#2	21.53	7.57	2510	49.9
#3	21.08	7.60	2917	14.56
#4	21.42	7.67	2254	16.07

#5	20.88	7.7	3202	3.42
#6	20.48	6.6	538	5.9

4.2 **MP abundance in surface water and sediment samples**

The analysis of MP samples from both rivers revealed a diverse array of particle shapes, including fibres, fragments, and pellets. The shape distribution of MPs is a critical factor in understanding their sources, behaviour, and potential ecological impacts. Typical MP particles recovered from surface water in both the Msunduzi River and Swartkops River are illustrated in Figure 10, showcasing the visual diversity of these pollutants. There were four different colours of MPs observed including blue, transparent, dark blue, and red, which may reflect the range of plastic products commonly found in the environment and their origins. In the Msunduzi River (Figure 11A), fibres emerged as the predominant shape in both surface water (60%) and sediment samples (59%), particularly at the IA site, where the concentration reached 42 particles/L in surface water. In sediment samples collected from the AA, fibres accounted for 36 particles/L. This dominance of fibres indicate significant pollution from textile sources, such as washing machine effluents and textile industry discharges. The presence of fibres aligns with global observations, such as those from the textile industrial area in Shaoxing City, China, where fibres were found to be the most common type of MP due to effluent from textile factories (Deng *et al.*, 2020). Additionally, pellets were notably more prevalent at the IA site, with 26 particles/L in surface water and an even higher concentration of 39 particles/L in sediment, indicating a significant accumulation in the riverbed. Similarly, the Swartkops River (Figure 11B) exhibited a similar trend, with fibres being the dominant shape across all sampling sites. The AA site recorded the highest concentration of fibres in surface water, at 38 particles/500ml, while the WWTP site showed 29 particles/500ml. In sediment samples, the AA site again showed a high concentration of fibres, at 18 particles/500ml, whereas fragments and pellets were more abundant at the AA site, with 31 particles/500ml. This shape distribution analysis underscores the complexities of MP pollution, emphasizing the need for targeted management strategies to address specific types of MPs based on their shapes and the environments from which they are collected.

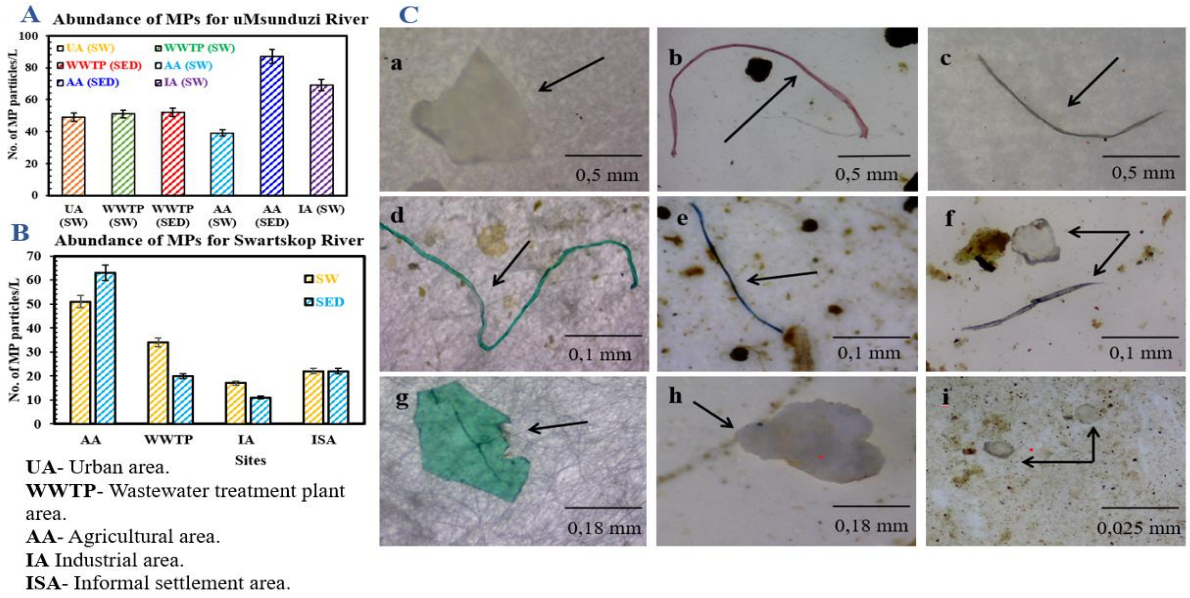

Figure 10: Abundance of MPs was found in all four sampling sites for surface water and sediment samples in the Msunduzi River (A) and Swartkops River (B). Images of different shapes of MPs in both rivers (C). The arrow indicates fragment (a), fibres (b-e), pellet and fibre (f), fragments (g), foam (h), and pellet (i)

4.3 Shape distribution of MPs: Fibbers, Fragments, and Pellets

The analysis of MP samples from both rivers revealed a diverse array of particle shapes, including fibres, fragments, and pellets. The shape distribution of MPs is a critical factor in understanding their sources, behaviour, and potential ecological impacts. Typical MP particles recovered from surface water in both the Msunduzi River and Swartkops River are illustrated in Figure 10C, showcasing the visual diversity of these pollutants. There were four different colours of MPs observed including blue, transparent, dark blue, and red, which may reflect the range of plastic products commonly found in the environment and their origins. In the Msunduzi River (Figure 11A), fibres emerged as the predominant shape in both surface water (60%) and sediment samples (59%), particularly at the IA site, where the concentration reached 42 particles/L in surface water. In sediment samples collected from the AA, fibres accounted for 36 particles/L. This dominance of fibres indicate significant pollution from textile sources, such as washing machine effluents and textile industry discharges. The presence of fibres aligns with global observations, such as those from the textile industrial area in Shaoxing City, China, where fibres were found to be the most common type of MP due to effluent from textile factories (Deng *et al.*, 2020). Additionally, pellets were notably more prevalent at the IA site, with 26 particles/L in surface water and an even higher concentration of 39 particles/L in sediment, indicating a significant accumulation in the riverbed.

The Swartkops River (Figure 11B) exhibited a similar trend, with fibres being the dominant shape across all sampling sites. The AA site recorded the highest concentration of fibres in surface water, at 38 particles/500ml, while the WWTP site showed 29 particles/500ml. In sediment samples, the AA site again showed a high concentration of fibres, at 18 particles/500ml, whereas fragments and pellets were more abundant at the AA site, with 31 particles/500ml. This shape distribution analysis underscores the complexities of MP pollution, emphasizing the need for targeted management strategies to address specific types of MPs based on their shapes and the environments from which they are collected.

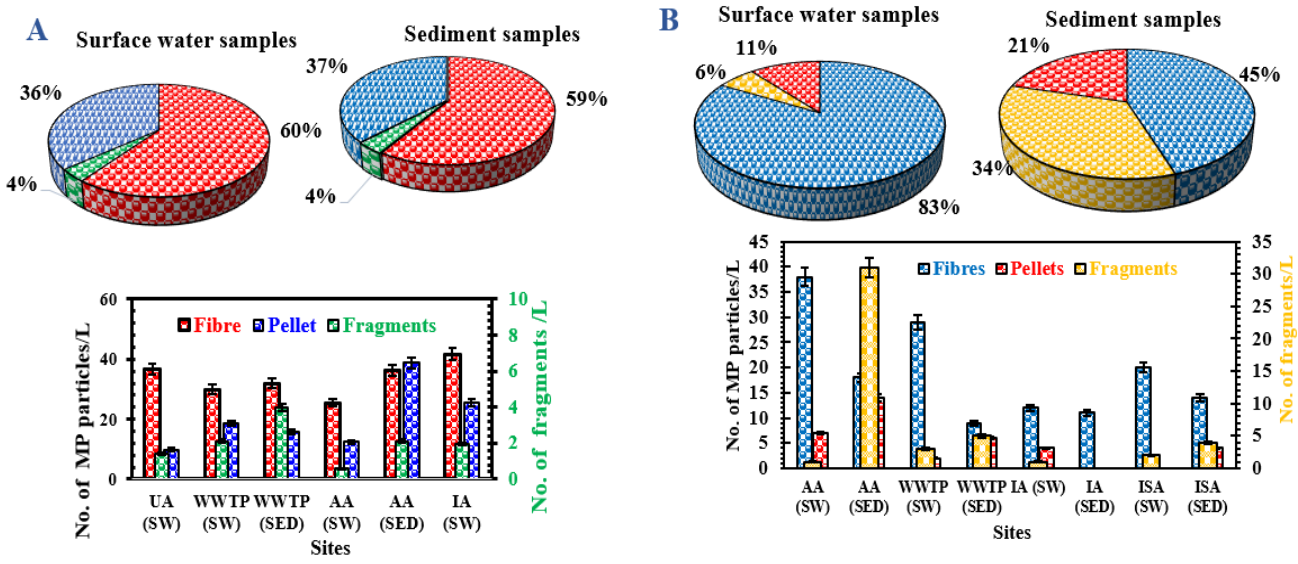

Figure 11: Shape distribution of MP particles and percentage of shape type in the Msunduzi (A) and Swartkops (B) River

4.5 Size variation of MPs across sites

The size variation of MPs in the Msunduzi River and Swartkops River reveals significant insights into the characteristics of plastic pollution across different environments, as illustrated by the bar charts in Figures 12A and B. The distribution of MPs was categorized into four size classes: 0.5 mm, 0.18 mm, 0.1 mm, and 0.025 mm, with distinct patterns observed in both surface water and sediment samples. In the Msunduzi River, larger MPs (0.5 mm) were predominantly found in surface water samples, particularly at the UA site, where they constituted 40% of the total MPs, and at the AA site, accounting for 36%. Larger MPs are often derived from fragmented consumer products, packaging, and synthetic fibres that have not yet undergone extensive environmental

degradation (Saad *et al*., 2022, Sulistyowati *et al*., 2022). The high presence of these larger particles in ISA, like that along the Swartkops River, aligns with findings from other studies, such as the research on the Cisadane River in Indonesia, which found that poorly managed urban waste directly contributes to the high prevalence of larger MPs (Sulistyowati *et al*., 2022). A comparable study of the South African Vaal River by Saad (2022) found that larger MPs were more common in regions with considerable human activity and inadequate waste management (Saad *et al.*, 2022). This trend suggests that larger particles are more effectively transported within the water column, potentially due to their buoyant nature. The 0.18 mm size class showed a peak concentration at the IA site, representing 29% of the total MPs, which indicates a direct correlation between industrial discharge and the prevalence of this size class. While smaller size classes (0.1 mm and 0.025 mm) were present, they were less dominant, particularly at the AA site, where the 0.025 mm class made up 17% of the MPs. In contrast, sediment samples from the Msunduzi River displayed a more balanced size distribution. Notably, smaller particles (0.025 mm) were more prevalent at the WWTP site (35%) and AA site (26%), highlighting the role of sediments in trapping these smaller MPs. This accumulation can have significant implications for benthic organisms, as smaller MPs may be ingested by various aquatic species. In the Swartkops River, surface water samples similarly exhibited a dominance of larger MPs (0.5 mm), particularly at the ISA site, where they comprised 68% of the total MPs, followed by the WWTP site (47%). The smaller size classes were less common, with the 0.025 mm size class only accounting for 7% at the AA site. Conversely, in sediment samples, the 0.025 mm size class emerged as the most abundant, particularly at the ISA site (50%) and AA site (49%). These findings emphasize the importance of considering both surface water and sediment matrices in evaluating MP pollution dynamics, as they provide critical insights into the different pollution sources of the MP in the aquatic ecosystems.

The Spearman correlation test was run to determine the relationship between MP sizes and abundance in surface water and sediment samples across the sites. The surface water (Msunduzi River) for UA demonstrated a strong statistically significant correlation with $r = 0.9509$ and p-value = 0.0491 whereas the other sites (WWTP, AA, and IA) showed insignificant correlation with p-value > 0.05. Whereas in the sediment samples WWTP site indicated almost no correlation ($r = -0.05499$) while the AA site demonstrated a moderate negative correlation ($r = -0.6833$).

Furthermore, the Spearman correlation further revealed varying degrees of correlation for the Swartkops River between the sites and habitats (surface water and sediment samples), though none of the relationships are statistically significant ($p > 0.05$). Strong positive correlations were observed for surface water at AA ($r = 0.768$, WWTP ($r = 0.7595$), and ISA ($r = 0.8522$), as well as

sediment for ISA (r = 0.9363). Whereas sediment samples for the AA (r = -0.666) revealed a moderate negative correlation and a strong negative correlation at WWTP sediment samples (**Table S5**).

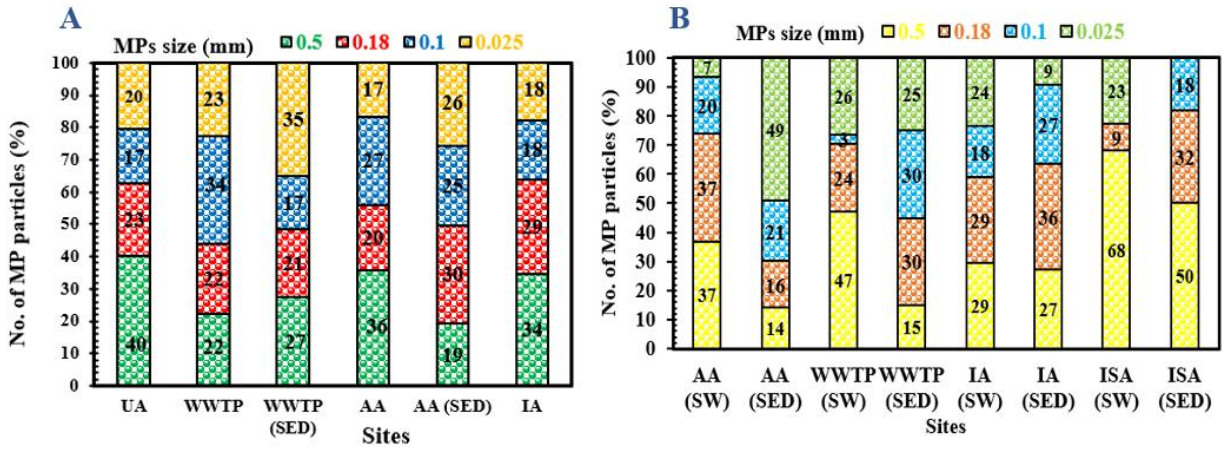

Figure 12: Size distribution for surface water and sediment samples in Msunduzi (A) and Swartkops (B) rivers

Table 13: Interpretation of correlation data for the sites (Msunduzi and Swartkops rivers)

Category	Pearson r	Strength of Correlation	P-value	Significant	R-Squared
Msunduzi River					
UA (SW)	0.9509	Very strong positive correlation	0.0491	Yes	0.9043
WWTP (SW)	-0.4352	Weak negative correlation	0.5648	No	0.1894
WWTP (SED	-0.05499	Very weak negative	0.945	No	0.003024
AA (SW)	0.8391	Strong positive correlation	0.1609	No	0.7041
AA (SED)	-0.6833	Moderate negative	0.3167	No	0.4668
IA (SW)	0.9213	Very strong positive correlation	0.0787	No	0.8487
Swartkops River					
AA (SW)	0.768	Strong positive	0.232	No	0.5898
AA (SED)	-0.666	Moderate Negative	0.334	No	0.4435
WWTP (SW)	0.7595	Strong positive	0.2405	No	0.5769
WWTP (SED	-0.8121	Strong Negative	0.1879	No	0.6594
IA (SW)	0.631	Moderate positive	0.369	No	0.3981
IA (SED)	0.4199	Weak Positive	0.5801	No	0.1763
ISA (SW)	0.8522	Very strong positive	0.1478	No	0.7263
ISA (SED)	0.9363	Very strong positive	0.0637	No	0.8767

4.6 MPs detection by Pyro-GC/MS

The detection of MPs in the Swartkops River sites using Pyro-GC/MS analysis indicates a diverse range of pyrolysis products that point towards different plastic pollutants. At the AA site the most

dominant pyrolysis products identified were 2,4-Dimethylhept-1-ene (23%), Benzene (15%), Hexanal (11%), Bicyclo [2.1.1] hexan-2-ol, 2-ethenyl-(4%) 1-undecene, 7-methyl-(4%) Benzene, 1,2-dimethyl-(3%), as shown in Table 14. Pyro compound 2,4-Dimethylhept-1-ene (23%) is present in high composition, which is associated with PE or PP (Šunta *et al*., 2021). Its high percentage indicates that agricultural activities near the Swartkops River likely involve significant use of these plastics, potentially in irrigation pipes, plastic sheeting, or packaging. Pyro compound Benzene is an aromatic compound that was probably derived from PS or PVC. This suggests a notable presence of consumer or industrial waste in the area, possibly from plastic containers, packaging, or insulation materials (Lou *et al.*, 2022). Hexanal is a linear chain aldehyde that may result from the degradation of polymers such as PE and PP (Vilakati *et al.*, 2021). Bicyclo [2.1.1] hexan-2-ol, 2-ethenyl- (4%), a minor component, this compound could be indicative of specialty plastics or additives which was probably derived from blending pyrolysis of PE and PP (Mahapatra *et al.*, 2024). The 1-Undecene, 7-methyl is a long chain linear structure pyro product that could be derived from PE and PP commonly used in packaging materials. The one minor pyro product, Benzene, 1,2-dimethyl- (also known as o-Xylene) is used in the production of styrene, which is a key monomer for polystyrene (Santos *et al*., 2023).

In the WWTP site pyro-GC/MS analysis of MPs detected in the surface water revealed the presence of several pyrolysis products: 1,3-Dioxolan-4-one, 2-(1,1-dimethylethyl)-5-(1-methylethyl)-, (2s-cis)-: (56.7%), Propyphenazone (3%), and n-Hexadecenoic acid (6%). These findings indicate that most detected MPs are likely composed of synthetic polymers or additives, with 1,3-Dioxolan-4-one being the dominant pyrolysis product. The compound 1,3-Dioxolan-4-one, 2-(1,1-dimethylethyl)-5-(1-methylethyl)- is a pyrolysis by-product, and while it may not directly point to a specific type of plastic, it can be associated with synthetic materials or additives used in plastic production (Gazzotti *et al.*, 2022). This type of compound might originate from polymers such as polyesters, polycarbonates, or certain synthetic resins, which degrade during pyrolysis. The other compound, propyphenazone is a non-steroidal anti-inflammatory drug (NSAID) commonly used for its analgesic (pain-relieving) and antipyretic (fever-reducing) properties, which is associated with pharmaceutical drugs (Phong *et al.,* 2024). n-Hexadecenoic acid (6.1%) is the potential pyro product of MPs of PE and PP. These polymers are widely used in packaging and household products (Lou *et al.,* 2022).

At the IA site, Hexacosane (87.7%) is a straight alkane comprising 26 carbon atoms. This was a major compound that indicated the presence of PE, especially high-density polyethylene (HDPE) and low-density polyethylene (LDPE). The Pentafluoropropionic acid (3.8%) is a pyrolysis

product of fluorinated polymers, particularly polytetrafluoroethylene (PTFE) and related fluoropolymers. During pyrolysis, these polymers can decompose and release various fluorinated compounds, including pentafluoropropionic acid (Vaganov *et al.*, 2019). Nonacosanol (3.65%), a long-chain fatty alcohol, is not a common pyrolysis product of typical synthetic plastics like PE, PP, or PS. Instead, it is more likely to arise from natural waxes or biopolymers, such as those found in plant materials or certain biodegradable plastics. It can be associated with the pyrolysis of natural substances like polysaccharides or lipid-based materials, rather than traditional petroleum-based plastics (Jaafar *et al.*, 2022). Propyphenazone (3.1%) was detected, which is a pharmaceutical drug, not a polymer pyroproduct. The ISA site features R-(-)-Cyclohexylethylamine (35.88%), which is an organic compound that can form as a pyrolysis byproduct of certain polymers, such as polyamides (nylon) and PS. Additionally, it has been reported to be found in rubber products like tires, suggesting potential contributions from these sources as well (Seiwert *et al.,* 2020). The 2,4-dimethylhept-1-ene (23.96%) compound is produced from the degradation of PE and PP (Šunta *et al*., 2021). The Bicyclo[4.2.0]octa-1,3,5-triene (6.41%), also known as "barrelene," is a strained hydrocarbon structure, and polylefin or polystyrene, when subjected to high heat or catalytic degradation derived from PS, this aromatic compound further indicates the presence of this ISA site (Mahapatra *et al*., 2024). 7-Methyl-1-undecene is a pyrolysis product primarily associated with the thermal degradation of certain types of polyolefins, such as PP and PE. These polymers, when subjected to high temperatures, can break down and form a range of hydrocarbons, including 7-methyl-1-undecene (Lou *et al*., 2022).

The presence of MPs in the AA site sediment samples in the Swartkops River indicated by pyrolysis-GC/MS analysis, points to potential plastic contamination from agricultural materials. The identified compounds are 2-Propanone 1-hydroxy-(8.51%), Benzene (8.62%), and 2-Oxiranylmethyl acetate (7.68%). The 2-Propanone, 1-hydroxy- (commonly known as acetone) is a pyrolysis product of various polymers, particularly those containing carbonyl groups, likely derived from polycarbonate (PC) and PS (Al-Hakami *et al*., 2024). The Benzene, ethenyl- (8.62%) indicated contamination, the primary monomer of PS, which is commonly found in packaging materials and can enter the environment through agricultural waste or plastic mulch (Santos *et al*., 2023), while the detection of 2-Oxiranylmethyl acetate (7.68%), derived from cellulose acetate, in sediment samples suggests that agricultural activities may contribute to MP pollution in the form of cellulose acetate. Cellulose acetate is considered a bioplastic; it can still degrade into MP particles under certain conditions (Zhao *et al.*, 2022).

The pyro compound detected in the WWTP site sediment sample was 2,4-Dimethylhept-1-ene (11.5%), 1-Decene (6.8%), 1-Undecene (4.71%), and 1-Dodecene (4.11%). All these compounds are long-chain hydrocarbons primarily derived from PE (Leslie *et al*., 2022). The Benzene ethenyl- (39.25%) in the IA site sediment sample is the key pyrolyzate aromatic compound, which was produced from PS polymer (Santos *et al.,* 2023). The other pyrolyzate compounds 1-decene (6.48%), and 1-undecene (5.1%), 1-dodecene (6.71%) and cetene (7.94%) are long-chain hydrocarbons primarily derived from PE (Leslie *et al.*, 2022). The dominance of Benzene and ethenyl suggests industrial discharge, while the presence of alkenes like 1-decene indicates potential contamination from polyolefin plastics. The primary Pyrolyzate compounds detected in the ISA sediment sample were 2,4-Hexadiyne (25.82%), Benzene, ethenyl- (10.27%), and Benzene, methyl (3.63%). Compound 2,4-hexadiyne is also cellulose acetate, which is a bioplastic and used as a film base in photography, as a component in some coatings, and as a frame material for eyeglasses; it is also used as a synthetic fibre in the manufacture of cigarette filters and playing cards. During pyrolysis, polybutadiene can break down and form various unsaturated hydrocarbons, including 2,4-hexadiyne (Zhao *et al*., 2022). The other compounds, Benzene, ethenyl- and Benzene, methyl are primary monomers of PS, which are commonly found in packaging materials and can enter the environment through agricultural waste or plastic mulch (Santos *et al.*, 2023). These findings suggest the sediment is heavily impacted by plastic debris, possibly from treated wastewater discharges.

The detection of MPs in surface water samples from the UA site near the Msunduzi River using Py-GCMS analysis reveals a diverse range of pyrolysis products, indicating various plastic pollutants. The amount of 1,30-Triacontanediol (40.9%), Heptacosane (31.26%), and Nonacos-1-ene (18.43%) were detected as pyroproducts, indicating a dominance of PE, commonly found in urban waste (Šunta *et al*., 2021). High concentrations of Heptacosane (31.26%) and Nonacos-1-ene (18.43%) were also detected. Heptacosane is saturated hydrocarbon formed from the breakdown of synthetic polymers, suggesting urban plastic pollution, and Nonacos-1-ene unsaturated hydrocarbon typically derived from PE, commonly found in urban environments due to high plastic use (Jaafar *et al.*, 2022, Leslie *et al.*, 2022). These compounds reflect the degradation of long-chain hydrocarbons characteristic of these widely used plastics in packaging, containers, and consumer products. The pyro-GC/MS analysis of MPs detected in the surface water sample of the WWTP site at Msunduzi River revealed the presence of several pyrolysis products. Benzene (60.33%), Propyphenazone (8.18%), Benzene ethenyl- (5.13%) and Benzaldehyde (3.78%). The presence of Benzene, and Benzene ethenyl- indicates significant PS degradation, a material

prevalent in consumer waste treated at wastewater effluent (Lou *et al*., 2022), while Propyphenazone related pharmaceutical production analgesic drugs, suggests that sewage pollution is not limited to plastics, but also includes pharmaceutical contaminants, indicative of a diverse range of pollutants entering wastewater systems (Phong *et al.*, 2024). Pyrolyzed compounds like Benzaldehyde is aromatic ring structure molecules derived from PS, PP, and PVC (Santos *et al*., 2023, Lou *et al.*, 2022).

MPs detected in AA site surface water samples included compound Benzene, ethenyl- (25.15%), 2,4-Hexadiyne (24.78%), Benzene, methyl- (6.54%), and Benzaldehyde (5.26%). The Benzene, ethenyl-, Benzene, methyl- indicating the presence of PS, while 2,4-Hexadiyne product of ABS plastic or cellulose acetate plastics (Zhao *et al.*, 2022, Lou *et al.*, 2022). The Benzaldehyde products of PS, PP, and PVC. The major pyrolyzate compounds detected in the surface water sample from the IA sites were traced i.e., Tetratetracontane (9.94%), Hexacosane (9.22%), 1-Heptadecene (4.5%) and 1-Hexanol, 2-ethyl- (5.09%). Tetratetracontane and hexacosane are a long-chain alkane commonly associated with the degradation of PE (Jaafar *et al*., 2022). It may originate from plastic packaging, industrial wraps, or other polymer-based materials used in manufacturing and transport. 1-Heptadecene is unsaturated hydrocarbon associated with the degradation of polyethylene or other polyolefins. It could be linked to industrial by-products or the breakdown of lubricants and additives in plastic manufacturing processes (Leslie *et al.*, 2022). 1-Hexanol, 2-ethyl- is a common plasticizer or additive used in industrial plastics and may also derive from the breakdown of plastic products like PVC or other polymeric materials (Leslie *et al*., 2022).

In the WWTP site sediment samples in Msunduzi River, Heneicosyl heptafluorobutyrate (72.78%), this compound is a likely derivative of Polytetrafluoroethylene (PTFE), and 1,19-Eicosadiene (23.32%) long-chain diene, is another product of PE degradation. Heneicosyl heptafluorobutyrate (72.78%) is a fluorinated ester, potentially derived from fluoropolymer coatings or fluorinated surfactants used in industrial applications (Leslie *et al*., 2022). These compounds are commonly found in non-stick coatings, waterproofing agents, and firefighting foams (PFAS-related products). Fluorinated chemicals are persistent in the environment and often end up in wastewater systems. 1,19-Eicosadiene is a long-chain hydrocarbon, typically associated with the degradation or breakdown of polyolefins like PE (Leslie *et al.*, 2022). These plastics are commonly used in packaging, textiles, and other consumer products, and their degradation can release such hydrocarbons into wastewater. The AA site sediment samples, Hexacosane (59.27%), Octacosane(27.43%), and Tetratetracontane (9.7%) are long-chain hydrocarbons commonly

associated with the breakdown of PE, which are extensively used in agricultural activities (Jaafar *et al*., 2022). Additionally, some of these long-chain hydrocarbons can also be linked to lubricants, waxes, and residues from pesticides or fertilizers used in farming. The presence of these compounds suggests plastic degradation and possible contamination from agricultural activities. Overall, the pyrolysis products identified across different sites highlight the complexity and diversity of plastic contamination in South African rivers. This analysis not only identifies the types of plastics present but also provides insights into their degradation processes and potential environmental implications, thereby informing strategies for pollution management and mitigation in these ecosystems.

Table 14: Characteristic pyrolyzate compounds for Msunduzi River and Swartkops River samples.

Pyrolyzate compounds	**Spectral peak area (%)**	**Retention time (min)**	**Chemical formula; PubChem CID**	**Molecular structure**	**Probable produced from**	**References**
Swartskop River						
	Site AA (SW)					
2,4-Dimethylhept-1-ene	23.24	4.747	C_9H_{18}; 12338	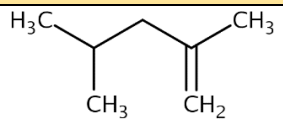	PP, PE, PS, PVC	(La Nasa *et al.* 2020, Santos *et al.*, 2023)
Benzene	15.58	2.293	C_6H_6; 241		PVC, PS	(Santos et al., 2023)
Hexanal	11.96	2.163	$C_6H_{12}O$; 618	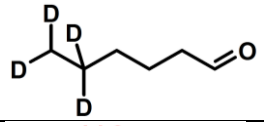	PE, PP, PS	(Vilakati *et al.*, 2021)
Bicyclo[2.1.1]hexan 2-ol, 2-ethenyl-	4.71	5.985	$C_8H_{12}O$; 560888	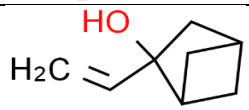	Blending Pyrolysis of PE, PP	(Mahapatra *et al.*, 2024)
1-Undecene, 7-methyl-	4.13	17.749	$C_{12}H_{24}$; 522554	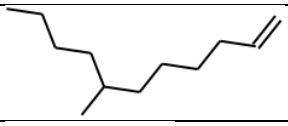	PP, PE	(Leslie *et al.*, 2022)
Benzene, 1,2-dimethyl-	3.08	4.747	C_8H_{10}; 7237	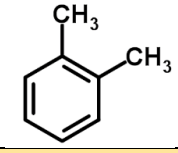	PS	(Santos *et al.*, 2023)
	Site WWTP (SW)					
1,3-Dioxolan-4-one, 2-(1,1-dimethylethyl 5-(1-methylethyl)-, (2s-cis)-	56.77	48.56	$C_{10}H_{18}O_3$; 91701869	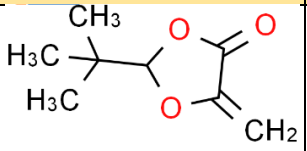	Nylon, PET	(Gazzotti et al. 2022)

Propyphenazone	3.94	14.676	$C_{14}H_{18}N_2O$; 3778	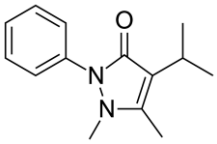	Pharmadrugs	(Phong et al., 2024)
n-Hexadecanoic acid	6.1	33.374	$C_{16}H_{32}O_2$; 98	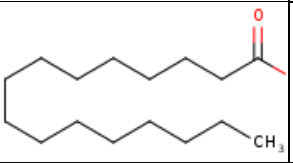	PE, PP	(Lou *et al.*, 2022)
	IA (SW)					
Hexacosane	87.78	41.54	$C_{26}H_{54}$; 1240	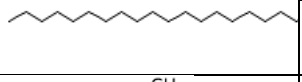	PE (HDPE/LDP pyrolytics)	(Jaafar *et al.*, 2022)
Pentafluoropropionic acid, hexadecyl ester	3.89	36.976	$C_{19}H_{33}F_5O_2$; 525401	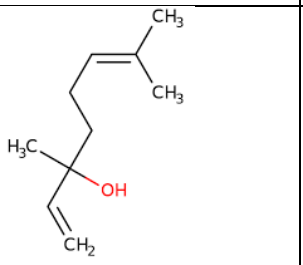	Polytetrafluoroethylene (PTFE)	(Vaganov *et al* 2019)
Nonacosanol	3.65	36.528	$C_{29}H_{60}O$; 243696	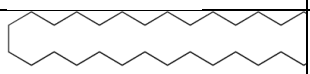	PE, PP	(Jaafar *et al.*, 2022)
Propyphenazone	3.1	15.235	$C_{14}H_{18}N_2O$; 3778	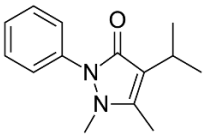	Pharma drugs	(Phong *et al.*, 2024)
	ISA (SW)					
R-(-)-Cyclohexylethylamine	35.88	2.178	$C_8H_{17}N$; 110733	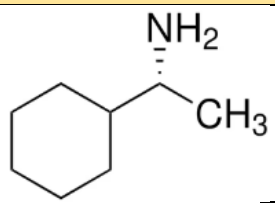	Nylone, PS	(Seiwert *et al.*, 2020)
2,4-Dimethylhept-1-ene	23.96	4.754	C_9H_{18}; 12338	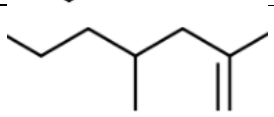	PE, PP, PS, PVC	(Šunta *et al.*, 2021)
Bicyclo[4.2.0]octa-1,3,5-triene	6.41	5.998	C_8H_8; 69667	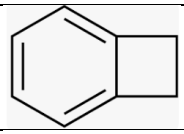	Blending Pyrolysis of PE, PP	(Mahapatra *et al.*, 2024)
7-Methyl-1-undecene	4.57	17.755	$C_{12}H_{24}$; 522554	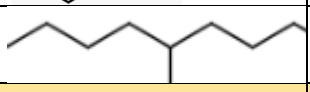	PE, PP	(Lou *et al.*, 2022)
	AA (Sediment)					
2-Propanone, 1-hydroxy-	8.51	2.267	$C_3H_6O_2$; 829	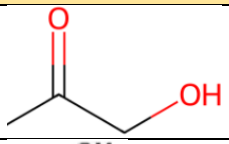	PS, PC	(Al-Hakami *et al.*, 2024)
Benzene, ethenyl-	8.62	5.983	C_8H_8; 7501	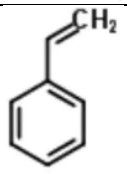	PS	(Santos *et al.*, 2023)

2-Oxiranylmethyl acetate	7.68	3.436	$C_5H_8O_3$; 110839	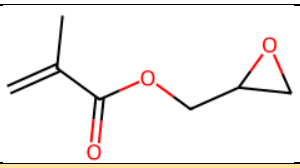	Cellulose acetate	(Zhao *et al.*, 2022)
	WWTP (Sediment)					
2,4-Dimethylhept-1-ene	11.46	4.784	C_9H_{18}; 12338	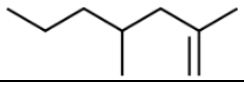	PE, PP	(Leslie *et al.*, 2022)
1-Decene	6.77	8.729	$C_{10}H_{20}$; 1338		PE	
1-Undecene	4.71	11.714	$C_{11}H_{22}$; 1319		PE	
1-Dodecene	4.11	14.679	$C_{12}H_{24}$; 8183	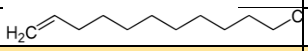	PE, Nylone	
	IA (Sediment)					
Benzene, ethenyl-	39.25	5.999	C_8H_8; 7501	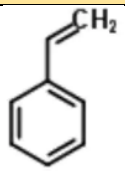	PS	(Santos *et al*., 2023)
1-Decene	6.48	8.717	$C_{10}H_{20}$; 1338		PE	(Leslie *et al.*, 2022)
1-Undecene	5.1	11.714	$C_{11}H_{22}$; 1319	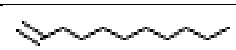	PE	
1-Dodecene	6.71	14.69	$C_{12}H_{24}$; 8183	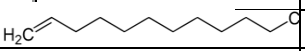	PE	
Cetene	7.94	22.808	$C_{16}H_{32}$; 1239	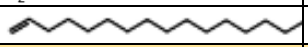	PE	
	ISA (Sediment)					
2,4-Hexadiyne	25.82	2.281	C_6H_6; 13772	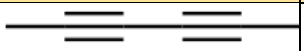	ABS plastic, cellulose acetate plastics	(Zhao *et al.*, 2022)
Benzene, ethenyl-	10.27	5.994	C_8H_8; 7501	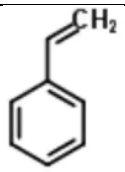	PS	(Santos *et al.*, 2023)
Benzene, methyl-	3.63	3.461	C_7H_8; 1140	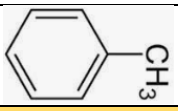	PS	(Santos et al., 2023)
Msunduzi River						
	UA (SW)					
1,30-Triacontanedio	40.96	33.856	$C_{30}H_{62}O_2$; 543982		PE	(Šunta *et al.*, 2021)
Heptacosane	31.26	42.12	$C_{27}H_{56}$; 1163	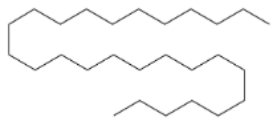	PE (HDPE/LDP	(Jaafar *et al.*, 2022)
Nonacos-1-ene	18.43	38.783	$C_{29}H_{58}$; 156989	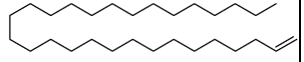	PE	(Leslie *et al.*, 2022)
	WWTP (SW)					

Benzene	60.33	2.285	C_6H_6; 241	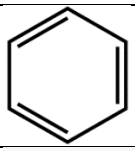	PS, PET, PVC	(Santos et al., 2023)
Propyphenazone	8.18	15.235	$C_{14}H_{18}N_2O$; 3778	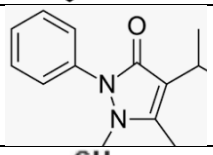	Pharmadrugs	(Phong *et al.*, 2024)
Benzene, ethenyl-	5.13	5.984	C_8H_8; 7501	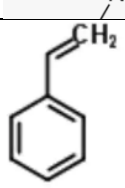	PS	(Santos *et al.*, 2023)
Benzaldehyde	3.78	7.943	C_7H_6O; 240	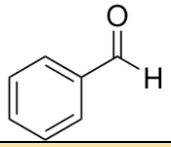	PS, PP, PE and nylom	(Akoueson *et al.*, 2021)
	AA (SW)					
Benzene, ethenyl-	25.15	6.004	C_8H_8; 7501	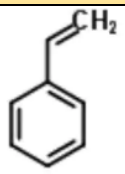	PS	(Santos *et al.*, 2023)
2,4-Hexadiyne	24.78	2.282	C_6H_6; 13772	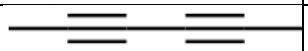	ABS plastic, cellulose acetate plastics	(Zhao *et al.*, 2022)
Benzene, methyl-	6.54	3.453	C_7H_8; 1140	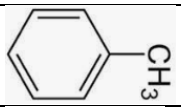	PS	(Santos *et al.*, 2023)
Benzaldehyde	5.26	7.943	C_7H_6O; 240	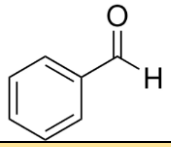	PS, PP, PE and nylon	(Akoueson *et al.*, 2021)
	IA (SW)					
Tetratetracontane	9.94	29.56	$C_{44}H_{90}$; 2349	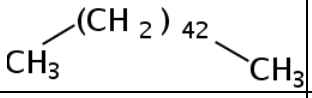	PE	(Jaafar *et al.*, 2022)
Hexacosane	9.22	31.554	$C_{26}H_{54}$; 1240		PE (HDPE/LDP pyrolytics)	(Jaafar *et al.*, 2022)
1-Hexanol, 2-ethyl-	5.09	9.916	$C_8H_{18}O$; 772	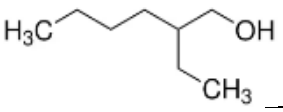	PE	(Leslie *et al.*, 2022)
1-Heptadecene	4.5	31.786	$C_{17}H_{34}$; 2321	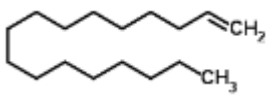	PE	(Leslie *et al.*, 2022)
	WWTP (Sediment)					
Heneicosyl heptafluorobutyrate	72.78	41.09	$C_{25}H_{43}F_7O_2$; 13932483	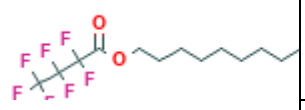	Polytetrafluoroet ylene (PTFE)	(Leslie *et al.*, 2022)
1,19-Eicosadiene	23.32	48.681	$C_{20}H_{38}$; 519006		PE	(Jaafar *et al.*, 2022)
	AA (Sediment)					

Hexacosane	59.27	32.724	$C_{26}H_{54}$; 1240	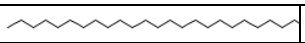	PE	(Jaafar *et al*., 2022)
Octacosane	27.43	32.27	$C_{28}H_{58}$; 124008	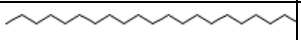	PE	
Tetratetracontane	9.7	31.52	$C_{44}H_{90}$; 2349	$CH_3(CH_2)_{42}CH_3$	PE	

4.7 ATR-FTIR data analysis of samples collected from sites near the Swartkops and Msunduzi rivers for MP detection

4.7.1 Surface water samples analysis from various active sites near the Swartkops River

The MP samples analysis by ATR-FTIR highlighted significant spectral peaks corresponding to distinct functional groups, reflecting the chemical nature of the pollutants (Figure 13). ATR-FTIR analysis in surface water samples from WWTP sites of Swartkops River showed significant peaks 1720 cm^{-1}, 1250 cm^{-1}, 1100 cm^{-1}, and 700 cm^{-1} could be attributed to different functional groups commonly associated with the compounds mentioned (Figure 13A). The spectral band near 1720 cm^{-1} corresponds to the C=O (carbonyl) stretching vibration, which is characteristic of esters, aldehydes, or carboxylic acids. In the WWTP sample, it could be linked to n-hexadecanoic acid (palmitic acid) or 1,3-Dioxolan-4-one due to their ester/carboxyl functionalities. Another peak near 1250 cm^{-1} might correspond to C–O stretching vibrations, which are common in esters and ethers. It could be attributed to the ester group in 1,3-Dioxolan-4-one. Peak near 1100 cm^{-1}: This is generally assigned to C–O–C stretching in ethers or alcohols, likely from 1,3-Dioxolan-4-one or the ester group in n-Hexadecanoic acid. Peak near 700 cm^{-1}: This is often associated with out-of-plane C–H bending, which can occur in aromatic compounds like propyphenazone. In the AA site samples intense peaks showed near 1708 cm^{-1} is commonly associated with carbonyl (C=O) stretching, which suggests the presence of aldehydes, ketones, or carboxylic acids (likely related to compounds like Hexanal). The spectral band near 1543 cm^{-1} corresponds to aromatic ring stretching, possibly indicating the presence of an aromatic compound like Benzene or a derivative (e.g., 7-methyl-Benzene). The spectral band near 1093 cm^{-1} typically indicative of C-O or C-N stretching, which could relate to alcohols (Bicyclo[2.1.1]hexan-2-ol) or ether groups. A spectral band near 3750 cm^{-1} is associated with O-H stretching, suggesting the presence of hydroxyl groups, possibly from an alcohol like Bicyclo[2.1.1]hexan-2-ol.

In the IA site sample intense peaks showed near 1708 cm^{-1} and 1543 cm^{-1} both are associated with carbonyl (C=O) stretching in propyphenazone. An additional intense peak at 3750 cm^{-1} peak could either be from Nonacosanol (due to its hydroxyl group) or atmospheric moisture. Spectral band near 1708 cm^{-1} typically associated with a carbonyl (C=O) stretching in compounds like amides,

esters, or ketones. it could be linked to the amine group present in R-(-)-Cyclohexylethylamine, although it's unusual for simple amines to have such a strong C=O stretch. R-(-)-Cyclohexylethylamine, an amine, is the most likely candidate responsible for peaks near 1543 mc^{-1} and 3750 cm^{-1} (N-H bending and stretching). Spectral band 3750 cm^{-1} more common for hydroxyl groups (O-H stretch) rather than amine N-H stretches

4.7.2 Sediment samples analysis from various active sites near the Swartkops River

ATR-FTIR analysis of sediment samples from WWTP and AA sites of Swartkops River showed significant peaks corresponding to various functional groups (Figure 13B). The common spectral band in WWTP and AA sites near 1708 cm^{-1} represents the C=O stretching in aromatic ring compounds like 2-Propanone (acetone) or ethenyl-2-Oxiranylmethyl acetate, as both contain carbonyl groups., which confirm the presence of polystyrene, and spectral band 1543 cm^{-1} possibly due to the presence of both the carbonyl group and the aromatic structure in 1-Hydroxybenzene (Phenol) suggesting the presence of a benzene ring. In IA and ISA sample some common peaks near 1092 cm^{-1} is associated with the C–C stretching or C–O stretching vibrations, which can be indicative of various hydrocarbons, including alkenes and aromatic compounds (Benzene, ethenyl-; 1-Decene; 1-Undecene; 1-Dodecene; Cetene; 2,4-Hexadiyne; Benzene, methyl-). These peaks may most closely relate to the aromatic compounds (like benzene derivatives) and alkenes. Additionally, there is one inverted peak showed near 2320 cm^{-1} is attributed to CO_2 from the atmosphere interacts with the sample or the spectrometer.

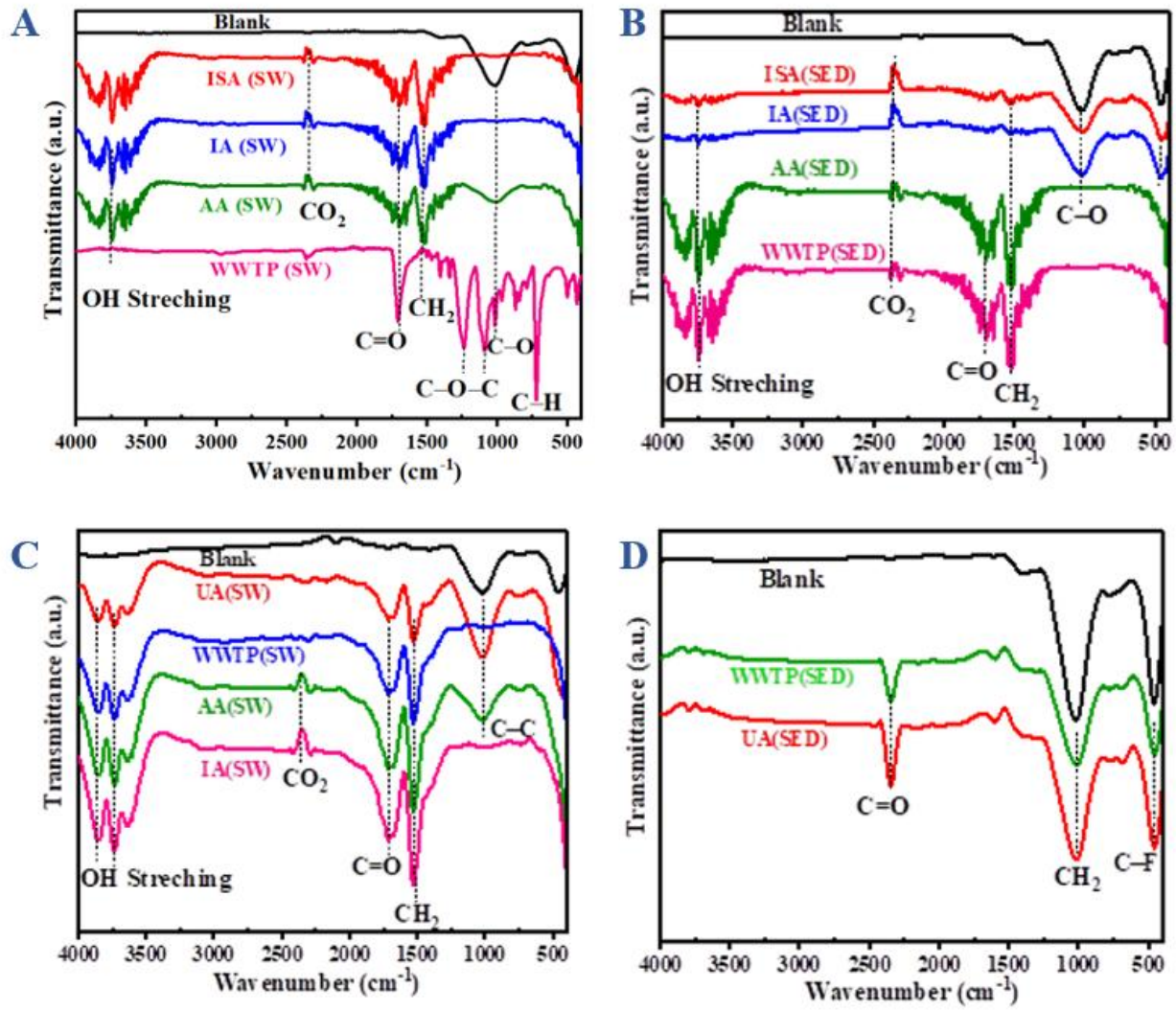

Figure 13: ATR-FTIR analysis for the Swartkops River: (A) Surface water samples and (B) Sediment samples; for the Msunduzi River: (C) Surface water samples and (D) Sediment samples.

4.7.3 ATR-FTIR data analysis of samples collected from sites near the Msunduzi rivers for MP detection

4.7.3.1 Surface water samples analysis from various active sites near the Msunduzi River

The MP detected in the Msunduzi River analysed by ATR-FTIR in surface water samples collected from various active sites showed the various functional groups indicating the significant presence of MPs (Figure 13C). The spectral band in the UA sample near 1002 cm^{-1} is typically associated with C–C stretching vibrations in aliphatic compounds, which could be observed in Heptacosane or Nonacos-1-ene. While the spectral band 1509 cm^{-1} corresponds to C=C bending or aromatic skeletal vibrations in aromatic compounds, possibly linked to Benzene and Ethenyl-Benzaldehyde. Another intense peak near 1702 cm^{-1} indicative of C=O stretching, which is characteristic of

carbonyl compounds like esters or aldehydes corresponding to compound 1,30-Triacontanediol. The spectral band in the WWTP sample near 1509 cm^{-1} is typically associated with the C=C stretching vibrations in aromatic compounds, indicating the presence of a conjugated system, common in benzene and its derivatives. The spectral band near 1509 cm^{-1} is typically associated with the C=O stretching vibrations, suggesting the presence of carbonyl groups, which could be linked to compounds like benzaldehyde.

ATR-FTIR spectra of the AA site sample showed intense peaks near 1002 cm^{-1}, 1509 cm^{-1}, 1702 cm^{-1}, and 3750 cm^{-1}. The peak at approximately 1002 cm^{-1} is typically associated with C–H bending vibrations, while the peak around 1509 cm^{-1} often corresponds to C=C stretching in alkenes and is related to Benzene, methyl- (Toluene). The peak near 1702 cm^{-1} can be attributed to the carbonyl (C=O) stretching of aldehydes such as benzaldehyde. Lastly, the peak at 3750 cm^{-1} may indicate the presence of hydroxyl groups (–OH) in compounds related to the presence of Ethenyl-2,4-Hexadiyne.

ATR-FTIR spectral band 1509 cm^{-1} is typically associated with C=C stretching vibrations in alkenes (like 1-heptadecene) or could be related to aromatic compounds. Another band near 1702 cm^{-1} associated by carbonyl (C=O) stretching vibrations, which is often seen in aldehydes, ketones, or carboxylic acids. It may correspond to 1-hexanol, 2-ethyl- or similar compounds with carbonyl functional groups. The spectral band near 3750 cm^{-1} indicative of O-H stretching vibrations, typical for alcohols (like 1-hexanol, 2-ethyl-) or phenolic compounds.

4.7.3.2 Sediment samples analysis from various active sites near the Msunduzi River

ATR-FTIR analysis of sediment samples from AA and WWTP sites of Msunduzi River showed significant peaks corresponding to various functional groups (Figure 13D). The common spectral band in WWTP and AA sites near 1092 cm^{-1} is typically related to the C-O stretching vibrations, which can be present in Heneicosyl heptafluorobutyrate (due to the ester functional group) and also in long-chain hydrocarbons. A spectral band near 470 cm^{-1} indicates out-of-plane bending vibrations, possibly associated with alkyl chains or certain halogenated compounds. But here it is related to halogenated compounds Heneicosyl heptafluorobutyrate. A spectral band near 2340 cm^{-1} typically represents the C≡C stretching vibrations or may indicate the presence of carbon dioxide (CO_2) if it's a broader band. In the context of your compounds, it could relate to the presence of unsaturated bonds in 1,19-Eicosadiene. The peaks near 470 cm^{-1} and 1092 cm^{-1} are likely linked to long-chain alkanes like Hexacosane or Octacosane, Tetratetracontane. Long-chain alkanes often

exhibit such low-energy vibrations due to their structure. The peak at 2340 cm^{-1} may not be directly associated with the compounds listed but could indicate the presence of ambient CO_2.

4.8 Profiling of microbial community associated with MPs and seasonal variations in microbial community composition in Msunduzi River system

The present study explored the differences in bacterial community composition and diversity between the surface water and plastisphere in a riverine ecosystem, with different pollution sources. The adequacy of sampling was estimated through a rarefaction curve, and the results showed an exhaustive sampling with the populations containing most of the microbial communities from each sampling site. Surface water comprised significantly (Wilcoxon, $p = 0.0012$) higher microbial communities compared to the plastisphere (Figure 14a). This difference was consistent when microbial richness was calculated for different sampling sites, such as Site 1, Site 2, Site 3 and Site 4 (Figure 14b) (Kruskal-Wallis, $p = 0.00011$). Overall, on average, surface water harboured about 7% higher bacterial taxa than the plastisphere. Bray–Curtis based cluster analysis between the samples revealed that the bacterial communities in the surface water and plastisphere from different sites formed two separate clusters. Principal coordinated analysis (PCoA) revealed that the microbial community composition in plastisphere and surface water differed significantly ($p < 0.05$) in the first and second dimension for both sampling sites (Figure 20a), and habitat (surface water and plastic) (Figure 14b). Permutational multivariate analysis of variance) also showed significant differences in community composition both between the sites (PERMANOVA $F = 4.5709$; $R^2 = 0.13$, $p < 0.001$) and habitat (PERMANOVA $F = 16.386$; $R^2 = 0.15$, $p < 0.001$). Geographic proximity calculated in terms of beta-diversity also exerted a significant effect on microbial communities, with different samples clustering based on their sites and habitat (Figure 21a). The major bacterial phyla also showed significant ($p < 0.05$) differences both between sites and habitats (Figure 15).

The major bacterial phyla detected were Proteobacteria, Bacteroidetes, Actinobacteria, Firmicutes, Cyanobacteria (Figure 16a). Moreover, a significant difference ($p < 0.05$) was observed in the relative abundances of Proteobacteria, Acidobacteria, Fusobacteria, Bacteroidetes, and Actinobacteria both between the sites, habitat (plastisphere and surface water) and season (winter and summer) (Figure 16b).

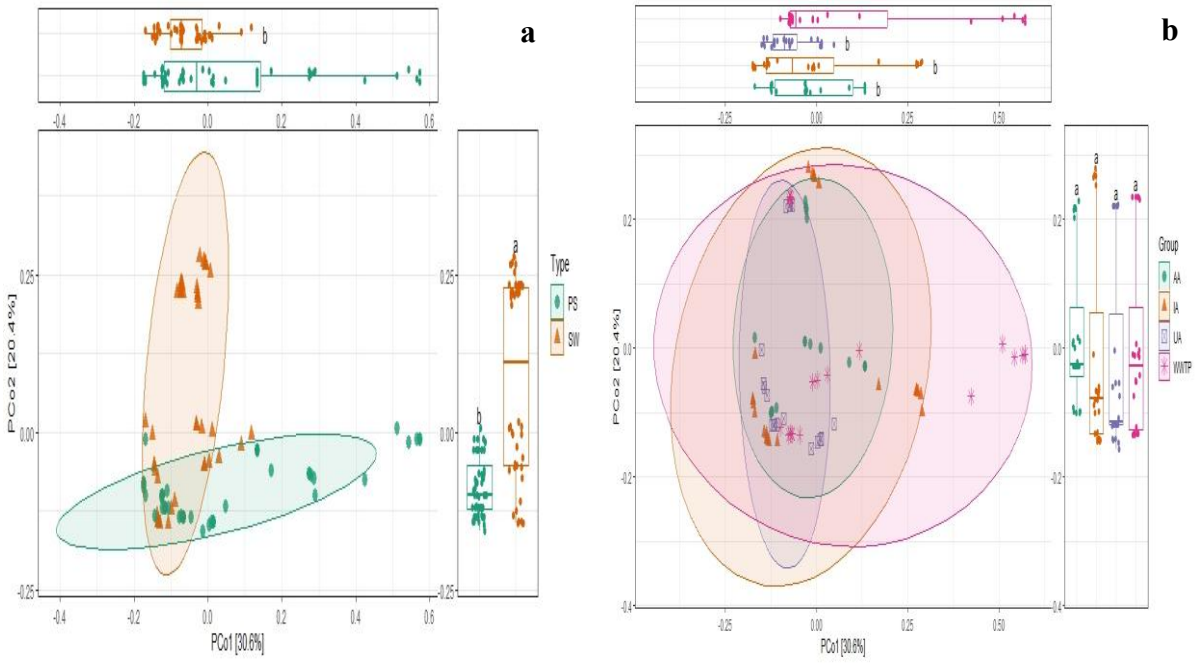

Figure 14. Bacterial community composition in surface water and plastisphere: a) habitats (surface-water and Plastisphere) and b) Principal coordinate analysis showing significantly distinct microbial community between different sampling sites (PERMANOVA)

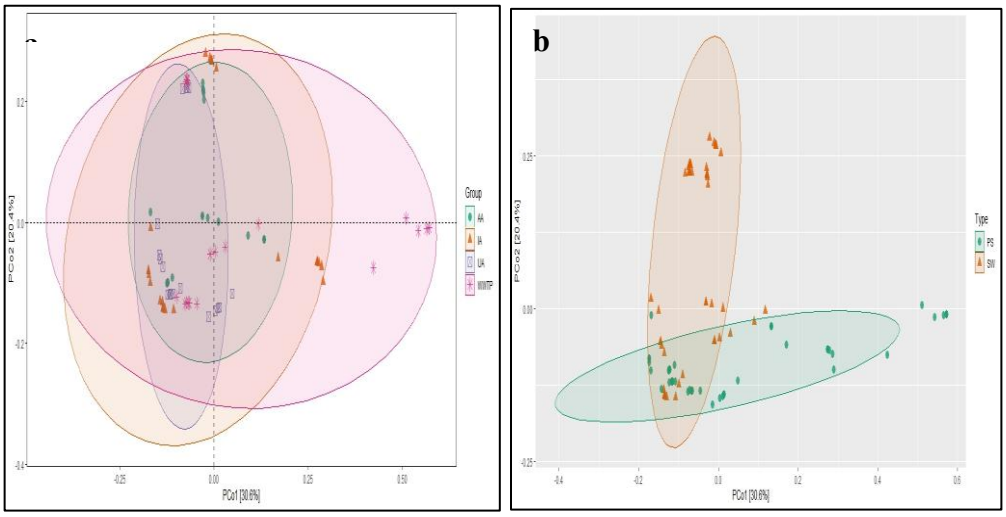

Figure 15: Changes in microbial community structure and composition: PCOA analysis depicting differences microbial communities, (a) across sites, (b) habitats (surface-water and plastisphere)

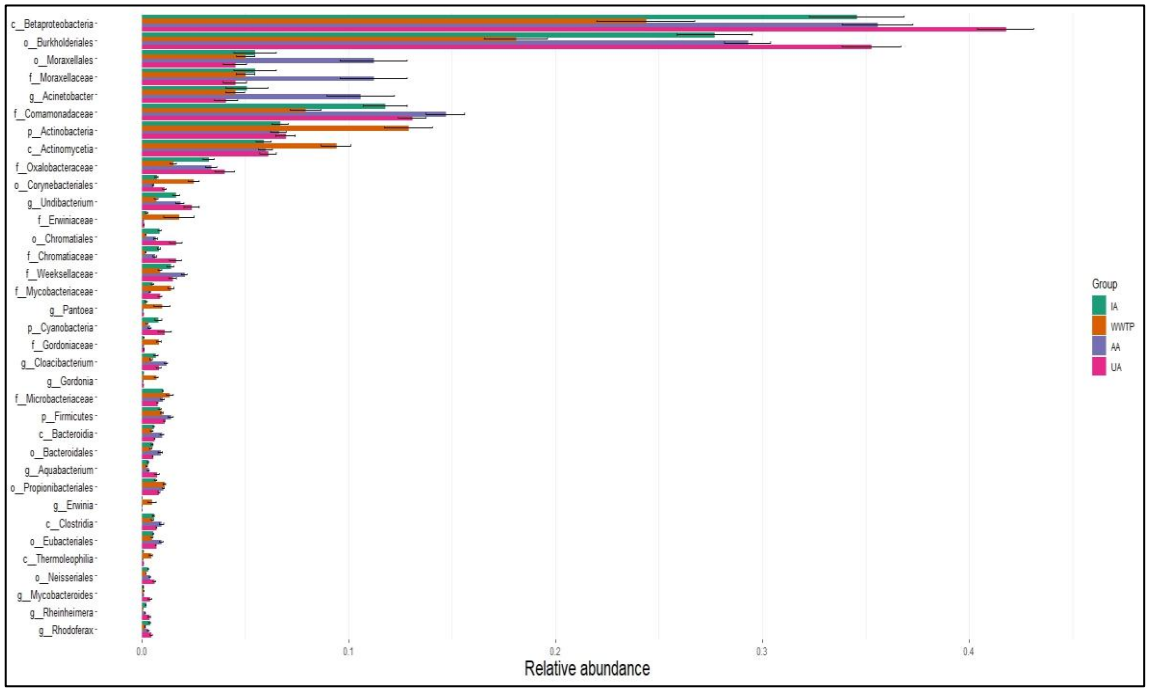

Figure 16a: Bar plot showing the relative abundance of bacterial communities across different sampling sites ($p < 0.05$)

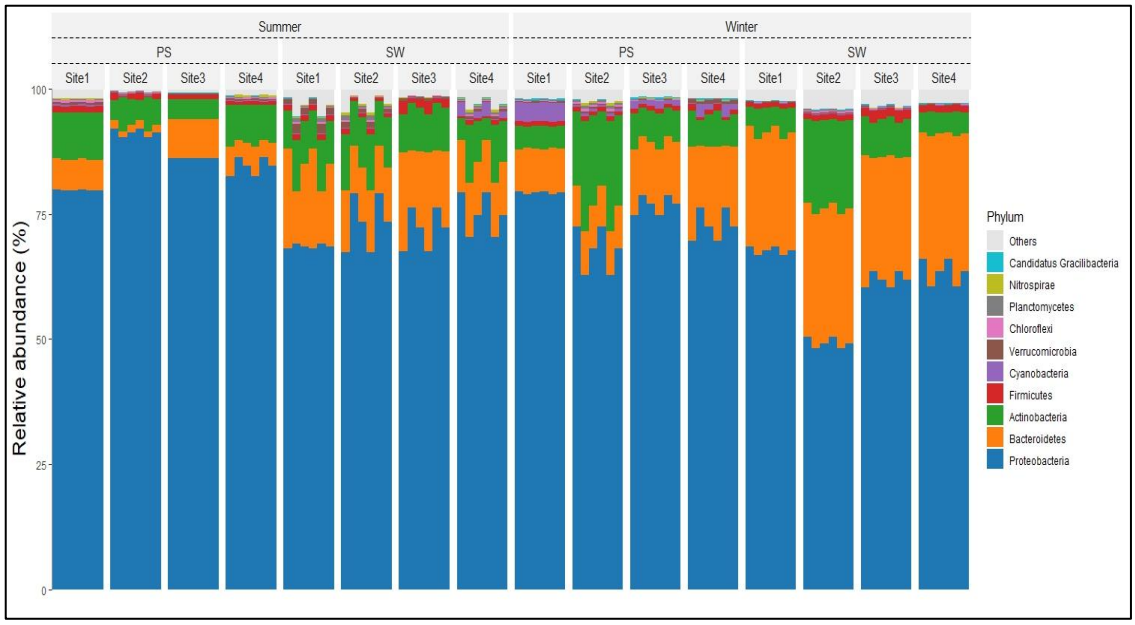

Figure 16b: Bar plot showing the relative abundance of bacterial communities across the sampling sites, habitats and season

4.9. The Unique, differentially enriched microbial taxa and biomarkers of surface water and plastisphere

Differences in community structure was estimated between the surface water and plastisphere. LEfSe analysis (LDA >3) was used to identify the differentially abundant taxa that varied between the sampling, habitat and season. First, the LEfSe analysis identified 20 discriminative bacterial taxa with significant ($p < 0.001$) variations in their relative abundance between the sites (IA, UA, WWTP and AA), habitat (surface water and plastisphere) and season (summer and winter). The samples from WWTP site were differentially enriched with Actinobacteria, Actionomycteia, Corynebacteriales, Micrococcales, Erwiniaceae and Mycobacteriaceae (Figure 22a). On the other hand, the samples from IA group, exhibited a significant presence of only 1 genus (Undibacterium), while as samples from AA site showed the significant presence of Comamonadaceae, Moraxellaceae, Weeksellaceae, Moraxellales, Actinobacter (Figure 17). Similarly, the samples from UA exhibited the presence of Betaproteobacteria, Oxalobacteraceae, Chromitiaceae, Sphaerotilus, Burkholderiales, Chromatiales, Sphaerotius, and Acidovorax (Figure 17b). In case of habitat and season, LEfSe analysis showed the presence of unique bacterial taxa in both surface water and plastisphere and summer and winter seasons and these taxa accounted for a considerable proportion (Figure 17c). In case of habitat, surface water recruited more unique taxa (52) than the plastisphere (21) and found a significant difference ($p < 0.05$) with surface water enriched bacterial groups out-numbering the plastisphere enriched taxa. Additionally, we employed a statistical and machine- learning based random-forest model level to find the most significant features distinguishing the microbial communities in sampling sites and in habitat. The top fifteen taxa at genus level with an accuracy rate of 99.97% were selected as biomarkers to differentiate both between the sites and the habitats. Among the identified biomarkers most of the taxa were significantly higher in surface water compared to plastisphere.

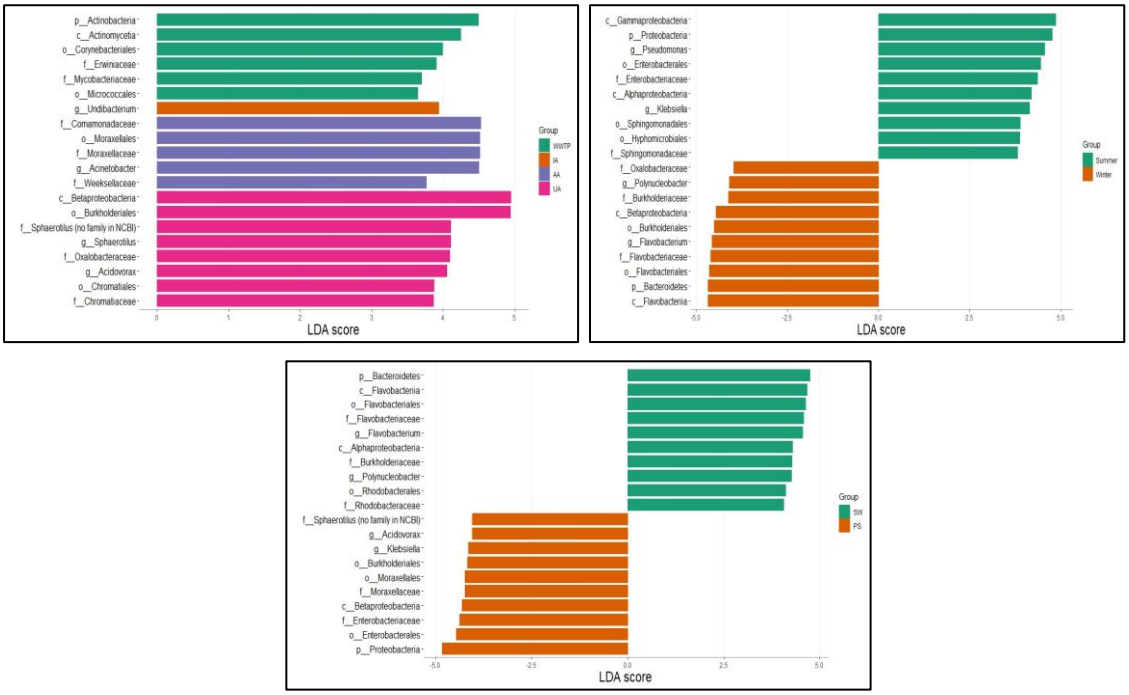

Figure 17: Differential characteristics of microbiome between different: a) sampling sites; b) habitats (surface-water and plastisphere) and c) seasons (summer vs winter)

4.10 Functional diversity of surface water and plastisphere microbiome

First, we analysed the functional profiles of the identified microbial communities by using FAPROTAX. The analysis revealed significant differences ($p < 0.05$) in the relative abundance of key microbial functions between different pollution sites. These differences were consistent when microbial functional composition was observed between different habitats, such as surface water and plastisphere ($p < 0.05$). The key microbial functions included are related to biogeochemical cycling such as carbon, sulphur and nitrogen, pathogenicity, xenobiotic degradation. In addition to these ecologically relevant functions, we characterized the functional profiles of surface water and plastisphere microbiome. Therefore, using the KEGG and COG-based pathway enrichment analysis, the functional potential of the microbial communities between the different sampling sites and habitats (surface water and plastisphere) was annotated to evaluate the impact of different pollution sources and microbial community changes on different metabolic functions (Figure 18a-d). The KEGG and COG-based annotations revealed significant variations in the relative abundance of different genes and their associated pathways both across the sampling sites and habitats. Overall, the relative abundance of the enzymatic genes (EC) retrieved from the KEGG database across the sampling sites and habitats are presented in (Figure 18a-d). We observed

significant variations in the relative abundance of key functional enzymes (Fig 18a-b), with a clear separation between the sampling sites and habitat in NMDS analysis (UA vs. WWTP, Anosim, p = 0.01; UA vs. AA, Anosim, p = 0.006; UA vs. IA, Anosim, p = 0.151; WWTP vs. AA, Anosim, p = 0.01; WWTP vs. IA, Anosim, p = 0.10; AA vs. IA, Anosim, p = 0.087) and between the habitats (SW vs. PS, Anosim, p = 0.001). To observe the key functional differences across the sampling locations and between the habitats, we looked for the differentially abundant pathways associated with the identified enzymes. Significant variations were observed in functional pathways all the samples were interspersed with significant differences between the both between the sampling locations and habitat in NMDS analysis ((UA vs. WWTP, Anosim, p = 0.006; UA vs. AA, Anosim, p = 0.05; UA vs. IA, Anosim, p = 0.13; WWTP vs. AA, Anosim, p = 0.006; WWTP vs. IA, Anosim, p = 0.01; AA vs. IA, Anosim, p = 0.09) and between the habitats (SW vs. PS, Anosim, p = 0.001). The major pathways were associated with amino acid transport and metabolism, energy production and conversion, transport and metabolism of ions, signal transduction, lipid metabolism, metabolism and transport of nucleotides, biosynthesis, and transport of secondary metabolites, sugar metabolism, defence mechanisms, transcription, signal transduction, cell motility and secretion, biogenesis etc.

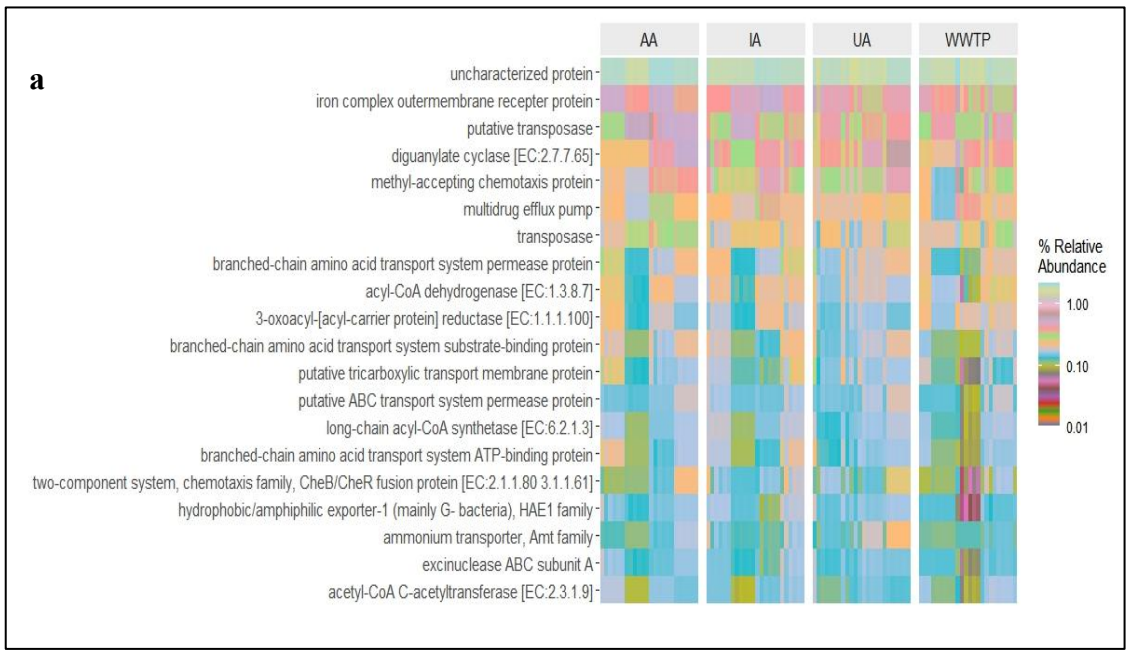

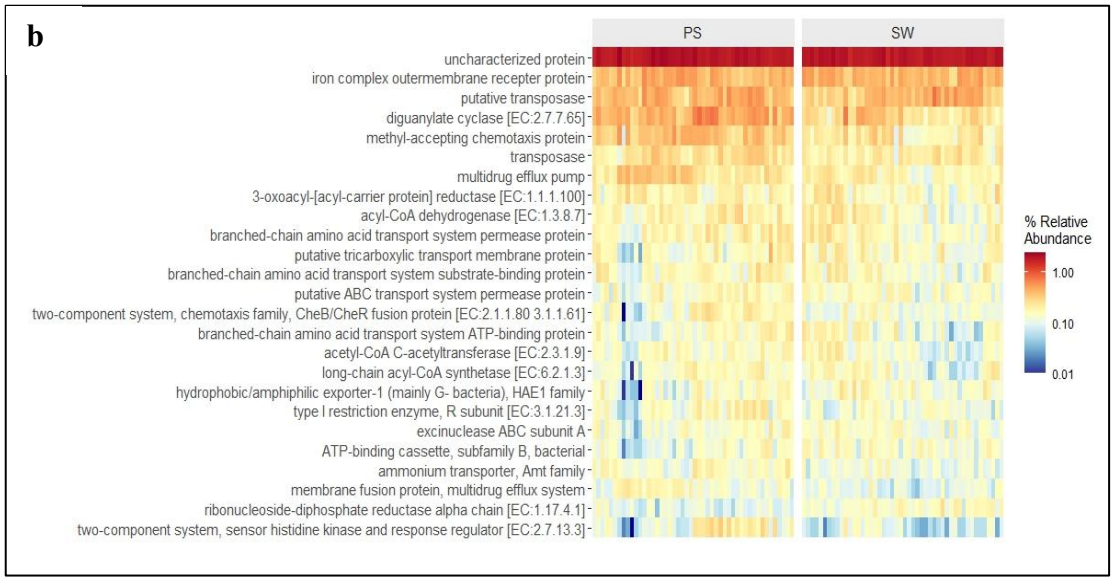

Figure 18a: Overview of functional gene abundances. Relative abundance of the 20 most abundant KEGG pathways across: a) different sampling sites, b) across habitats (surface water: SW) and plastisphere PS); and

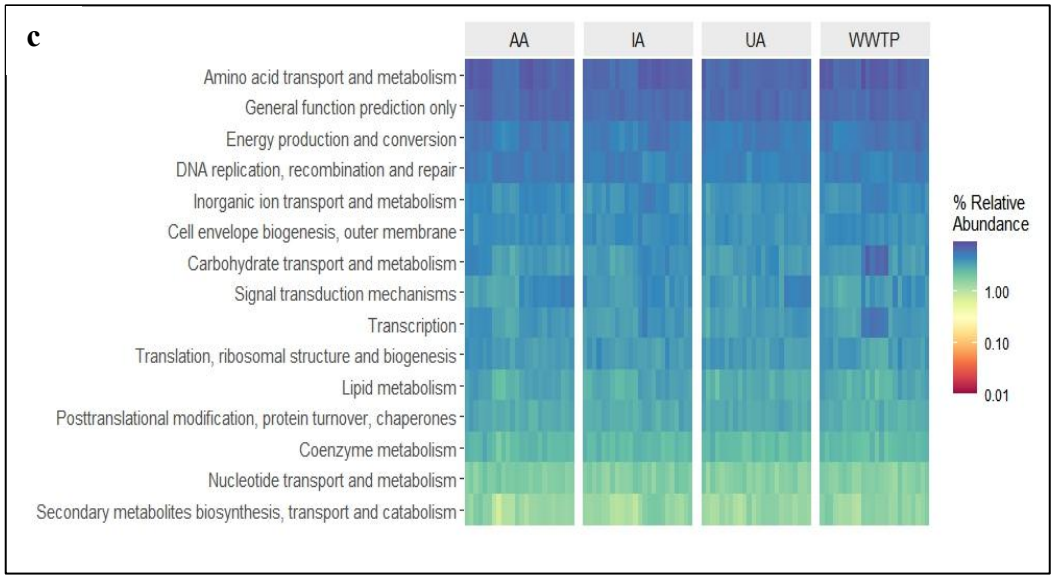

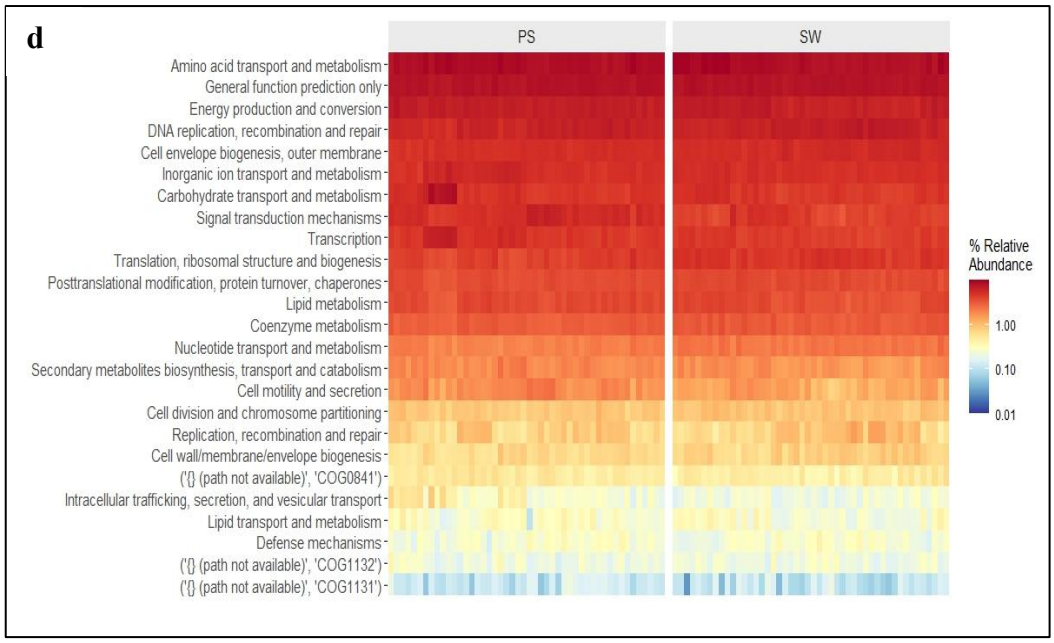

Fig 18b Relative abundance of the 25 most abundant COG genes: c) across different sampling sites and d) across habitats (surface water: SW and plastisphere: PS)

4.11 Factors shaping surface water and plastisphere microbiome

Using the distance decay model and accounting for experimental variables, we tested whether microbial richness was associated with pollution sources. For all the sites the model revealed that microbial communities in plastisphere and surrounding environments is significantly positively associated with the type and source of pollution (UA: $R^2 = 0.83$, $p = 0.015$; WWTP = $R^2 = 0.88$, $p = 0.0072$, AA: $R^2 = 0.85$, $p = 0.0075$, IA: $R^2 = 0.95$, $p = 0.0011$) (Figure 25a-d). Moreover, bray-Curtis dissimilarity analysis showed that expect pH all environmental factors also affected microbial community structure and composition both across the sites and habitat. To further explore the key environmental drivers for microbiome in surface water and plastisphere, Mantel analysis was performed to elucidate which environmental factors were significantly related to microbial community (Figure 19). Results showed that temperature, dissolved oxygen, pH, salinity, total dissolved solids and specific conductivity had a significant effect on microbial community both across the sampling sites and habitats (Figure 20).

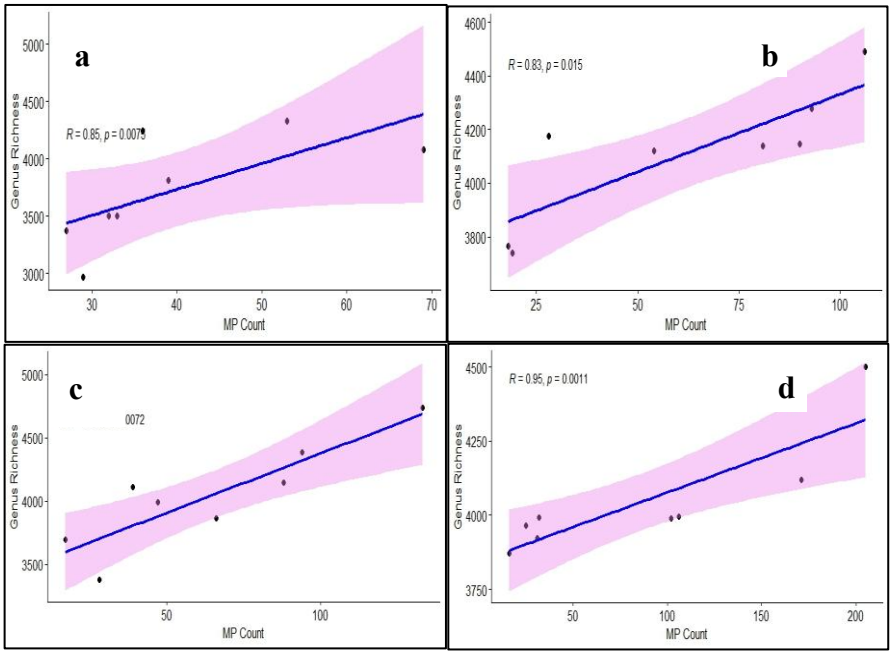

Figure 19: Correlation between MP (MP) and microbial diversity. Each dot represents a sample (a) Urban area (UA), (b) wastewater treatment plant (WWTP), (c) agricultural area (AA), (d) industrial area (IA)

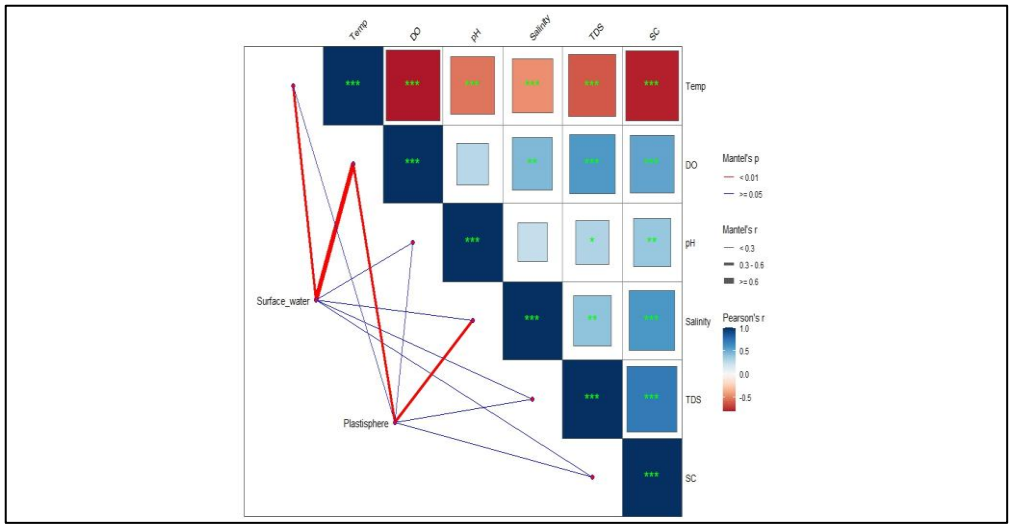

Figure 20: Drivers of microbial communities in surface water and plastisphere. Mantel analysis showing the correlation between key environmental variables and bacterial community composition.

4.12 Profiling of microbial community associated with MPs and seasonal variations in microbial community composition in Swartkops River system

Similar to Msunduzi River, the surface water in Swartkops River comprised significantly (Wilcoxon, $p = 0.018$) higher microbial diversity than plastisphere (Figure 21). The difference was consistent when the microbial diversity was estimated across the different sampling sites, such as UA, WWTP, IA and AA (Figure 21b) (Kruskal-Wallis, $p = 0.03$). Beta diversity using Bray-Curti's dissimilarity analysis between the samples showed that the microbial diversity in surface water and plastisphere from different sampling sites formed two separate clusters. Principal coordinated analysis (PCoA) also explained difference in microbial community composition in the first and second dimension of the plot both across the sampling sites and in the first and second dimension (Figure 21a), and habitat (surface water and plastic) ($p < 0.05$) (Figure 21b). PERMANOVA also showed significant differences in microbial community across the sites (PERMANOVA $F = 3.82$; $R^2 = 0.19$, $p < 0.003$) and habitat (PERMANOVA $F = 18.86$; $R^2 = 0.35$, $p < 0.0009$). Geographic proximity estimated in terms of beta-diversity was found to have a significant impact on microbial communities, with samples clustering based on their sites/ pollution sources and habitat (SW and PS). The major phyla also revealed significant ($p < 0.05$) differences both across the sampling sites and habitat (Figure 22a). The major bacterial phyla detected were Proteobacteria, Bacteroidetes, Actinobacteria, Chloroflexi, Verrucomicrobia, and Cyanobacteria (Figure 22a). Moreover, a significant difference ($p < 0.05$) was observed in the relative abundances of Proteobacteria,

Bacteroidetes, Actinobacteria, and Cyanobacteria, both between the sites, habitat (plastisphere and surface water) and season (winter and summer) (Figure 22b).

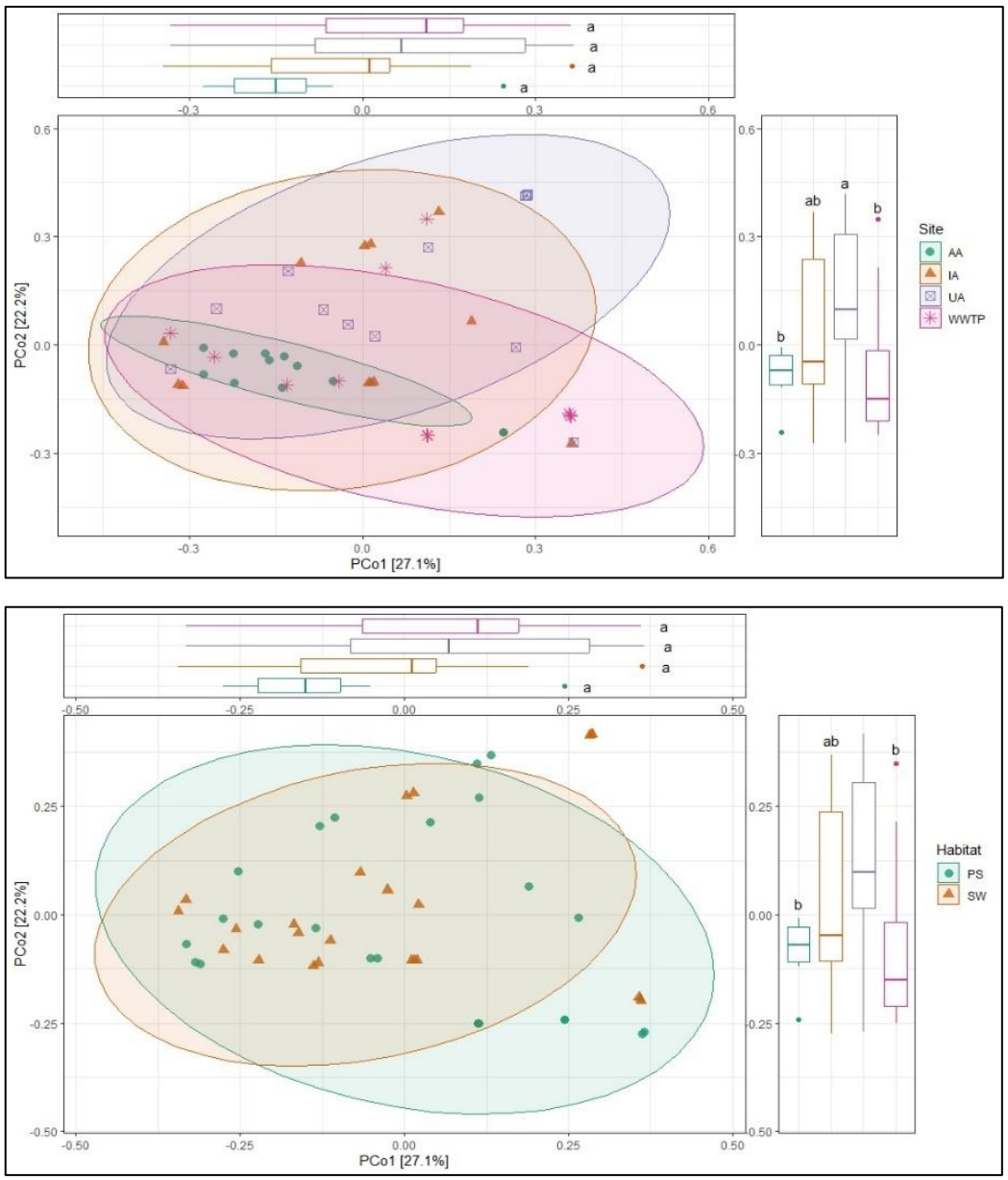

Figure 21**:** Microbial community composition in surface water and plastisphere: a) across sampling sites and b) habitats (SW and PS). Principal coordinate analysis showing significantly distinct microbial communities between different sampling sites (PERMANOVA). (c and d) showing Changes in microbial community structure and composition: PCOA analysis depicting differences in microbial communities, (c) across sites, (d) habitats (surface-water and plastisphere).

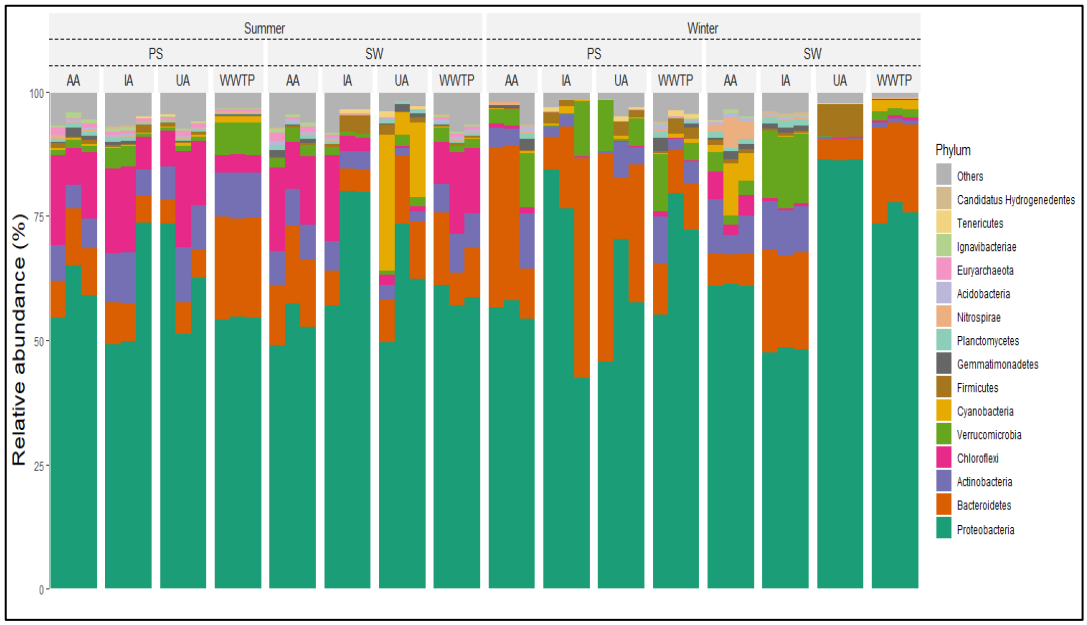

Figure 22a: Bar plot showing the relative abundance of bacterial communities across different sampling sites ($p < 0.05$)

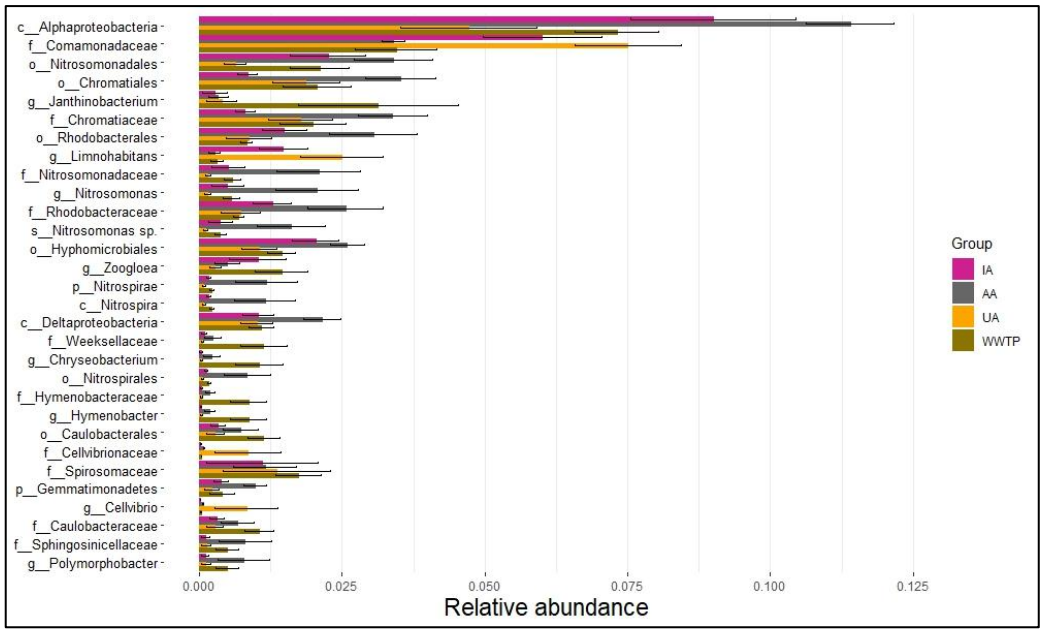

Figure 22b: Bar plot showing the relative abundance of bacterial communities across the sampling sites.

4.13 Unique and differentially abundant microbial communities in Swartkops River system

Differences in microbial community structure were evaluated between surface water and plastisphere. LEfSe analysis (LDA >3) was used to identify the differentially enriched microbial taxa that varied between the sampling sites, habitat and season. LEfSe analysis identified different

bacterial taxa with significant ($p < 0.05$) variations in relative abundance between the sampling sites (UA, WWTP, IA and AA), habitat (surface water and plastisphere) and season (summer and winter). The samples from IA and UA site were differentially enriched with Alphaproteobacteria, Nitrosomonadales, Chromatiales, Chromatiaceae, Rhodobacterales, Nitrosomonadaceae, and Nitrosomonas (Figure 23a). On the other hand, the samples from AA group showed a significant presence of Janthinobacterium, Zoogloea, Weeksellaceae, Chryseobacterium, while samples from WWTP site exhibited the significant presence of Comamonadaceae, and Limnohabitans (Figure 29a). Similarly, in the case of habitat and season, LEfSe analysis showed the presence of unique bacterial taxa in both surface water and plastisphere and summer and winter seasons, accounting for a considerable proportion (Figure 23). In the case of habitat, surface water was significantly enriched with unique taxa (21) than the plastisphere (9) ($p < 0.05$). Similarly, the summer season was significantly enriched with unique taxa (22) than the winter season (7) ($p < 0.05$). Overall, from the results, it was observed that surface water had significantly enriched with unique microbial taxa than the plastisphere ($p < 0.05$).

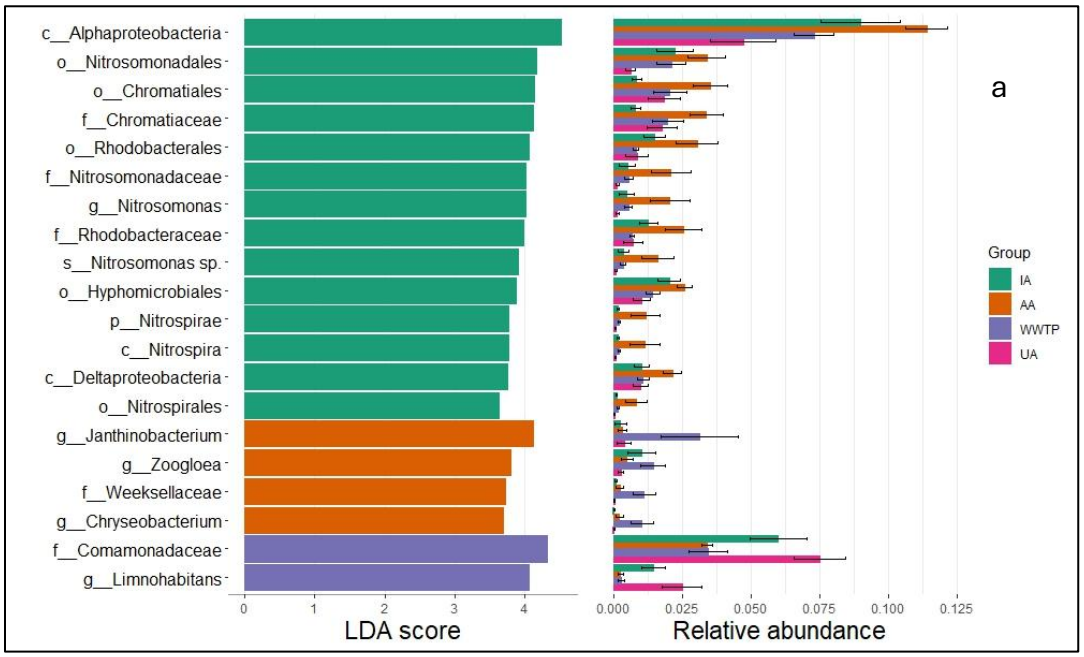

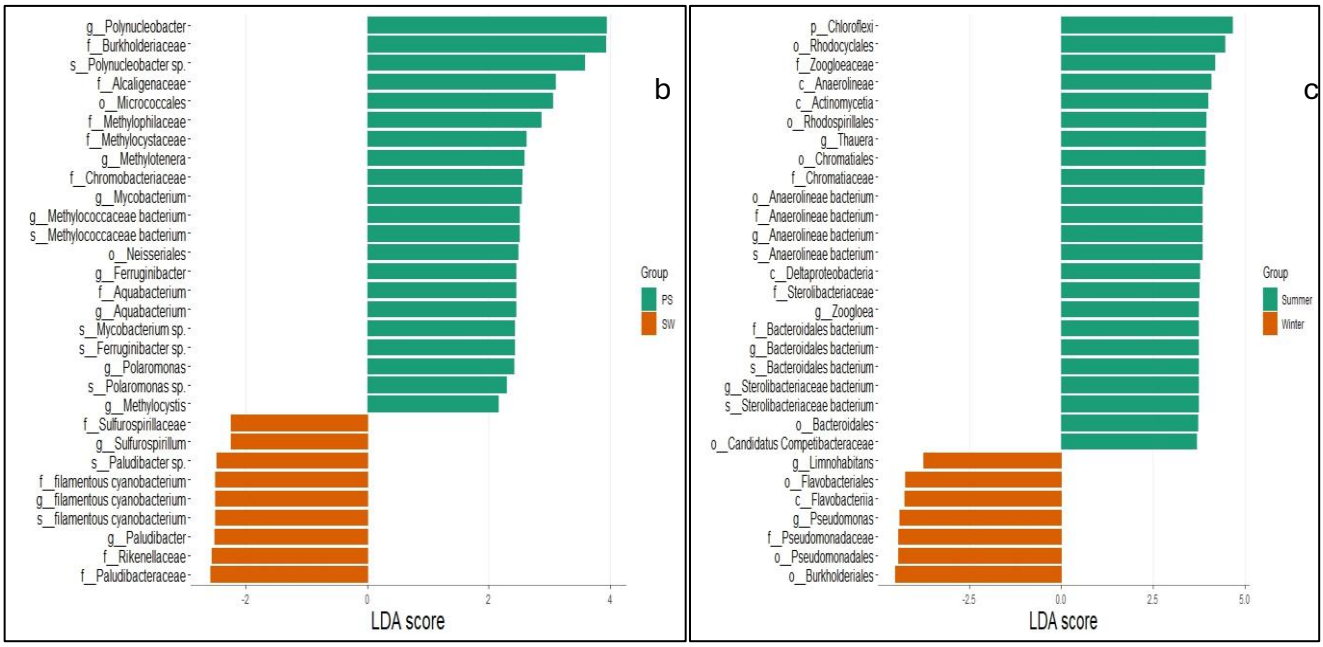

Figure 23: Differential characteristics of microbiome between different: a) sampling sites; b) habitats (surface-water and plastisphere) and c) seasons (summer vs winter)

4.14 Functional diversity of surface water and plastisphere microbiome in Swartkops River

The functional potential of microbial communities was annotated using KEGG and COG databases and presented as heatmaps (Figure 24a, b). The results revealed significant ($p < 0.05$) variations in the relative abundances of functional genes and their associated pathways both across the sampling sites and habitats (Figure 24a). The major pathways identified were associated with general functions prediction, amino acid transport and metabolism, energy production and conversion, DNA replication, recombination and repair, cell envelope biogenesis and outer membrane, signal transduction mechanism, nucleotide transport and metabolism, coenzyme metabolism, carbohydrates, and ions metabolism, nucleotides and lipid metabolism, transcription, biosynthesis, and transport of secondary metabolites, defence mechanisms, energy production and conversion (figure 24a). From the results, a significant variation in the relative abundance of key functional enzymes (figure 24b), with a clear separation between the sampling sites and habitat in NMDS analysis (UA vs. WWTP, Anosim, $p = 0.004$; UA vs. AA, Anosim, $p = 0.002$; UA vs. IA, Anosim, $p = 0.021$; WWTP vs. AA, Anosim, $p = 0.009$; WWTP vs. IA, Anosim, $p = 0.09$; AA vs. IA, Anosim, $p = 0.0028$) and between the habitats (SW vs. PS, Anosim, $p = 0.003$). Significant variations were also observed in functional pathways all the samples were interspersed with significant differences between the both between the sampling locations and habitat in NMDS analysis ((UA vs. WWTP, Anosim, $p = 0.0009$; UA vs. AA, Anosim, $p = 0.0004$; UA vs. IA, Anosim, $p = 0.13$; WWTP vs. AA, Anosim, $p = 0.006$; WWTP vs. IA, Anosim, $p = 0.001$; AA vs.

IA, Anosim, p = 0.0003) and between the habitats (SW vs. PS, Anosim, p = 0.0002). The major pathways were associated with genetic information processing, signalling, cellular processes and transporters, metabolism and carbohydrate metabolism, environmental information processing and signal transduction and two component system, metabolism of nucleotides, energy production and conversion, transport and metabolism of ions, signal transduction, lipid metabolism, metabolism and transport of nucleotides, biosynthesis, and transport of secondary metabolites, sugar metabolism, defence mechanisms, transcription, signal transduction, cell motility and secretion, biogenesis etc.

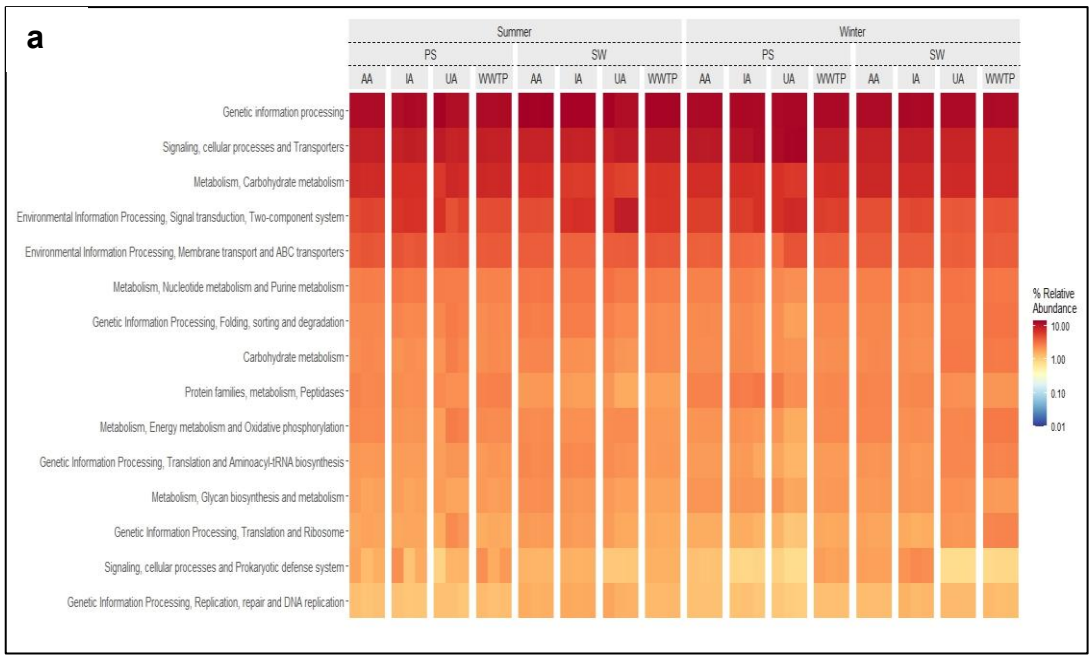

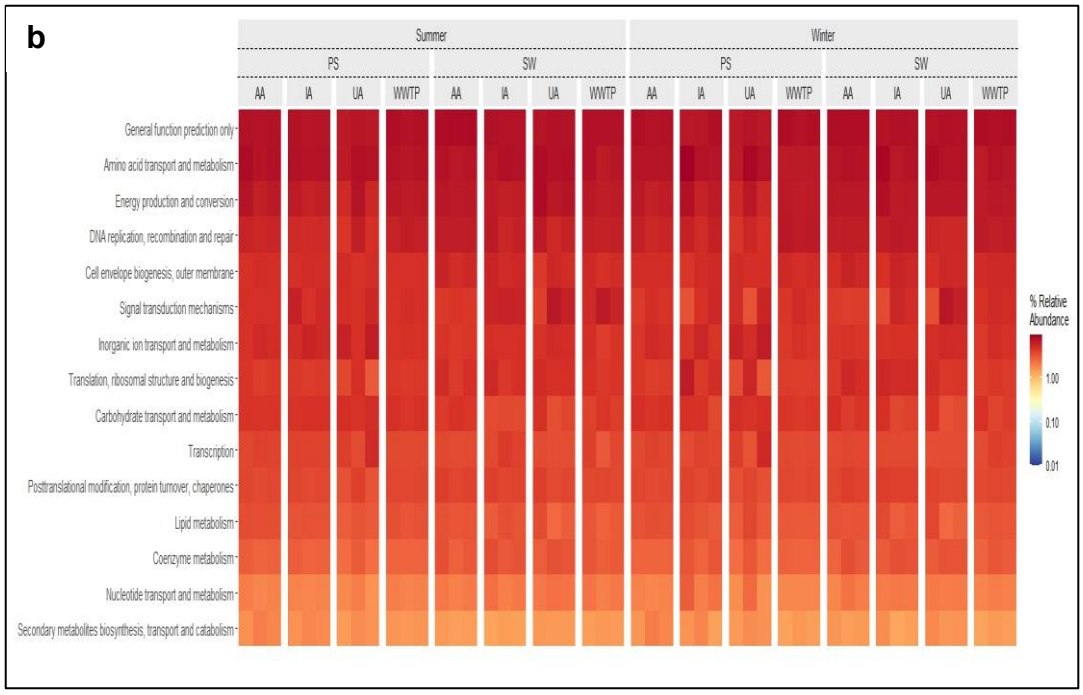

Figure 24: Overview of functional gene abundances. Relative abundance of the 15 most abundant KEGG pathways across: a) different sampling sites, b) across habitats (surface water: SW) and plastisphere PS)

4.15 Factors shaping surface water and plastisphere microbiome in Swartkops River

To evaluate the key environmental factors that shape the surface water and plastisphere microbiome in Swartkops River, we performed Mantel analysis, which elucidates the significant factors driving microbial communities (Figure 25). Results showed that temperature, turbidity, salinity, pH, salinity, had a significant effect on microbial community in surface water and plastisphere both across the sampling sites and habitats (Figure 25).

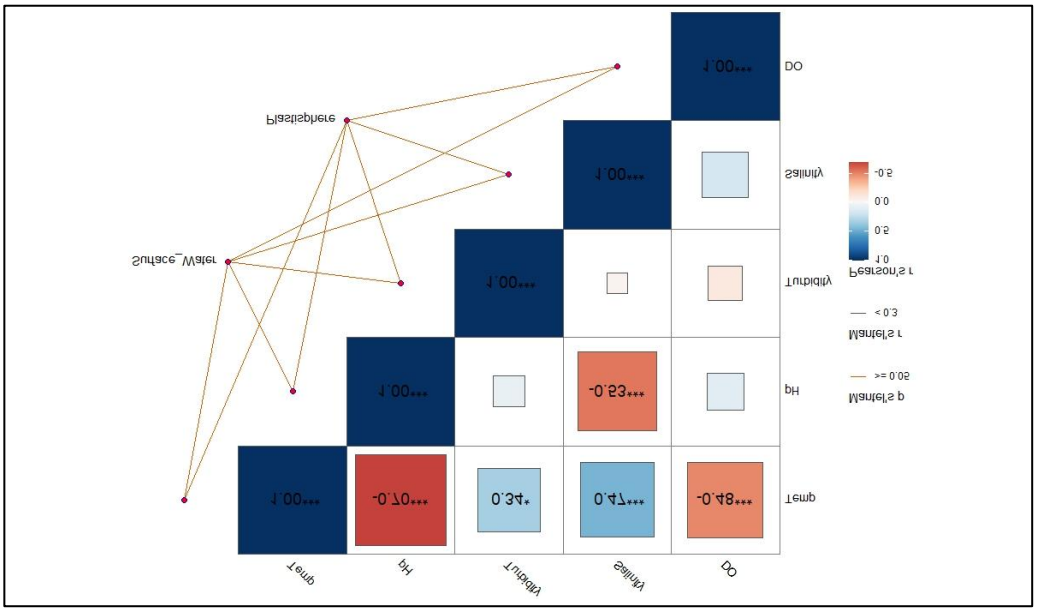

Figure 25: Mantel analysis showing the correlation between key environmental factors, bacterial community composition in surface water and plastisphere.

4.16 Metagenomic assembly and antimicrobial gene detection

See annexure 1 (Published article)

4.16 Microplastic transport model

4.16.1 Abundance of MPs

Through the sampling at the four locations over two sampling periods, a total of 3890 microparticles were detected from surface water. The highest number of MPs originated from Subcatchment 2, which is mainly industrial, followed by Subcatchment 3, which is an agricultural area, downstream of the Municipal Darvill Wastewater Treatment Works. Due to river access, sediment samples could only be taken from Subcatchment 3, and it was found that more MPs were sampled from sediments than from the water column. In terms of MP shape, fibers were dominant in surface water (65%) and pellets in sediment samples (48%). The size distribution of the MPs were categorized by sieves of 0.5, 0.18, 0.1 and 0.025 µm and resulted in surface water samples being: 33% (0.5 mm), 24% (0.18 µm), 24% (0.1 µm) and 20% (0.025 µm) and in sediment samples: 25% (0.5 µm), 28% (0.18 µm), 24% (0.1 µm) and 24% (0.025 µm). The number of MPs, categorized between winter and summer samples, is presented in Figure 26, which indicates that the concentration of MPs was higher in winter. This was due to the winter samples being taken after a large flooding event, as high discharge can induce remobilization of sediment MPs (de

Carvalho *et al.* 2022). However, the average surface water MPs in subcatchment 3 (downstream from rural townships) were constant for both sampling periods, which agrees with a study conducted by Wagner *et al.* (2019) who highlighted that MP concentrations only increased with river discharge in urban catchments when compared to rural catchments. The results also indicate that MP concentration during the flooding event was stronger in the urban and industrial catchments.

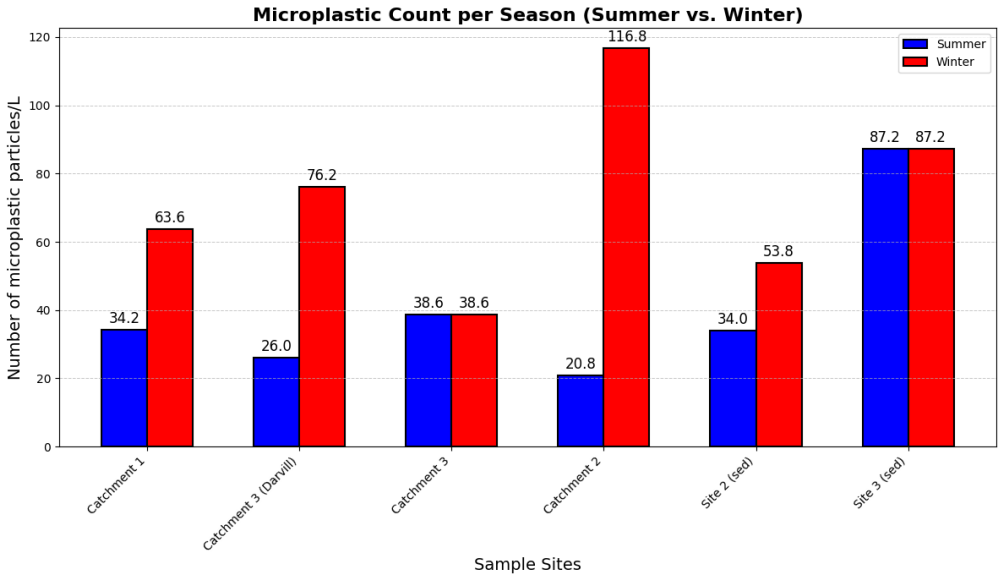

Figure 26: Number of sampled MPs per litre

4.17 Catchment hydrology

The catchment model for simulating fluxes of water through the heterogeneous landscape of the Msunduzi Catchment is presented together with a Monte Carlo (MC) analysis.

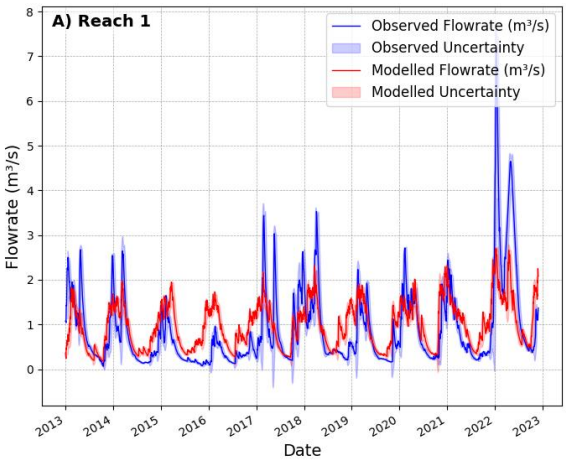
A) Reach 1
Observed Flowrate (m³/s)
Observed Uncertainty
Modelled Flowrate (m³/s)
Modelled Uncertainty
Flowrate (m³/s)
Date

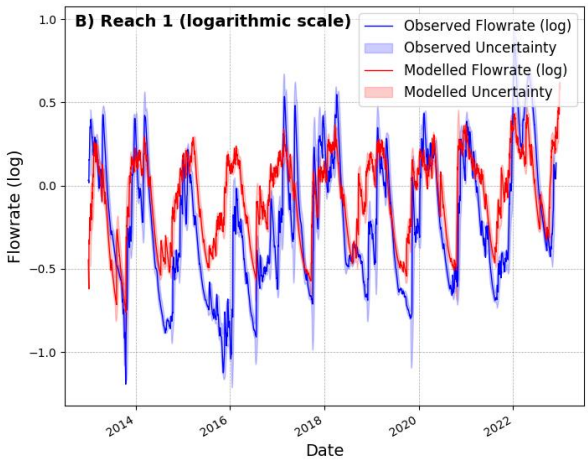
B) Reach 1 (logarithmic scale)
Observed Flowrate (log)
Observed Uncertainty
Modelled Flowrate (log)
Modelled Uncertainty
Flowrate (log)
Date

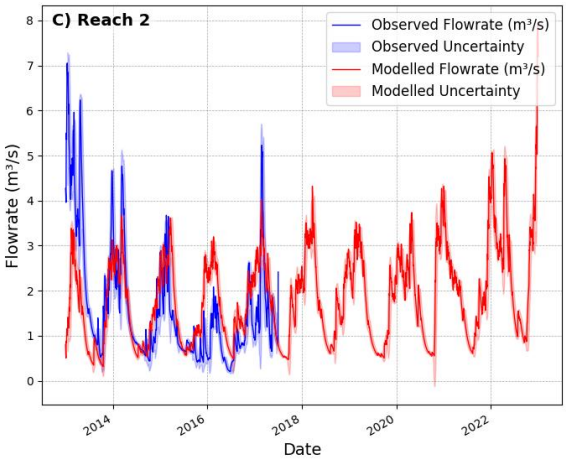
C) Reach 2
Observed Flowrate (m³/s)
Observed Uncertainty
Modelled Flowrate (m³/s)
Modelled Uncertainty
Flowrate (m³/s)
Date

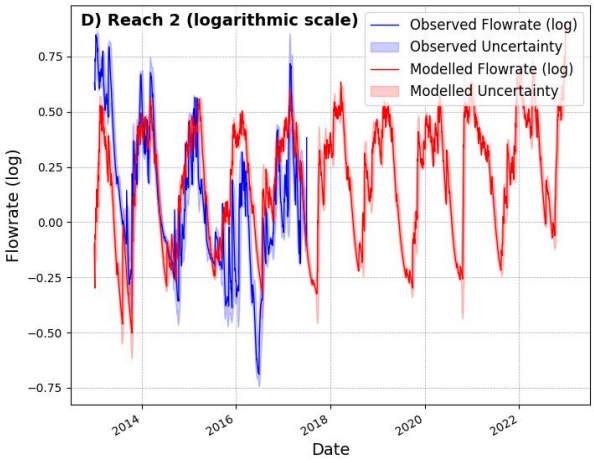
D) Reach 2 (logarithmic scale)
Observed Flowrate (log)
Observed Uncertainty
Modelled Flowrate (log)
Modelled Uncertainty
Flowrate (log)
Date

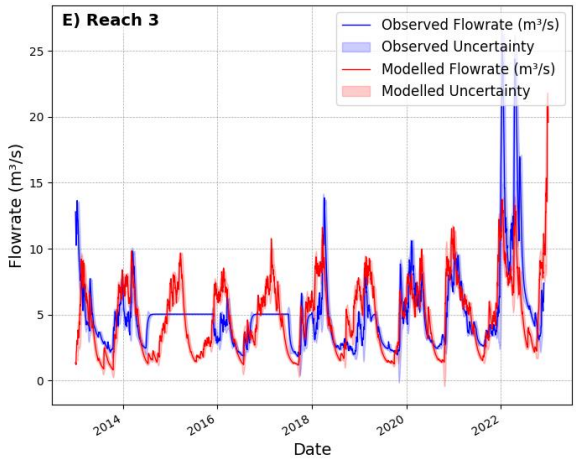
E) Reach 3
Observed Flowrate (m³/s)
Observed Uncertainty
Modelled Flowrate (m³/s)
Modelled Uncertainty
Flowrate (m³/s)
Date

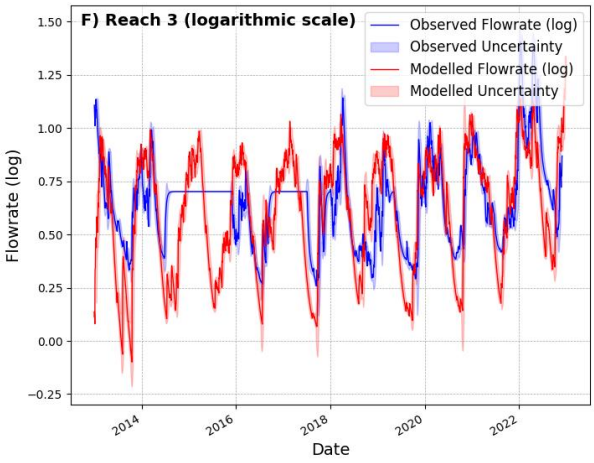
F) Reach 3 (logarithmic scale)
Observed Flowrate (log)
Observed Uncertainty
Modelled Flowrate (log)
Modelled Uncertainty
Flowrate (log)
Date

Figure 27: Plots (A), (C), and (E) represent observed and modelled flows at reach 1,2 and 3 respectively; and (B), (D), (F) represent log10 transformed observed and modelled flows at reach 1,2 and 3 respectively.

The NSE and logNS statistics for the reaches, presented in Table 15, fall in the moderate category Schober, Boer and Schwarte (2018), but there is a better fit between observed and modelled flow lower down in the catchment (reach 3). Preliminary manual calibrations indicated that the model performance was sensitive to sub-catchment-specific rainfall multipliers, which were used in the MC analysis.

Table 15*:* Calibration statistics for river water flow predictions in the three reaches. The Nash-Sutcliffe coefficient is a measure of the quality of the correlation between measured and predicted data.

Msunduzi Rive	**NSE**	**Log N-S**	**r2**
Reach 1	0.465	0.501	0.506
Reach 2	0.485	0.413	0.581
Reach 3	0.501	0.415	0.503

PERSiSt was able to reproduce the observed flow in the reaches using a time series of air temperature and precipitation, together with data on the different hydrological response types within the catchment. The INCA model framework, using quick runoff into soil water and groundwater buckets, was adequate for reproducing the observed flow patterns in the catchment. However, there may be some uncertainty in the input time series used as there were obvious errors with observed flow patterns. Model predictions did give consistent results throughout the catchment; however, prediction accuracy did increase going downstream of the catchment. This could be a result of many factors such as model structure not being appropriate for the upper locations of the catchment, or input time series and calibration data may be inaccurate. However, given that the predictions were relatively consistent and subcatchment-specific rainfall multipliers were amongst the most important parameters affecting model results, it can be concluded that the model results would be enhanced if additional timeseries per Subcatchment were used instead of single timeseries for the entire catchment. The model's under and over predictions for the certain observed years may be linked to water abstractions and wastewater discharges by local farmers and small settlements (Norling *et al.* 2024). The model performance was not affected by drought runoff fraction, indicating that low flow events do not need to be simulated for runoff estimates.

The hydrological model presented did show good simulations compared to observed data, however the modelling situation can be thought of as an inverse problem, Norling et al. (2024), in which results are simulated from incomplete data as calibrations were taken from 3 gauging stations due to data availability at internal points in the catchment not being available.

4.18 MP transport by reach

Figure 34 presents the simulated MP fluxes responding to the input scenarios described above for the three reaches in the catchment. The transport of MPs is strongly dependent on the reach flow, with intense flows causing the mobilization of larger MPs, which is visually evident in reach 3, as simulated MP peaks coincide with high flows. However, this is more evident with smaller and less dense MPs, which are transported more effectively downstream. The reach flows were also supplemented by daily runoff, as illustrated in Figure 35, which decisively contributed to reach 3 having greater MPs compared to reach 1 due to runoff being high from the built-up area of which the majority is in Subcatchment 2. The simulations of the reaches show that there is a strong hydrological control on the storage of heavier MPs within the reaches, which is influenced more by the size rather than density. The results in reach 3 also indicate that the discharge from the Municipal Darvill WWTW (flow volumes and sludge application) has a substantial increasing effect on the MP concentration volumes and their mobilization downstream, as concentration volumes are twofold compared to the upstream reaches.

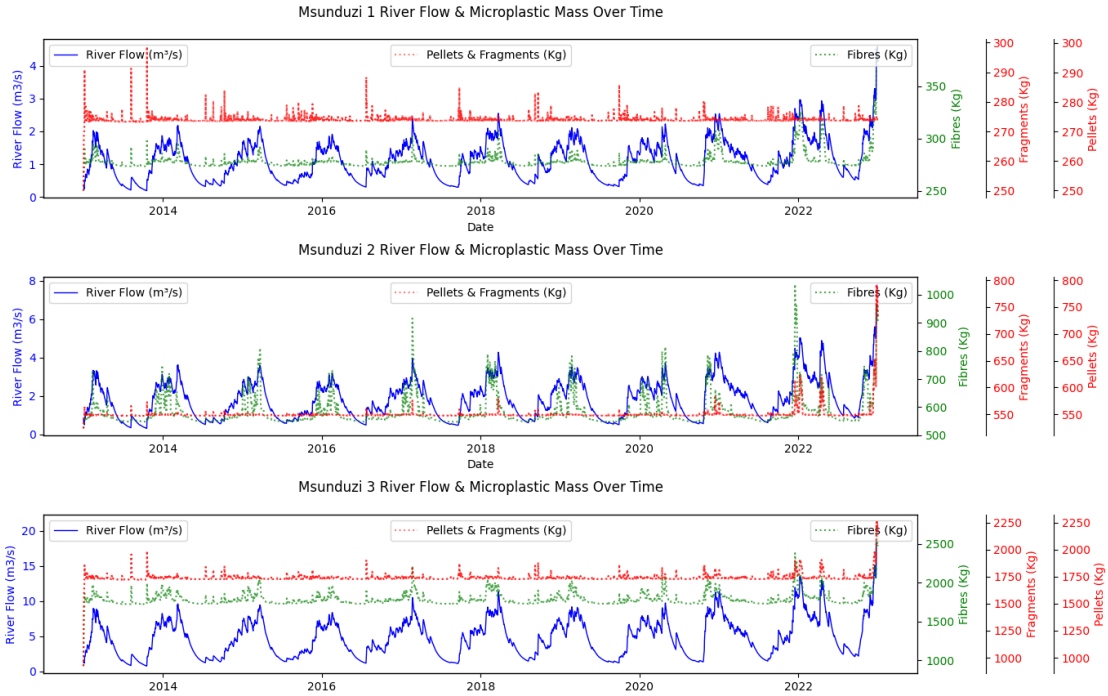

Figure 28: Simulated discharge fluxes of MPs per shape

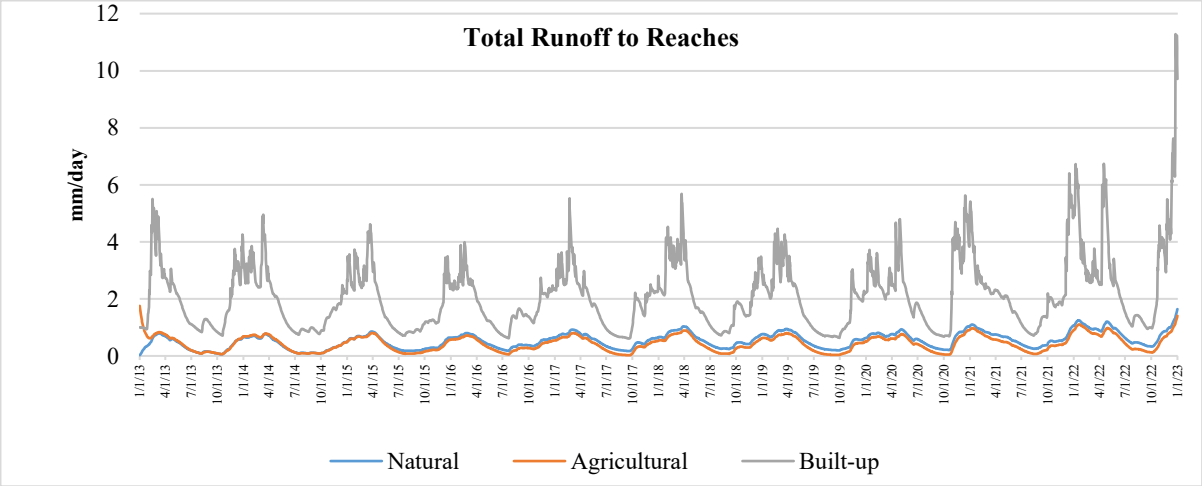

Figure 29: Total runoff to reaches due to landscape units

4.19 Assessment model predictability

Following the calibration using river hydrology datasets, the model was run to predict the MP dataset. In terms of the bed MPs, the model underestimated concentrations by a factor of 2-5, with predictions increasing towards the end of 2023, for all MP types when compared to the experimental dataset, shown in Figure 30. The underestimation can be attributed to the model not

considering biofouling of MPs, which increases its settling rate (Kaiser, Kowalski and Waniek 2017). The predicted suspended concentration, compared to the two sampled dates, varied as the winter samples (August) were collected after an intense flooding period, which resulted in all shape classes being a factor of greater than 3 when compared to the simulated concentrations. However, the winter samples (March) were relatively aligned with the simulated results. In Subcatchment 1, pellets were the most accurately predicted, being within a factor of 2. Fibers were the least accurately predicted, being within a factor of 6. Fragments were within a factor of 4. Subcatchment 2 followed the same pattern as Subcatchment 1, however, the simulated results were more accurate, with the model correctly predicting pellet concentration, and fibers and pellets being underestimated by a factor of less than 2. In Subcatchment 3, the model accurately predicted the concentration of fibers, but pellets and fragments were underestimated by a factor of 7. Given the confidence boundaries for measurements of MPs in river sediments as described by Norling et al. (2024), the model's predictive ability can be considered satisfactory.

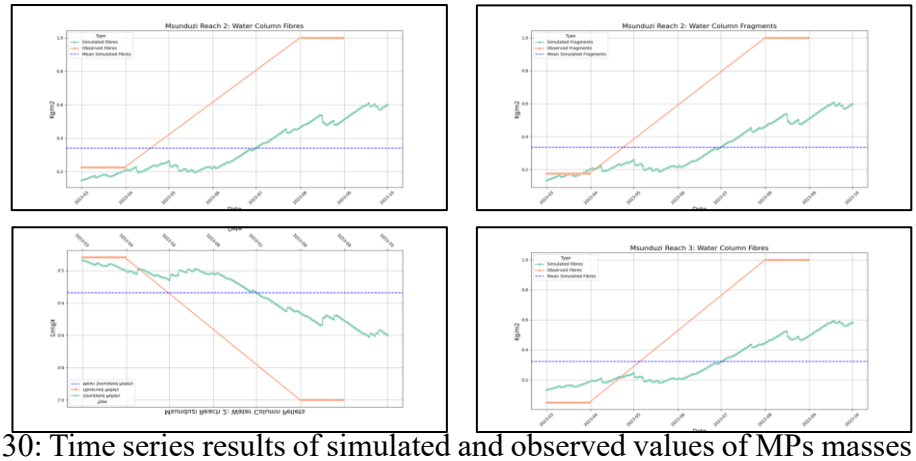

Figure 30: Time series results of simulated and observed values of MPs masses and concentrations in the riverbed and water column of the reaches of the Msunduzi River catchment.

4.20 Assessment of MP transport and fluxes in the catchment

Following model calibration and evaluation, analysis was done on the simulated fluxes of MPs in the catchment. The simulation represents how both regular flow and high-flow events affect the accumulation and release of MPs from river sediments. Low flows together with low runoff coincided with relatively constant levels of MPs as opposed to high flows, which deplete the stream bed, resulting in peaks of suspended MPs, as observed in 2022 when river flows peaked and sediment MP mass decreased (Figure 31). Figure 31 also shows the temporal variability of MP delivery from land to the river which ranges from 14 000 to 72 000 kg/year. It can be seen that in 2021 - 2022 there was drastic increase in MP delivery from land of 46 000 kg, which can be attributed to the flooding events as the high-water velocity facilitated the migration of more MP particles from source points.

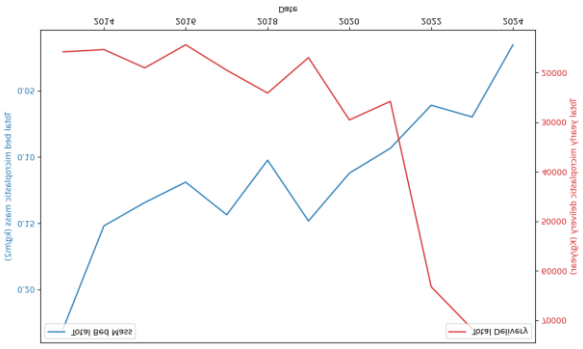

Figure 31: Total yearly MP delivery to the river (sum of all catchments) and total bed MP mass

The MP transport and mobilization in the Msunduzi River is governed by sediment initiation, which can be evaluated in terms of critical velocity and critical shear stress. The critical velocity method correlates initiation to flow velocity and the critical shear stress method correlates to bed shear stress (Jiang 2019). In order for the particles to move, one of three conditions needs to be satisfied as described below and in Figure 32 (Jiang 2019).

1. If Fd and Fl exceed W and Fc, the particle starts to roll.
2. If Fd overcomes Ff and Fc, the particle starts to slide.
3. If Fl overcomes W and vertical Fc, the particle floats.

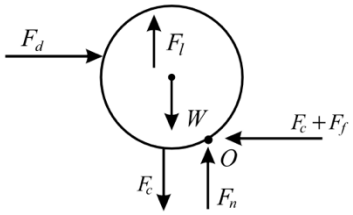

Figure 32: Forces on a bed particle, W (submerged weight). Fd (hydrodynamic darg), Fl (hydrodynamic lift), Fc (cohesion), Ff (friction), Fn (bed support force)

The MP initiation was evaluated based on Shields and Hjulstrom diagrams, presented in Figure 39 using Shields parameter and velocity. The variables used when calculating shields parameter is the MP size and density, gravitational acceleration, dynamic viscosity, reach shear stress (Figure 40a) and reach kinematic viscosity (Figure 33b), which are used to calculate the shear velocity, Reynolds Number and Shields Parameter (Figure 33d).

The resultant Shields Parameters, when analyzed with Figure 39a, indicate that fibres (1.75) and fragments (0.25) fall above the Shield curve, resulting in movement. The pellets, having a Shields Parameter of 0.02 and fall below the curve, indicating no mobilization. However, when comparing the reach flows (Figure 33c) to the Hjulstrom's Diagram, the bed MPs mobilize and are transported downstream due to high flows.

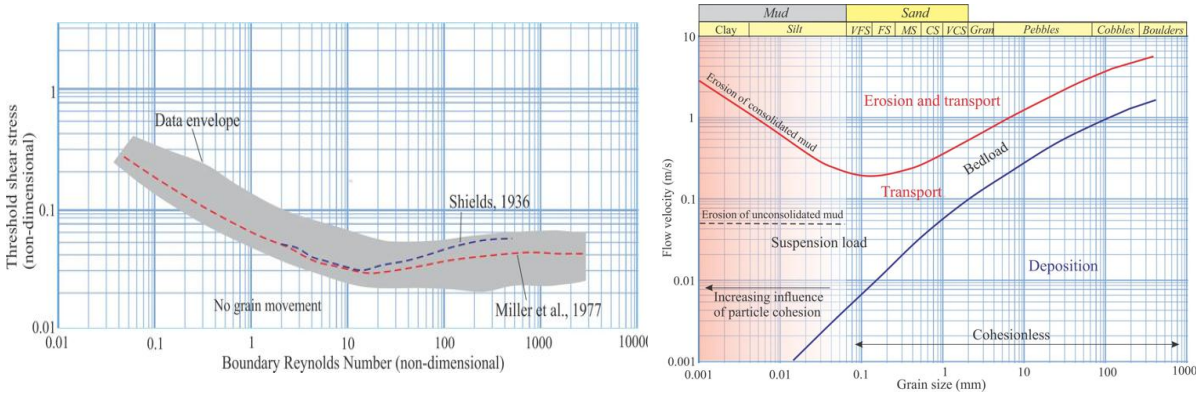

(a) (b)

Figure 33: (a) representing Shields Diagram ((Miller, McCave and Komar 1977) and (b) representing the Hjulstrom's Diagram ((Hjulström 1955)

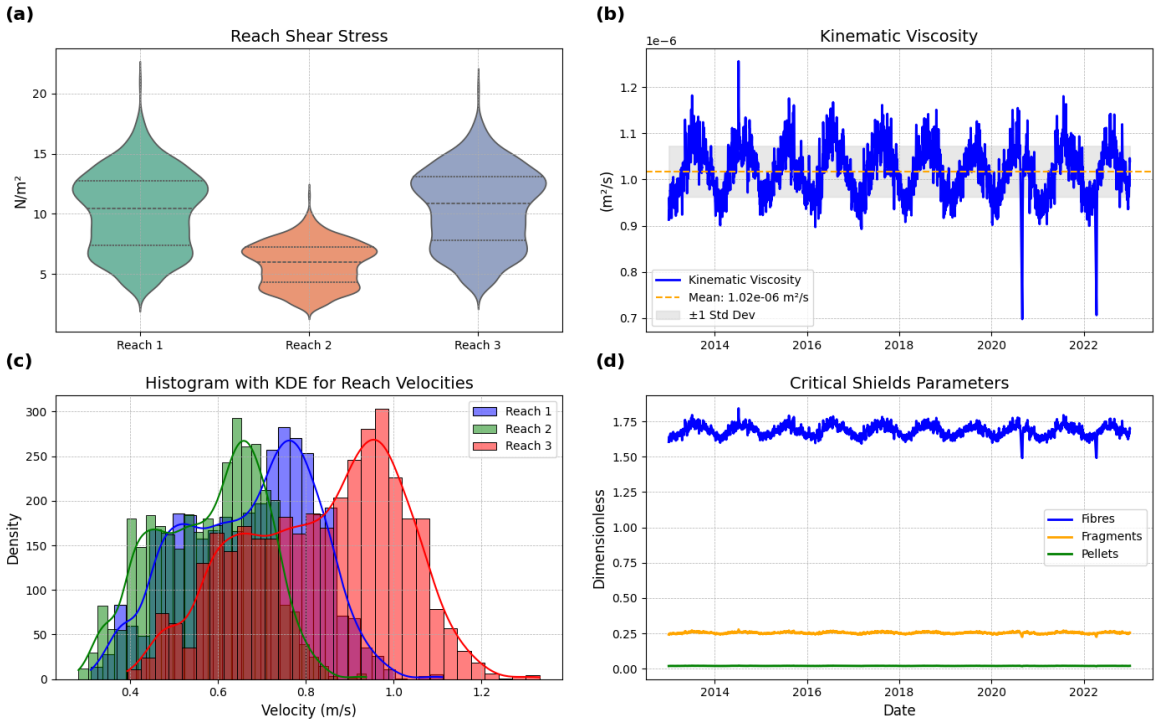

Figure 34 (a) Reach shear stress, (b) reach kinematic viscosity, (c) shear velocities and (d) critical Shield's parameter

Figure 35 illustrates the daily rate of MP bed entrainment along the Msunduzi River as a function of size, density, and sediment bed critical Shields Parameter. The potential for entrainment is present in all rivers reaches for fragments and pellets, except for fibres, which have a high critical Shields Parameter and are therefore not retained. It can be seen that MP entrainment increased in the lower reach of the Msunduzi Catchment, especially for larger MPs (pellets). Based on the

critical shear stress for entrainment and sediment bed critical Shields Parameter in Figure 36, all MPs are able to mobilize into suspension flow.

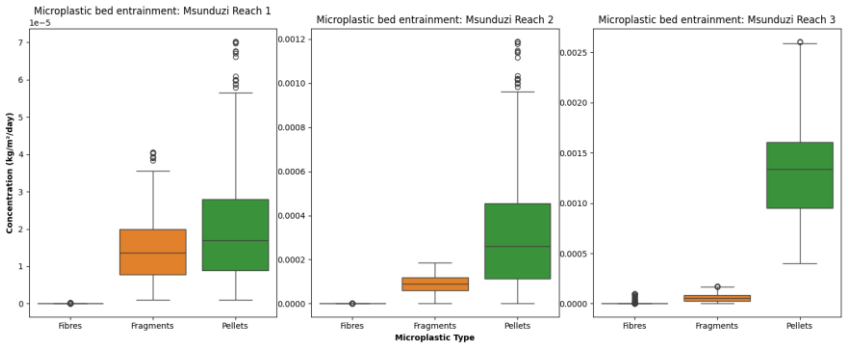

Figure 35: MP entrainment per subcatchment

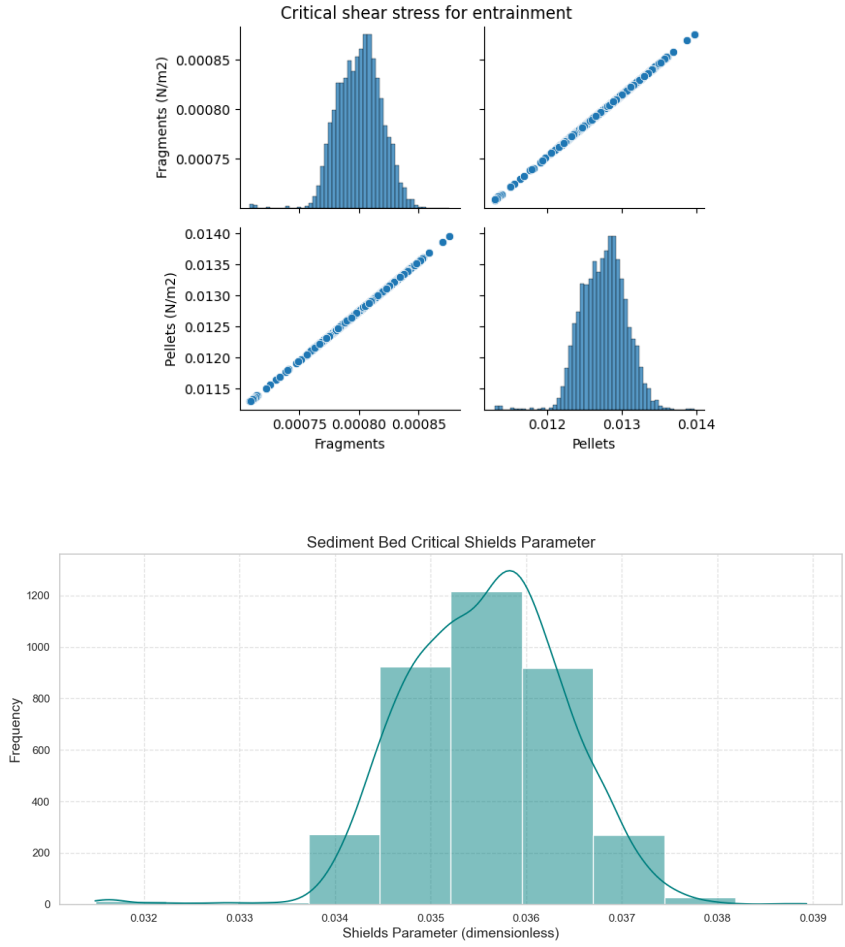

Figure 36: Shields Parameter for entrainment MP

CHAPTER 5: CONCLUSION

This comprehensive study undertook a multifaceted analysis of the Msunduzi and Swartkops rivers, aiming to unravel the intricate web of interactions between physicochemical parameters, land use patterns, microplastic (MP) contamination, and microbial community dynamics. The findings revealed a complex and concerning picture of environmental health, highlighting the urgent need for targeted interventions.

Land Use Impacts on water quality of the rivers

The analysis of physicochemical parameters revealed significant variations across sampling sites, indicating the influence of land use on surface water quality. In the Msunduzi River, while temperature and pH remained relatively stable, dissolved oxygen (DO) levels exhibited notable fluctuations. Sites #2 and #3, located in areas impacted by agricultural and urban runoff, respectively, demonstrated significantly lower DO concentrations. This decline in DO is a critical indicator of pollution, suggesting the influx of organic matter and pollutants that deplete oxygen levels. Similarly, in the Swartkops River, elevated electrical conductivity at Site #5, situated downstream of urban settlements, pointed to increased pollution, likely due to urban runoff and sewage discharge. Divergent turbidity levels across sites further underscored the impact of varying land use patterns, with higher turbidity indicating increased suspended solids, often associated with erosion and runoff. These findings underscore the direct and measurable impact of human activities on the water quality of the river systems.

Microplastic Contamination and Polymer Identification

The analysis of MP contamination in the selected sites revealed the pervasive presence of synthetic plastics in both river systems. The dominance of MP fibres, alongside fragments and pellets, highlighted the widespread distribution of MPs, likely originating from various sources, including textiles, packaging, and agricultural practices. ATR-FT-IR analysis provided valuable insights into the polymer composition of these MPs, identifying a diverse range of plastics, including polypropylene (PP), polystyrene (PS), polyethylene terephthalate (PET), polyethylene (PE), polycarbonate (PC), and polyamides (Nylon). The identification of specific polymers allowed for the tracing of potential pollution sources. Additionally, the higher concentrations of MPs in sediments compared to surface water further emphasized the accumulation of these pollutants, posing long-term risks to benthic ecosystems.

Microbial Community Dynamics and Functional Roles

The investigation of microbial communities associated with MPs revealed significant differences in diversity and composition between the sampling sites at surface water and plastisphere habitats. Surface water exhibited higher bacterial diversity and richness, suggesting a more diverse microbial community driven by various environmental factors. Proteobacteria emerged as the dominant phylum, followed by Bacteroidetes and Actinobacteria, reflecting the adaptability of these bacterial groups to diverse aquatic environments. LEfSe analysis identified unique biomarkers associated with different sites and habitats, indicating functional adaptations to MP presence. Notably, plastisphere samples showed enriched styrene degradation pathways, suggesting that MPs may serve as niches for pollutant-degrading microbes. This finding highlights the potential role of microbial communities in the biodegradation of MPs and associated pollutants, although the long-term implications of these processes remain unclear. The distance decay model further demonstrated a strong correlation between microbial diversity and pollution sources, emphasizing the influence of environmental stressors on microbial community structure. Additionally, the plastisphere emerged as a critical hotspot for the accumulation and proliferation of antibiotic resistance genes, mobile genetic elements, and potentially pathogenic bacteria. This highlights the plastisphere's role as a significant vector for the dissemination of antibiotic resistance and pathogens, posing serious environmental and public health risks. The persistence of MGEs and the observed enrichment of ARGs on plastic debris underscores the urgent need for further investigation and mitigation strategies to address the growing threat of antibiotic resistance in urban aquatic environments.

MP Flux Modelling and Prediction

The application of a dynamic model to assess MP fluxes along the Msunduzi River Catchment demonstrated the potential for predicting riverine MP fate. While the model yielded satisfactory predictions, its accuracy was limited by the absence of a comprehensive MP concentration database. The model highlighted the importance of considering seasonal and daily dynamics for accurate MP assessments, as opposed to relying on mean annual averages. The ability to model MP transport processes provides a valuable tool for identifying MP hotspots and developing targeted mitigation strategies. However, further refinement of modelling frameworks, incorporating hydrodynamic, ecological, and 3D modelling approaches, is necessary to enhance predictive capabilities. The absence of a sampled MP database can significantly impact model accuracy by limiting the calibration process.

Final Conclusion and Future Directions

Collectively, these findings underscore the urgent need for targeted mitigation strategies to address MP pollution and preserve the ecological health of these vital water resources. The multifaceted nature of MP contamination, originating from diverse sources and impacting various aspects of the aquatic environment, necessitates a holistic approach. Future research should prioritize building robust MP concentration databases, refining predictive models, and investigating the long-term impacts of MP-associated microbial communities on aquatic ecosystems as well as elucidating the specific mechanisms driving the enrichment of ARGs on the plastisphere and developing targeted interventions to minimize the spread of antibiotic resistance and pathogens in these critical ecosystems. Moreover, efforts should focus on implementing effective waste management practices, reducing plastic consumption, and promoting sustainable agricultural and industrial practices.

REFERENCES

Adam, V., Yang, T., Nowack, B., 2019. Toward an ecotoxicological risk assessment of microplastics: Comparison of available hazard and exposure data in freshwaters. Environ. Toxicol. Chem. 38, 436–447.

Alam, F.C., Sembiring, E., Muntalif, B.S., Suendo, V., 2019. Microplastic distribution in surface water and sediment river around slum and industrial area (case study: Ciwalengke River, Majalaya district, Indonesia). Chemosphere 224, 637–645.

Anderson, M.J., 2001. A new method for non-parametric multivariate analysis of variance. Austral Ecol. 26, 32–46.

Atugoda, T., Vithanage, M., Wijesekara, H., Bolan, N., Sarmah, A.K., Bank, M.S., You, S., Ok, Y.S., 2021. Interactions between microplastics, pharmaceuticals and personal care products: Implications for vector transport. Environ. Int. 149, 106367.

Bhagwat, G., Zhu, Q., O'Connor, W., Subashchandrabose, S., Grainge, I., Knight, R., Palanisami, T., 2021. Exploring the composition and functions of plastic microbiome using whole-genome sequencing. Environ. Sci. Technol. 55, 4899–4913.

Blair, R.M., Waldron, S., Phoenix, V.R., Gauchotte-Lindsay, C., 2019. Microscopy and elemental analysis characterisation of microplastics in sediment of a freshwater urban river in Scotland, UK. Environ. Sci. Pollut. Res. 26, 12491–12504.

Brown, E., MacDonald, A., Allen, S., Allen, D., 2023. The potential for a plastic recycling facility to release microplastic pollution and possible filtration remediation effectiveness. J. Hazard. Mater. Adv. 10, 100309. https://doi.org/https://doi.org/10.1016/j.hazadv.2023.100309

Browne, M.A., Crump, P., Niven, S.J., Teuten, E., Tonkin, A., Galloway, T., Thompson, R., 2011. Accumulation of microplastic on shorelines woldwide: sources and sinks. Environ. Sci. Technol. 45, 9175–9179.

Buchfink, B., Xie, C., Huson, D.H., 2015. Fast and sensitive protein alignment using DIAMOND. Nat. Methods 12, 59–60.

Campanale, C., Savino, I., Pojar, I., Massarelli, C., Uricchio, V.F., 2020. A practical overview of methodologies for sampling and analysis of microplastics in riverine environments. Sustainability 12, 6755.

Carney Almroth, B.M., Åström, L., Roslund, S., Petersson, H., Johansson, M., Persson, N.-K., 2018. Quantifying shedding of synthetic fibers from textiles; a source of microplastics released into the environment. Environ. Sci. Pollut. Res. 25, 1191–1199.

Castañeda, R.A., Avlijas, S., Simard, M.A., Ricciardi, A., 2014. Microplastic pollution in St. Lawrence river sediments. Can. J. Fish. Aquat. Sci. 71, 1767–1771.

Chen, Xiaoli, Castro, S.A., Liu, Q., Hu, W., Zhang, S., 2019. Practical considerations on performing and analyzing CLIP-seq experiments to identify transcriptomic-wide RNA-protein interactions. Methods 155, 49–57. https://doi.org/https://doi.org/10.1016/j.ymeth.2018.12.002

Chen, Xianchuan, Xiong, X., Jiang, X., Shi, H., Wu, C., 2019. Sinking of floating plastic debris caused by biofilm development in a freshwater lake. Chemosphere 222, 856–864.

Dahms, H.T.J., van Rensburg, G.J., Greenfield, R., 2020. The microplastic profile of an urban African stream. Sci. Total Environ. 731, 138893.

De Tender, C.A., Devriese, L.I., Haegeman, A., Maes, S., Ruttink, T., Dawyndt, P., 2015. Bacterial community profiling of plastic litter in the Belgian part of the North Sea. Environ. Sci. Technol. 49, 9629–9638.

de Villiers, S., 2019. Microfibre pollution hotspots in river sediments adjacent to South Africa's coastline. Water Sa 45, 97–102.

Di, M., Wang, J., 2018. Microplastics in surface waters and sediments of the Three Gorges Reservoir, China. Sci. Total Environ. 616, 1620–1627.

Ding, L., fan Mao, R., Guo, X., Yang, X., Zhang, Q., Yang, C., 2019. Microplastics in surface waters and sediments of the Wei River, in the northwest of China. Sci. Total Environ. 667, 427–434.

Dris, R., Gasperi, J., Tassin, B., 2018. Sources and fate of microplastics in urban areas: a focus on Paris megacity. Freshw. microplastics Emerg. Environ. Contam. 69–83.

Eriksen, M., Mason, S., Wilson, S., Box, C., Zellers, A., Edwards, W., Farley, H., Amato, S., 2013. Microplastic pollution in the surface waters of the Laurentian Great Lakes. Mar. Pollut. Bull. 77, 177–182.

Fan, Y., Zheng, K., Zhu, Z., Chen, G., Peng, X., 2019. Distribution, sedimentary record, and persistence of microplastics in the Pearl River catchment, China. Environ. Pollut. 251, 862–870.

Frei, S., Piehl, S., Gilfedder, B.S., Löder, M.G.J., Krutzke, J., Wilhelm, L., Laforsch, C., 2019. Occurence of microplastics in the hyporheic zone of rivers. Sci. Rep. 9, 15256.

Fu, L., Niu, B., Zhu, Z., Wu, S., Li, W., 2012. CD-HIT: accelerated for clustering the next-generation sequencing data. Bioinformatics 28, 3150–3152.

Gerolin, C.R., Pupim, F.N., Sawakuchi, A.O., Grohmann, C.H., Labuto, G., Semensatto, D., 2020. Microplastics in sediments from Amazon rivers, Brazil. Sci. Total Environ. 749, 141604.

Gola, D., Tyagi, P.K., Arya, A., Chauhan, N., Agarwal, M., Singh, S.K., Gola, S., 2021. The impact of microplastics on marine environment: A review. Environ. Nanotechnology, Monit. Manag. 16, 100552.

Golwala, H., Zhang, X., Iskander, S.M., Smith, A.L., 2021. Solid waste: An overlooked source of microplastics to the environment. Sci. Total Environ. 769, 144581.

Guerranti, C., Cannas, S., Scopetani, C., Fastelli, P., Cincinelli, A., Renzi, M., 2017. Plastic litter in aquatic environments of Maremma Regional Park (Tyrrhenian Sea, Italy): Contribution by the Ombrone river and levels in marine sediments. Mar. Pollut. Bull. 117, 366–370.

He, B., Goonetilleke, A., Ayoko, G.A., Rintoul, L., 2020. Abundance, distribution patterns, and identification of microplastics in Brisbane River sediments, Australia. Sci. Total Environ. 700, 134467.

Hidalgo-Ruz, V., Gutow, L., Thompson, R.C., Thiel, M., 2012. Microplastics in the marine environment: a review of the methods used for identification and quantification. Environ. Sci. Technol. 46, 3060–3075.

Horton, A.A., Svendsen, C., Williams, R.J., Spurgeon, D.J., Lahive, E., 2017. Large microplastic

particles in sediments of tributaries of the River Thames, UK–Abundance, sources and methods for effective quantification. Mar. Pollut. Bull. 114, 218–226.

Hou, L., Kumar, D., Yoo, C.G., Gitsov, I., Majumder, E.L.-W., 2021. Conversion and removal strategies for microplastics in wastewater treatment plants and landfills. Chem. Eng. J. 406, 126715.

Huang, Z., Hu, B., Wang, H., 2023. Analytical methods for microplastics in the environment: a review. Environ. Chem. Lett. 21, 383–401.

Jiang, J.-Q., 2018. Occurrence of microplastics and its pollution in the environment: A review. Sustain. Prod. Consum. 13, 16–23.

Kapp, K.J., Yeatman, E., 2018. Microplastic hotspots in the Snake and Lower Columbia rivers: A journey from the Greater Yellowstone Ecosystem to the Pacific Ocean. Environ. Pollut. 241, 1082–1090.

Karbalaei, S., Hanachi, P., Walker, T.R., Cole, M., 2018. Occurrence, sources, human health impacts and mitigation of microplastic pollution. Environ. Sci. Pollut. Res. 25, 36046–36063.

Kasamesiri, P., Thaimuangphol, W., 2020. Microplastics ingestion by freshwater fish in the Chi River, Thailand. Geomate J. 18, 114–119.

Khan, S.A., Khan, S.B., Khan, L.U., Farooq, A., Akhtar, K., Asiri, A.M., 2018. Fourier transform infrared spectroscopy: fundamentals and application in functional groups and nanomaterials characterization. Handb. Mater. Charact. 317–344.

Klein, S., Worch, E., Knepper, T.P., 2015. Occurrence and spatial distribution of microplastics in river shore sediments of the Rhine-Main area in Germany. Environ. Sci. Technol. 49, 6070–6076.

Kumar, R., Sharma, P., Manna, C., Jain, M., 2021. Abundance, interaction, ingestion, ecological concerns, and mitigation policies of microplastic pollution in riverine ecosystem: A review. Sci. Total Environ. 782, 146695.

Lebreton, L.C.M., Van Der Zwet, J., Damsteeg, J.-W., Slat, B., Andrady, A., Reisser, J., 2017. River plastic emissions to the world's oceans. Nat. Commun. 8, 15611.

Lechthaler, S., Schwarzbauer, J., Reicherter, K., Stauch, G., Schüttrumpf, H., 2020. Regional study of microplastics in surface waters and deep sea sediments south of the Algarve Coast. Reg. Stud. Mar. Sci. 40, 101488.

Li, C., Wang, Lifei, Ji, S., Chang, M., Wang, Longfei, Gan, Y., Liu, J., 2021. The ecology of the plastisphere: microbial composition, function, assembly, and network in the freshwater and seawater ecosystems. Water Res. 202, 117428.

Li, D., Liu, C.-M., Luo, R., Sadakane, K., Lam, T.-W., 2015. MEGAHIT: an ultra-fast single-node solution for large and complex metagenomics assembly via succinct de Bruijn graph. Bioinformatics 31, 1674–1676.

Li, R., Li, Y., Kristiansen, K., Wang, J., 2008. SOAP: short oligonucleotide alignment program. Bioinformatics 24, 713–714. https://doi.org/10.1093/bioinformatics/btn025

Liaw, A., Wiener, M., 2002. Classification and regression by randomForest. R news 2, 18–22.

Lu, L., Luo, T., Zhao, Y., Cai, C., Fu, Z., Jin, Y., 2019. Interaction between microplastics and microorganism as well as gut microbiota: A consideration on environmental animal and

human health. Sci. Total Environ. 667, 94–100.

Malla-Pradhan, R., Suwunwong, T., Phoungthong, K., Joshi, T.P., Pradhan, B.L., 2022. Microplastic pollution in urban Lake Phewa, Nepal: the first report on abundance and composition in surface water of lake in different seasons. Environ. Sci. Pollut. Res. 29, 39928–39936. https://doi.org/10.1007/s11356-021-18301-9

Malla, M.A., Dubey, A., Kumar, A., Yadav, S., 2023. Unlocking the biotechnological and environmental perspectives of microplastic degradation in soil-ecosystems using metagenomics. Process Saf. Environ. Prot. 170, 372–379. https://doi.org/https://doi.org/10.1016/j.psep.2022.11.084

Mani, T., Hauk, A., Walter, U., Burkhardt-Holm, P., 2015. Microplastics profile along the Rhine River. Sci. Rep. 5, 17988.

Marsay, K.S., Ambrosino, A.C., Koucherov, Y., Davidov, K., Figueiredo, N., Yakovenko, I., Itzahri, S., Martins, M., Sobral, P., Oren, M., 2023. The geographical and seasonal effects on the composition of marine microplastic and its microbial communities: The case study of Israel and Portugal. Front. Microbiol. 14, 1089926.

Mason, S.A., Garneau, D., Sutton, R., Chu, Y., Ehmann, K., Barnes, J., Fink, P., Papazissimos, D., Rogers, D.L., 2016. Microplastic pollution is widely detected in US municipal wastewater treatment plant effluent. Environ. Pollut. 218, 1045–1054.

McCormick, A., Hoellein, T.J., Mason, S.A., Schluep, J., Kelly, J.J., 2014. Microplastic is an abundant and distinct microbial habitat in an urban river. Environ. Sci. Technol. 48, 11863–11871.

Meijer, L.J.J., Van Emmerik, T., Van Der Ent, R., Schmidt, C., Lebreton, L., 2021. More than 1000 rivers account for 80% of global riverine plastic emissions into the ocean. Sci. Adv. 7, eaaz5803.

Miller, R.Z., Watts, A.J.R., Winslow, B.O., Galloway, T.S., Barrows, A.P.W., 2017. Mountains to the sea: river study of plastic and non-plastic microfiber pollution in the northeast USA. Mar. Pollut. Bull. 124, 245–251.

Moore, C.J., Lattin, G.L., Zellers, A.F., 2011. Quantity and type of plastic debris flowing from two urban rivers to coastal waters and beaches of Southern California. Rev. Gestão Costeira Integr. Integr. Coast. Zo. Manag. 11, 65–73.

Murphy, F., Ewins, C., Carbonnier, F., Quinn, B., 2016. Wastewater treatment works (WwTW) as a source of microplastics in the aquatic environment. Environ. Sci. Technol. 50, 5800–5808.

Nel, H.A., Dalu, T., Wasserman, R.J., 2018. Sinks and sources: Assessing microplastic abundance in river sediment and deposit feeders in an Austral temperate urban river system. Sci. Total Environ. 612, 950–956.

Noguchi, H., Park, J., Takagi, T., 2006. MetaGene: prokaryotic gene finding from environmental genome shotgun sequences. Nucleic Acids Res. 34, 5623–5630.

Nuelle, M.-T., Dekiff, J.H., Remy, D., Fries, E., 2014. A new analytical approach for monitoring microplastics in marine sediments. Environ. Pollut. 184, 161–169. https://doi.org/https://doi.org/10.1016/j.envpol.2013.07.027

Oberbeckmann, S., Loeder, M.G.J., Gerdts, G., Osborn, A.M., 2014. Spatial and seasonal variation in diversity and structure of microbial biofilms on marine plastics in Northern European

waters. FEMS Microbiol. Ecol. 90, 478–492.

Oksanen, J., 2010. Vegan: community ecology package. http//vegan. r-forge. r-project. org/.

Oksanen, J., Kindt, R., Legendre, P., O'Hara, B., Stevens, M.H.H., Oksanen, M.J., Suggests, M., 2007. The vegan package. Community Ecol. Packag. 10, 719.

Omura, T., Isobe, N., Miura, T., Ishii, S., Mori, M., Ishitani, Y., Kimura, S., Hidaka, K., Komiyama, K., Suzuki, M., Kasuya, K., Nomaki, H., Nakajima, R., Tsuchiya, M., Kawagucci, S., Mori, H., Nakayama, A., Kunioka, M., Kamino, K., Iwata, T., 2024. Microbial decomposition of biodegradable plastics on the deep-sea floor. Nat. Commun. 15, 568. https://doi.org/10.1038/s41467-023-44368-8

Peng, G., Xu, P., Zhu, B., Bai, M., Li, D., 2018. Microplastics in freshwater river sediments in Shanghai, China: a case study of risk assessment in mega-cities. Environ. Pollut. 234, 448–456.

Philippe, A., Noël, C., Eyheraguibel, B., Briand, J.-F., Paul-Pont, I., Ghiglione, J.-F., Coton, E., Burgaud, G., 2023. Fungal diversity and dynamics during long-term immersion of conventional and biodegradable plastics in the marine environment. Diversity 15, 579.

Pinnell, L.J., Turner, J.W., 2020. Temporal changes in water temperature and salinity drive the formation of a reversible plastic-specific microbial community. FEMS Microbiol. Ecol. 96, fiaa230.

Ratre, P., Nazeer, N., Soni, N., Kaur, P., Tiwari, R., Mishra, P.K., 2024. Smart carbon-based sensors for the detection of non-coding RNAs associated with exposure to micro (nano) plastics: an artificial intelligence perspective. Environ. Sci. Pollut. Res. 1–24.

Rodrigues, M.O., Abrantes, N., Gonçalves, F.J.M., Nogueira, H., Marques, J.C., Gonçalves, A.M.M., 2018. Spatial and temporal distribution of microplastics in water and sediments of a freshwater system (Antuã River, Portugal). Sci. Total Environ. 633, 1549–1559.

Rüthi, J., Rast, B.M., Qi, W., Perez-Mon, C., Pardi-Comensoli, L., Brunner, I., Frey, B., 2023. The plastisphere microbiome in alpine soils alters the microbial genetic potential for plastic degradation and biogeochemical cycling. J. Hazard. Mater. 441, 129941.

Schell, T., Hurley, R., Nizzetto, L., Rico, A., Vighi, M., 2021. Spatio-temporal distribution of microplastics in a Mediterranean river catchment: the importance of wastewater as an environmental pathway. J. Hazard. Mater. 420, 126481.

Scherer, C., Weber, A., Stock, F., Vurusic, S., Egerci, H., Kochleus, C., Arendt, N., Foeldi, C., Dierkes, G., Wagner, M., 2020. Comparative assessment of microplastics in water and sediment of a large European river. Sci. Total Environ. 738, 139866.

Schmidt, C., Kumar, R., Yang, S., Büttner, O., 2020. Microplastic particle emission from wastewater treatment plant effluents into river networks in Germany: Loads, spatial patterns of concentrations and potential toxicity. Sci. Total Environ. 737, 139544.

Shen, M., Zhu, Y., Zhang, Y., Zeng, G., Wen, X., Yi, H., Ye, S., Ren, X., Song, B., 2019. Micro (nano) plastics: unignorable vectors for organisms. Mar. Pollut. Bull. 139, 328–331.

Singh, R., Kumar, R., Sharma, P., 2022. Microplastic in the subsurface system: Extraction and characterization from sediments of River Ganga near Patna, Bihar, in: Advances in Remediation Techniques for Polluted Soils and Groundwater. Elsevier, pp. 191–217.

Sun, J., Dai, X., Wang, Q., Van Loosdrecht, M.C.M., Ni, B.-J., 2019. Microplastics in wastewater treatment plants: Detection, occurrence and removal. Water Res. 152, 21–37.

Tamames, J., Puente-Sánchez, F., 2019. SqueezeMeta, a highly portable, fully automatic metagenomic analysis pipeline. Front. Microbiol. 9, 3349.

Thakur, B., Singh, Jaswinder, Singh, Joginder, Angmo, D., Vig, A.P., 2023a. Biodegradation of different types of microplastics: Molecular mechanism and degradation efficiency. Sci. Total Environ. 877, 162912.

Turner, A., Arnold, R., Williams, T., 2020. Weathering and persistence of plastic in the marine environment: Lessons from LEGO. Environ. Pollut. 262, 114299.

Uogintė, I., Pleskytė, S., Pauraitė, J., Lujanienė, G., 2022. Seasonal variation and complex analysis of microplastic distribution in different WWTP treatment stages in Lithuania. Environ. Monit. Assess. 194, 829.

Uurasjärvi, E., Hartikainen, S., Setälä, O., Lehtiniemi, M., Koistinen, A., 2020. Microplastic concentrations, size distribution, and polymer types in the surface waters of a northern European lake. Water Environ. Res. 92, 149–156.

Van Emmerik, T., Kieu-Le, T.-C., Loozen, M., Van Oeveren, K., Strady, E., Bui, X.-T., Egger, M., Gasperi, J., Lebreton, L., Nguyen, P.-D., 2018. A methodology to characterize riverine macroplastic emission into the ocean. Front. Mar. Sci. 5, 372.

Wang, J., Peng, J., Tan, Z., Gao, Y., Zhan, Z., Chen, Q., Cai, L., 2017. Microplastics in the surface sediments from the Beijiang River littoral zone: composition, abundance, surface textures and interaction with heavy metals. Chemosphere 171, 248–258.

Weideman, E.A., Perold, V., Ryan, P.G., 2019. Little evidence that dams in the Orange–Vaal River system trap floating microplastics or microfibres. Mar. Pollut. Bull. 149, 110664.

Xu, C., Zhang, B., Gu, C., Shen, C., Yin, S., Aamir, M., Li, F., 2020. Are we underestimating the sources of microplastic pollution in terrestrial environment? J. Hazard. Mater. 400, 123228.

Yang, Y., Liu, W., Zhang, Z., Grossart, H.-P., Gadd, G.M., 2020. Microplastics provide new microbial niches in aquatic environments. Appl. Microbiol. Biotechnol. 104, 6501–6511. https://doi.org/10.1007/s00253-020-10704-x

Zhang, J.L., Ma, K.P., 2014. spaa: an R package for computing species association and niche overlap. Res. Prog. Biodivers. Conserv. China 10, 165–174.

Zhang, K., Xiong, X., Hu, H., Wu, C., Bi, Y., Wu, Y., Zhou, B., Lam, P.K.S., Liu, J., 2017. Occurrence and characteristics of microplastic pollution in Xiangxi Bay of Three Gorges Reservoir, China. Environ. Sci. Technol. 51, 3794–3801.

Zhang, S.-J., Zeng, Y.-H., Zhu, J.-M., Cai, Z.-H., Zhou, J., 2022. The structure and assembly mechanisms of plastisphere microbial community in natural marine environment. J. Hazard. Mater. 421, 126780. https://doi.org/https://doi.org/10.1016/j.jhazmat.2021.126780

Zhang, Y., Kang, S., Allen, S., Allen, D., Gao, T., Sillanpää, M., 2020. Atmospheric microplastics: A review on current status and perspectives. Earth-Science Rev. 203, 103118.

Zheng, Y., Li, J., Cao, W., Liu, X., Jiang, F., Ding, J., Yin, X., Sun, C., 2019. Distribution characteristics of microplastics in the seawater and sediment: a case study in Jiaozhou Bay, China. Sci. Total Environ. 674, 27–35.

Zhu, D., Ma, J., Li, G., Rillig, M.C., Zhu, Y.-G., 2022. Soil plastispheres as hotspots of antibiotic resistance genes and potential pathogens. ISME J. 16, 521–532. https://doi.org/10.1038/s41396-021-01103-9

Zhu, X.-T., Yi, J., Qiang, L.-Y., Cheng, J.-P., 2018. Distribution and settlement of microplastics in the surface sediment of Yangtze Estuary. Huan jing ke xue= Huanjing kexue 39, 2067–2074.

Ziajahromi, S., Neale, P.A., Leusch, F.D.L., 2016. Wastewater treatment plant effluent as a source of microplastics: review of the fate, chemical interactions and potential risks to aquatic organisms. Water Sci. Technol. 74, 2253–2269.

Annexure 1:

Muneer Ahmad Malla, Malambule Nomalihle, Jonathan Featherston, Arvind Kumar, Isaac D. Amoah, Arshad Ismail, Faizal Bux, Sheena Kumari, 2025. Comprehensive profiling and risk assessment of antibiotic resistomes in surface water and plastisphere by integrated shotgun metagenomics, Journal of Hazardous Materials, Volume 487, 137180, ISSN 0304-3894, https://doi.org/10.1016/j.jhazmat.2025.137180.